SIMULATION-ASSISTED URBAN MICROCLIMATE EVALUATION OF VERTICAL GREENERY ON HOUSING DESIGN MORPHOLOGY IN TIRANA, ALBANIA.

A THESIS SUBMITTED TO
THE FACULTY OF ARCHITECTURE AND ENGINEERING
OF
EPOKA UNIVERSITY

BY

REI GOGA

IN PARTIAL FULFILLMENT OF THE REQUIREMENTS
FOR
THE DEGREE OF MASTER OF SCIENCE
IN
ARCHITECTURE

JUNE, 2023

Approval sheet of the Thesis

This is to certify that we have read this thesis entitled **"Simulation-assisted urban microclimate evaluation of vertical greenery on housing design morphology in Tirana, Albania."** and that in our opinion it is fully adequate, in scope and quality, as a thesis for the degree of Master of Science.

_____

Assoc. Prof. Dr. Edmond Manahasa
Head of Department
Date: June, 20, 2023

Examining Committee Members:

Prof. Dr. Sokol Dervishi (Architecture) _____

Dr. Fabio Naselli (Architecture) _____

Dr. Ina Dervishi (Architecture) _____

I hereby declare that all information in this document has been obtained and presented in accordance with academic rules and ethical conduct. I also declare that, as required by these rules and conduct, I have fully cited and referenced all material and results that are not original to this work.

Name Surname: Rei Goga

Signature: _____

ABSTRACT

SIMULATION-ASSISTED URBAN MICROCLIMATE EVALUATION OF VERTICAL GREENERY ON HOUSING DESIGN MORPHOLOGY IN TIRANA, ALBANIA

Goga, Rei

M.Sc., Department of Architecture

Supervisor: Prof. Dr. Sokol Dervishi

Co supervisor: Dr. Ina Dervishi

Greenery use in buildings has become a trend and a topic of discussions amongst the built environment community and abroad. One of the major elements affecting the dispersion of modern environmentally friendly building envelopes is the need to better the performance of the targeted buildings.

With cityscapes expanding both horizontally and vertically, green washed buildings seem to appear more often on the scene of recently permitted buildings even though the evidence to back up their claims on environmental performance lack strong backing from scientific studies. As a result, the early design evaluation process on these large parts of urban fabric is critical. While many studies have analyzed and evaluated, different scenarios that consist of different types of greenery use there is a gap in literature regarding whether greenwashing relates to outdoor thermal comfort, and if so, how much of an impact it has. This paper will attempt to answer this question by analyzing a real case scenario, using simulations to obtain data on two different optimization scenarios that follow greenwashing techniques based on literature. The goal of this paper is to guide and assist planners in Tirana and other cities with similar climate circumstances to make the right decisions when planning new neighborhoods.

Keywords: *morphology, thermal comfort, courtyards, macroscale, microscale, impact, optimization, sustainable, early-design, planning, UTCI*

ABSTRAKT

VLERËSIMI I PROJEKTIMIT NË FAZE TË HERSHME PËR KOMFORTIN TERMIK TË JASHTËM QË OFRON GJELBËRIMI VERTIKAL NË TIRANË, SHQIPËRI

Goga, Rei

Master Shkencor, Departamenti i Arkitektures

Udhëheqësi: Prof. Dr. Sokol Dervishi

Bashkë udhëheqës: Dr. Ina Dervishi

Përfshirja e gjelbërimit horizontal dhe vertikal në ndertim tashmë është një tendencë e spikatur arkitektonike globale. Një nga elementët kryesorë që ka ndikuar në shpërndarjen e këtij stili të veshjes së ndertesave ka qënë dhe mbetet nevoja për të rritur performancën termike dhe energjitike të ndertesave dhe uljen e ndikimeve negative të këtyre të fundit në mjedis.

Zgjerimi urban i qyteteve në aspektin vertikal si dhe atë horizontal ka lënë gjithmon e më shumë vend per aplikimim e modeleve të ndryshme të gjelbërimit edhe pse në shumë raste mungojnë evidencat shkencore të cilat vërtetojnë ndikimin pozitiv të ndërtesave të gjelbëruara në mjedis. Për këtë arsye analizimi i hershëm, prej fazës së projektimit të hapësirave urbane të cilat kanë pjesë të tyre ndërtesa të gjelbëruara është kritik dhe tejet i nevojshëm. Ndërsa shumë studime kanë vlerësuar dhe analizuar skenare të ndryhsme të përdorimit të gjelbërimit si pjesë e veshjes së jashtme të ndërtesave, ekziston një boshllëk në literaturë lidhur me korrelacionin e mundshëm midis komfortit termik të jashtëm dhe ndërtesave të gjelbëruara. Ky studim do të përpiqet ti përgjigjet kësaj pyetje duke analizuar një zonë urbane ekzistuese në Tiranë, ku do të provohen dhe më pas analizohen performancat termike të dy llojeve të gjelbërimit në ndërtesa, atij vertikal dhe horizontal. Duke përdorur programe të avancuara simulimi do të analizohet komforti termik i jashtëm ne shkallë mikro dhe makro per zonën urbane të zgjedhur.

Qëllimi i këtij punimi është të udhëzojë planifikuesit në Tiranë dhe qytete të tjera me rrethana të ngjashme klimatike për t'i ndihmuar ata të marrin vendimet e duhura kur planifikojnë lagje të reja në të cilat mund të përdoret gjelbërimi si pjesë e ndërtimit.

Fjalët kyçe: *morfologji, komfort termik, oborre të brendshme, shkallë macro, shkallë micro, impakt, optimizim, qëndrueshmëri në aspekt mjedisor, projektim i hershëm, planifikim urban, UTCI*

ACKNOWLEDGEMENTS

Acknowledgements should be written here. Times New Roman, 12 pt. Indentaion should be “Special first line, 12 mm”. Line spacing should be 1.5 lines with 6 pt before and 6 pt after.

TABLE OF CONTENTS

ABSTRACT III

ABSTRAKT V

ACKNOWLEDGEMENTS VII

LIST OF TABLES XIV

LIST OF FIGURES XVII

CHAPTER 1 1

INTRODUCTION 1

1.1 Overview 1

1.2 Motivation & Background 2

1.3 Thesis objective 4

1.4 Organization of the thesis 5

CHAPTER 2 6

LITERATURE REVIEW 6

2.1 Theoretical background 6

2.1.1. Environmental comfort 6

2.1.2. Courtyards 6

2.1.3. Albedo materials 7

2.1.4. Greenery usage in urban scale 8

2.1.5. UTCI 9

2.2 Previously related studies 10

2.2.1. “Studying impact of infrastructure development on urban microclimate: Integrated multiparameter analysis using Open-FOAM” 10

2.2.2. “Assessing the impact of urban microclimate on building energy demand by coupling CFD and building performance simulation” 10

2.2.3. “Detailed investigation of vegetation effects on microclimate by means of computational fluid dynamics (CFD) in a tropical urban environment” 11

2.2.4. “Urban microclimate and energy consumption: A multi-objective parametric urban design approach for dense subtropical cities” 12

2.2.5. “Impact of urban morphology on urban microclimate and building energy loads.” 12

2.2.6. “Analyzing impacts of urban morphological variables and density on outdoor microclimate for tropical cities: A review and a framework proposal for future research directions.” 13

2.2.7. “Impact of reflective materials on urban canyon albedo, outdoor and indoor microclimates.” 14

2.2.8. “Assessing local heat stress and air quality with the use of remote sensing and pedestrian perception in urban microclimate simulations” 15

2.3 Aim and Originality 18

CHAPTER 3 19

METHODOLOGY 19

3.1 Overview 19

3.2 Climatic context 20

3.3 Case study selection 23

3.3.1 Site selection 23

3.3.2 Site description 24

3.4 Computational simulation 35

3.4.1. Software description 35

3.4.2. Software data input 37

3.4.3. Software data output 37

CHAPTER 4 40

RESULTS AND DISCUSSIONS 40

4.1 Overview 40

4.2 Micro scale 41

4.2.1 Courtyard 01 41

4.2.2 Courtyard 02 42

4.2.3 Courtyard 03 43

4.2.4 Courtyard 04 43

4.2.5 Courtyard 05 44

4.2.6 Courtyard 06 45

4.2.7 Courtyard 07 46

4.2.8 Courtyard 08 46

4.2.9 Courtyard 09 48

4.2.10 Courtyard 10 49

4.2.11 Courtyard 11 49

4.2.12 Courtyard 12 51

4.2.13 Courtyard 13 52

4.2.14 Courtyard 14 52

4.2.15 Courtyard 15 54

4.2.16 Courtyard 16 55

4.2.17 Courtyard 17 56
4.2.18 Courtyard 18 56
4.2.19 Courtyard 19 57
4.2.20 Courtyard 20 58
4.2.21 Courtyard 21 59
4.2.22 Courtyard 22 60
4.2.23 Courtyard 23 61
4.2.24 Courtyard 24 62
4.2.25 Courtyard 25 62
4.2.26 Courtyard 26 63
4.2.27 Courtyard 27 64
4.2.28 Courtyard 28 65
4.2.29 Courtyard 29 66
4.2.30 Courtyard 30 67
4.2.31 Courtyard 31 68
4.2.32 Courtyard 32 69
4.2.33 Courtyard 33 70
4.3 Macroscale 71
CHAPTER 5 77
OPTIMIZATION 77
5.1 Overview 77
5.2 Microscale 78
5.2.1 Courtyard 01 78
5.2.2 Courtyard 02 79

5.2.3 Courtyard 03 81
5.2.4 Courtyard 04 82
5.2.5 Courtyard 05 84
5.2.6 Courtyard 06 85
5.2.7 Courtyard 07 86
5.2.8 Courtyard 08 88
5.2.9 Courtyard 09 89
5.2.10 Courtyard 10 91
5.2.11 Courtyard 11 92
5.2.12 Courtyard 12 94
5.2.13 Courtyard 13 95
5.2.14 Courtyard 14 97
5.2.15 Courtyard 15 99
5.2.16 Courtyard 16 100
5.2.17 Courtyard 17 102
5.2.18 Courtyard 18 103
5.2.19 Courtyard 19 105
5.2.20 Courtyard 20 106
5.2.21 Courtyard 21 108
5.2.22 Courtyard 22 109
5.2.23 Courtyard 23 111
5.2.24 Courtyard 24 112
5.2.25 Courtyard 25 113
5.2.26 Courtyard 26 115
5.2.27 Courtyard 27 116
5.2.28 Courtyard 28 118

5.2.29 Courtyard 29 119
5.2.30 Courtyard 30 121
5.2.29 Courtyard 29 122
5.2.31 Courtyard 31 124
5.2.32 Courtyard 32 125
5.2.33 Courtyard 33 127
4.3 Macroscale 128
CHAPTER 6 132
CONCLUSIONS 132
6.1 Conclusions 132
6.2 Recommendations for further research 133
REFERENCES 134

LIST OF TABLES

Table 1. Functional area distributions on site 25

Table 2. Fully enclosed courtyard visualization (Plane, Axo, Section)..... 26

Table 3. Courtyards morphology indicators 28

Table 4. Non-enclosed Courtyards illustrations (Plane, Axo, Section) 29

Table 5. Non-enclosed Courtyards morphology indicators 34

Table 6. UTCI performance differences between optimization scenarios on “C01” .. 78

Table 7. UTCI performance differences between optimization scenarios on “C02” .. 79

Table 8. UTCI performance differences between optimization scenarios on “C03” .. 81

Table 9. UTCI performance differences between optimization scenarios on “C04” .. 82

Table 10. UTCI performance differences between optimization scenarios on “C05” 84

Table 11. UTCI performance differences between optimization scenarios on “C06” 85

Table 12. UTCI performance differences between optimization scenarios on “C07” 86

Table 13. UTCI performance differences between optimization scenarios on “C08” 88

Table 14. UTCI performance differences between optimization scenarios on “C09” 89

Table 15. UTCI performance differences between optimization scenarios on “C10” 91

Table 16. UTCI performance differences between optimization scenarios on “C11” 93

Table 17. UTCI performance differences between optimization scenarios on “C12” 94

Table 18. UTCI performance differences between optimization scenarios on “C13” 95

Table 19. UTCI performance differences between optimization scenarios on “C14” 97

Table 20. UTCI performance differences between optimization scenarios on “C15” 99

Table 21. UTCI performance differences between optimization scenarios on “C16” 100

Table 22. UTCI performance differences between optimization scenarios on “C17” 102

Table 23. UTCI performance differences between optimization scenarios on “C18” 103

Table 24. UTCI performance differences between optimization scenarios on “C19” 105

Table 25. UTCI performance differences between optimization scenarios on “C20” 106

Table 26. UTCI performance differences between optimization scenarios on “C21” 108

Table 27. UTCI performance differences between optimization scenarios on “C22” 110

Table 28. UTCI performance differences between optimization scenarios on “C23” 111

Table 29. UTCI performance differences between optimization scenarios on “C24” 112

Table 30. UTCI performance differences between optimization scenarios on “C25” 113

Table 31. UTCI performance differences between optimization scenarios on “C26” 115

Table 32. UTCI performance differences between optimization scenarios on “C27” 117

Table 33. UTCI performance differences between optimization scenarios on “C28” 118

Table 34. UTCI performance differences between optimization scenarios on “C29” 120

Table 35. UTCI performance differences between optimization scenarios on “C30” 121

Table 36. UTCI performance differences between optimization scenarios on “C29” 122

Table 37. UTCI performance differences between optimization scenarios on “C31” 124

Table 38. UTCI performance differences between optimization scenarios on “C32” 126

Table 39. UTCI performance differences between optimization scenarios on “C33” 127

Table 40. UTCI performance differences between both optimization 131

LIST OF FIGURES

Figure 1. Methodology framework of the research 20

Figure 2. Tirana’s annual temperatures 22

Figure 3. Site location 23

Figure 4. Mangalem 21 urban area site 24

Figure 5. Mangalem 21's outdoor areas/ courtyards 25

Figure 6. Illustrates the site buildings, and the cell like structure of the model..... 36

Figure 7. Illustrates the site python script used to obtain average values within courtyards..... 39

Figure 8. UTCI thermal stress categorization 40

Figure 9. Graphical illustration of UTCI performance of Courtyard 01..... 41

Figure 10. Graphical illustration of UTCI performance of Courtyard 02..... 42

Figure 11. Graphical illustration of UTCI performance of Courtyard 03..... 43

Figure 12. Graphical illustration of UTCI performance of Courtyard 04..... 44

Figure 13. Graphical illustration of UTCI performance of Courtyard 05..... 44

Figure 14. Graphical illustration of UTCI performance of Courtyard 06..... 45

Figure 15. Graphical illustration of UTCI performance of Courtyard 07..... 46

Figure 16. Graphical illustration of UTCI performance of Courtyard 08..... 47

Figure 17. Graphical illustration of UTCI performance of Courtyard 09..... 48

Figure 18. Graphical illustration of UTCI performance of Courtyard 10..... 49

Figure 19. Graphical illustration of UTCI performance of Courtyard 11..... 50

Figure 20. Graphical illustration of UTCI performance of Courtyard 12..... 51

Figure 21. Graphical illustration of UTCI performance of Courtyard 13..... 52

Figure 22. Graphical illustration of UTCI performance of Courtyard 14..... 53

Figure 23. Graphical illustration of UTCI performance of Courtyard 15 54

Figure 24. Graphical illustration of UTCI performance of Courtyard 16 55

Figure 25. Graphical illustration of UTCI performance of Courtyard 17 56

Figure 26. Graphical illustration of UTCI performance of Courtyard 18 57

Figure 27. Graphical illustration of UTCI performance of Courtyard 19 58

Figure 28. Graphical illustration of UTCI performance of Courtyard 20 58

Figure 29. Graphical illustration of UTCI performance of Courtyard 21 59

Figure 30. Graphical illustration of UTCI performance of Courtyard 22 60

Figure 31. Graphical illustration of UTCI performance of Courtyard 23 61

Figure 32. Graphical illustration of UTCI performance of Courtyard 24 62

Figure 33. Graphical illustration of UTCI performance of Courtyard 25 63

Figure 34. Graphical illustration of UTCI performance of Courtyard 26 64

Figure 35. Graphical illustration of UTCI performance of Courtyard 27 65

Figure 36. Graphical illustration of UTCI performance of Courtyard 28 66

Figure 37. Graphical illustration of UTCI performance of Courtyard 29 66

Figure 38. Graphical illustration of UTCI performance of Courtyard 30 67

Figure 39. Graphical illustration of UTCI performance of Courtyard 31 68

Figure 40. Graphical illustration of UTCI performance of Courtyard 32 69

Figure 41. Graphical illustration of UTCI performance of Courtyard 33 70

Figure 42. Graphical illustration of max UTCI performance of all courtyards 71

Figure 43. Graphical illustration of surface area morphological indicator 72

Figure 44. Graphical illustration of courtyard width over length morphological indicator..... 72

Figure 45.Graphical illustration of courtyard façade area morphological indicator ... 73

Figure 46. Graphical illustration of courtyard average depth morphological indicator 74

Figure 47. Graphical illustration of courtyard façade area over site area morphological indicator..... 75

Figure 48. Graphical illustration of max. UTCI performance of all courtyards 76

Figure 49. Graphical illustration of average UTCI performance of all courtyards..... 76

Figure 50. Graphical illustration of optimization scenarios..... 77

Figure 51. Graphical illustration of optimization UTCI performance of "C01"\..... 79

Figure 52. Graphical illustration of optimization UTCI performance of "C02"..... 80

Figure 53. Graphical illustration of optimization UTCI performance of "C03"..... 82

Figure 54. Graphical illustration of optimization UTCI performance of "C04"..... 83

Figure 55. Graphical illustration of optimization UTCI performance of "C05"..... 85

Figure 56. Graphical illustration of optimization UTCI performance of "C06"..... 86

Figure 57. Graphical illustration of optimization UTCI performance of "C07"..... 88

Figure 58. Graphical illustration of optimization UTCI performance of "C08"..... 89

Figure 59. Graphical illustration of optimization UTCI performance of "C09"..... 91

Figure 60. Graphical illustration of optimization UTCI performance of "C10"..... 92

Figure 61. Graphical illustration of optimization UTCI performance of "C10"..... 94

Figure 62. Graphical illustration of optimization UTCI performance of "C12"..... 95

Figure 63. Graphical illustration of optimization UTCI performance of “C13”..... 97

Figure 64. Graphical illustration of optimization UTCI performance of “C14”..... 98

Figure 65. Graphical illustration of optimization UTCI performance of “C15”..... 100

Figure 66. Graphical illustration of optimization UTCI performance of “C16”..... 101

Figure 67. Graphical illustration of optimization UTCI performance of “C17”..... 103

Figure 68. Graphical illustration of optimization UTCI performance of “C18”..... 104

Figure 69. Graphical illustration of optimization UTCI performance of “C19”..... 106

Figure 70. Graphical illustration of optimization UTCI performance of “C20”..... 107

Figure 71. Graphical illustration of optimization UTCI performance of “C21”..... 109

Figure 72. Graphical illustration of optimization UTCI performance of “C22”..... 110

Figure 73. Graphical illustration of optimization UTCI performance of “C23”..... 112

Figure 74. Graphical illustration of optimization UTCI performance of “C24”..... 113

Figure 75. Graphical illustration of optimization UTCI performance of “C25”..... 114

Figure 76. Graphical illustration of optimization UTCI performance of “C26”..... 116

Figure 77. Graphical illustration of optimization UTCI performance of “C27”..... 117

Figure 78. Graphical illustration of optimization UTCI performance of “C28”..... 119

Figure 79. Graphical illustration of optimization UTCI performance of “C29”..... 120

Figure 80. Graphical illustration of optimization UTCI performance of “C30”..... 122

Figure 81. Graphical illustration of optimization UTCI performance of “C29”..... 123

Figure 82. Graphical illustration of optimization UTCI performance of “C31”..... 125

Figure 83. Graphical illustration of optimization UTCI performance of “C32”..... 126

Figure 84. Graphical illustration of optimization UTCI performance of "C33"..... 128

Figure 85. Graphical illustration of max. UTCI performance of all scenarios 129

Figure 86. Graphical illustration of avg. UTCI performance of all scenarios 130

Figure 87. Potential air temperature map for s1 base at 14:00..... 138

Figure 88. Mean radiant temperature map for s1 base at 14:00..... 138

Figure 89. Wind speed map for s1 base at 14:00 139

Figure 90. Relative humidity map for s1 base at 14:00 139

Figure 91. Potential air temperature map for s3 green roof at 14:00 140

Figure 92. Mean radiant temperature map for s3 green roof at 14:00 140

Figure 93. Mean radiant temperature map for s3 green roof at 14:00 141

Figure 94. Potential air temperature map for s2 green facade at 14:00 141

Figure 95. Mean radiant temperature map for s2 green façade at 14:00..... 142

Figure 96. Relative humidity map for s2 green facade at 14:00 142

Figure 97. UTCI base model at 14:00..... 143

Figure 98. UTCI green roof model at 14:00..... 143

Figure 99. UTCI green façade model at 14:00..... 144

Figure 100. Courtyard 3D mesh illustration 144

Figure 101. Courtyard 3D mesh illustration 145

Figure 102. Courtyard 3D wind movement illustration..... 145

CHAPTER 1

INTRODUCTION

1.1 Overview

The issue of population density in urban areas has been a subject of significant concern in urban planning since the mid-20th century, and its importance has continued to grow over time. Urbanization witnessed a notable upsurge between 1990 and 2015, with the proportion of individuals residing in urban areas rising from 43% to 54%. It is projected that there will be a sustained increase, with a potential attainment of 80% by the year 2050. The significant influx of individuals towards urban areas has occurred due to various factors and has emerged as a crucial determinant in the formation of cities (Al-Kodmany & Ali, 2018). The number of megacities, defined as cities with a population exceeding 10,000, has also witnessed a notable surge. In 1990, the number of cities falling under this category was limited to one, whereas it is projected that by 2025, the count will increase to approximately 30. The proliferation of megacities globally is a matter of concern, particularly in light of projections indicating that their populace may escalate from 30,000 to 50,000, owing to an annual increase of 80 million individuals in the global population (Al-Kodmany & Ali, 2013).

The rapid expansion of cities vertically and horizontally has led to a vast number of issues impacting human life. Some of these issues are directly correlated with the built environments thermal performance. Even though major advancements have been made in the field of building energy and thermal comfort in building scale but on the other hand very little to no assessments have been made on large scale regarding outdoor human comfort.

1.2 Motivation & Background

According to the United Nations, one of the primary concerns of the built environment, particularly in vast urban fabrics, is energy poverty. Many individuals are deprived of energy and encounter difficulty in maintaining a sufficient degree of thermal comfort in their homes as energy expenses rise and energy services become inaccessible. Furthermore, energy poverty contributes to additional problems such as poor air quality, a lack of essential amenities, and socioeconomic inequities. As a result, addressing energy poverty is critical in order to enhance quality of life and reduce energy consumption in urban areas.

A number of studies have been conducted to examine the Balkan Peninsula's energy poverty, a region that has been severely afflicted by the issue. These studies have centered on residential building energy efficiency, energy poverty indicators, and the impact of energy poverty on daily life. According to a study conducted in Albania, energy poverty is a major issue, with nearly 70% of families having difficulty sustaining appropriate thermal comfort. Additionally, the study found that energy poverty is particularly widespread in rural areas and among low-income households. Overall, these studies indicate that addressing energy poverty in the region is critical to provide access to energy services and enhance the thermal comfort performance of large urban fabrics.

Addressing global environmental control issues is imperative for humanity. Our impact on the environment has risen significantly as the world's population has grown and our technical power has increased. Climate change, biodiversity loss, and poor-quality urban living conditions are all serious environmental issues that must be addressed to preserve a sustainable and healthy environment for future generations.

Sustainable urban design and performance-based design are essential for a variety of reasons, both on a global scale and within regional and national scales. Worldwide, the built environment has a tremendous impact with regard to the environment and the well-being of urban residents. The building and design of cities has the capacity to contribute to or alleviate environmental and social issues, such as climate change, air pollution, and socioeconomic inequality.

There is great emphasis on sustainability in the built environment in Europe. The European Union has put initiatives in place to encourage sustainable building

techniques, such as the Energy Performance of Buildings Directive (EPBD) and the Nearly Zero Energy Buildings (NZEB) criteria. These regulations establish criteria for building energy efficiency and promote the use of renewable energy sources.

The Balkans peninsula is also promoting sustainability in the built environment. Nations such as Serbia and Bosnia and Herzegovina have enacted national building codes that specify norms for energy efficiency and the use of renewable energy in buildings. Furthermore, several Balkan cities, including Belgrade and Sarajevo, have developed measures to improve the sustainability of the built environment including the use of sustainable materials, the promotion of green spaces, and the implementation of energy-efficient building technologies.

Another notable project in the promotion of sustainability in the built environment is the European Union's taxonomy. The taxonomy is a categorization system that seeks to provide a uniform and transparent framework for assessing the environmental performance of economic activities such as building construction and operation. The taxonomy comprises criteria for assessing the environmental implications of various operations and serves as a reference for investors and policymakers interested in promoting sustainable practices.

Overall, sustainable urban design and performance-based design are critical for tackling an array of environmental and socioeconomic challenges. It is possible to design cities that are livable and sustainable by considering the influence of the built environment on the environment and the well-being of people. The European Union's taxonomy is a significant endeavor in this area, offering a framework for evaluating the environmental performance of economic activities and supporting sustainable practices in the built environment.

Environmental control becomes considerably more crucial on a city scale. Cities are getting more densely inhabited as urbanization progresses, and their environmental challenges are becoming increasingly complex. Because of high levels of energy consumption and air pollution, urban heat islands are turning into a major concern in many cities. Mitigating techniques, such as increasing vegetation cover, planting street trees and green roofs, along with creating urban wetlands, have been proposed to solve this issue. Furthermore, built infrastructure such as cool pavements, reflective or cool roofs, and smart development can decrease energy use while simultaneously improving

air quality. These measures have been proven in scientific studies and articles to lower air temperature by up to 3-7°C in some instances, as well as reduce energy usage, enhance air quality, and minimize storm-water runoff.

Additionally, thermal comfort, both indoor and outdoor, is an important factor in urban environments. Buildings should be designed and constructed considering energy efficiency to maintain sufficient thermal comfort. Ventilation, insulation, and shading are all critical components of energy-efficient buildings because they minimize the amount of energy required for heating and cooling while also improving interior air quality. Cities may create healthier and sustainable environments for their residents by implementing these measures.

On the other hand, energy efficiency is a key component of both urban scale optimization and performance-based design. Energy-efficient buildings and urban areas can assist in decreasing the city's overall energy consumption, resulting in financial savings for inhabitants and companies as well as a reduction in the urban area's carbon footprint.

A comprehensive approach to large-scale urban fabric performance has been utilized in only a few instances (Abdollahzadeh & Biloria, 2022), and no research has addressed these concerns with the complete inclusion of impactful factors. This study was driven by a void in comprehensive scientific research.

1.3 Thesis objective

There is a void in the research about the effects of particular climatic settings on energy and thermal performance, despite the fact that building envelope materials and greenery are significant contributors to building energy performance and human and thermal comfort. As a result, the current study intends to determine the climatic effect on the early energy evaluation of the morphology of residential structures in the twenty-first century in Southeastern Europe, an area with a high degree of climatic variability. Through simulations, the influence of building morphology and vegetation on thermal outdoor comfort may be assessed and utilized as parameters and design guides for both new and existing homes in Southeast Europe and in places with climate patterns

comparable to those in the study region. Both better thermal comfort for the residents and financial gains for the local governments or private organizations are guaranteed.

1.4 Organization of the thesis

The structure of this thesis is organized into 6 chapters. The introduction, overview, and objective of the thesis are presented in the first chapter. In the second chapter, the literature review and studies related to this paper are presented. Chapter 3 presents the method used to conduct the study. In the fourth chapter, the results are illustrated and then discussed. The fifth chapter consists of optimizations and comparisons. Conclusions and references are immersed in the final sixth chapter.

CHAPTER 2

LITERATURE REVIEW

2.1 Theoretical background

2.1.1. Environmental comfort

Environmental comfort is a critical component of residential building design and construction. Indoor environmental parameters like temperature, humidity, and air quality can have considerable impact on inhabitants' health and productivity, according to a study published in the journal "Building and Environment" (Jia et al., 2022). A different study, published in "Indoor Air" (Fisk, 2018) indicated that poor indoor air quality might cause a plethora of health problems, including headaches and respiratory issues.

Furthermore, according to a study published in "Energy Reports" (Zoure & Genovese, 2023), natural ventilation can be an efficient technique to enhance indoor air quality while reducing the demand for mechanical heating and cooling systems. Green roofs can also assist in minimizing the urban heat island effect and increase thermal comfort in residential buildings, according to a study published in "Building and Environment " (Wang et al., 2022) Shading devices can also aid in the reduction of solar heat gain and boost thermal comfort in residential buildings. (Diz-Mellado et al., 2023)

These studies show the significance of incorporating indoor environmental factors in the design and construction of residential buildings to better occupants' health and productivity.

2.1.2. Courtyards

Courtyards have displayed a considerable impact on the energy consumption, human comfort, and thermal comfort of residential buildings. According to a study

published in "Frontiers of Architectural Research" (Tabadkani et al., 2022), courtyards can help minimize solar heat gain, resulting in reduced consumption of energy for cooling. Another research indicated that courtyards can assist in promoting natural ventilation in residential buildings, reducing energy consumption, and improving indoor air quality. (Zhu et al., 2023)

In addition, according to a study published in "Sustainable Cities and Society" (Lizana et al., 2022), courtyards can assist in increasing thermal comfort by providing shade and minimizing the urban heat island effect. The overall thermal comfort of the indoor environment can also be increased by courtyards. Courtyard oriented design contributes to higher levels of indoor and outdoor human comfort. (Leng et al., 2020)Lastly, by promoting passive solar design and minimizing the need for mechanical heating and cooling systems, courtyards can also reduce energy consumption. (Diz-Mellado et al., 2023)

Ultimately, these studies show that courtyards can have a considerable influence on the energy usage, human comfort, and thermal comfort of residential buildings. Courtyards can assist in energy use reduction by encouraging natural ventilation, lowering solar heat gain, and promoting passive solar design. They can also increase thermal comfort by shading and minimizing the urban heat island effect. Furthermore, by offering visual and auditory ties to nature, courtyards can promote human comfort. According to the studies, incorporating courtyards into the design of residential buildings can serve as a method to increase energy efficiency and the quality of the indoor environment.

2.1.3. Albedo materials

The usage of albedo materials in residential urban areas may have significant effects on residential building energy consumption and thermal comfort. According to a study published in "Sustainable Cities and Energy" (Lopez-Cabeza et al., 2022), using high albedo materials can minimize solar heat gain, resulting in reduced energy consumption for cooling. Another research published in "Solar Energy" (Enríquez et al., 2017) indicated that using albedo materials can lessen the urban heat island effect, improving thermal comfort in residential structures. A study published in

“Energy and Buildings” concluded that the utilization of albedo materials can assist in lowering pollutants in the air and increasing indoor air quality. (Taha et al., 1997)

These research findings illustrate that the usage of albedo materials in residential urban areas may result in significant impacts on residential building energy consumption and thermal comfort. Albedo materials can minimize solar heat gain, the urban heat island effect, and increase indoor air quality, all of which can reduce energy consumption and increase thermal comfort. The research implies that using albedo materials could create a more sustainable environment and boost community well-being.

2.1.4. Greenery usage in urban scale

The incorporation of various forms of greenery into urban residential blocks can have a substantial influence on energy consumption and outdoor-indoor thermal comfort. According to a study published in the journal "Energy and Buildings" (Vox et al., 2022), the use of vegetation and trees can help minimize solar heat gain, resulting in lower energy usage for cooling. A second study published in "Applied Thermal Engineering" (Mazzeo et al., 2022) indicated that using green roofs can help minimize the urban heat island effect, improving thermal comfort in residential buildings.

Moreover, according to a study published in "Urban Forestry & Urban Greenery" (Ysebaert et al., 2021), the usage of green walls can enhance indoor air quality by decreasing pollutants and increasing the amount of fresh air . Lastly, the use of different kinds of greenery lowers the energy consumption of residential buildings, notably in terms of heating and cooling. (Seyam, 2019)

These studies show that incorporating various forms of greenery into urban residential blocks can have significant positive impacts on energy usage and outdoor-indoor thermal comfort. The use of trees, green roofs, green walls, and other vegetation can aid in the reduction of solar heat gain, the reduction of the urban heat island effect, the improvement of indoor air quality, and the promotion of a more sustainable environment. Furthermore, the research show that using vegetation in urban residential blocks also promotes community well-being.

2.1.5. UTCI

The Universal Thermal Climate Index (UTCI) is a key instrument for assessing thermal comfort and forecasting thermal stress. According to the scientific literature, the UTCI has its origins from an approach proposed over 15 years ago by the International Society of Biometeorology (ISB) Commission (Zare et al., 2018), and has since been recognized as a standard for monitoring thermal stress in the European Union (ISO 7933:2004).The UTCI is a complete thermal condition indicator that takes into account the combined influence of air temperature, humidity, wind speed, and radiation as well as physiological data such as skin and core temperature, garment insulation, and metabolic rate (Jendritzky et al., 2011). This indicator is critical in the design and optimization of building and urban area performance, particularly in the context of climate change.

Prior to the establishment of the UTCI, other indices such as the Predicted Mean Vote (PMV) or the Physiological Equivalent Temperature (PET) were routinely employed for measuring thermal comfort. However, these indices fail to account for the effect of radiation, which can have a substantial impact on thermal sensation and stress. Furthermore, they fail to account for individual physiologic responses, which might result in varied amounts of thermal stress for individuals exposed to comparable environmental conditions.

Several studies have shown the value of including UTCI in the design and planning of buildings and urban areas. (Gómez et al., 2018), for example, demonstrated how the UTCI may be utilized to optimize the design of outdoor areas such as pedestrian zones or public squares through incorporating shade and cooling elements.

The UTCI is a vital instrument for analyzing thermal stress and enhancing building and urban design. Its introduction has greatly enhanced the understanding of thermal comfort and stress, and its use in design can result in more sustainable and comfortable environments.

$$UTCI = f(Ta, Vs, VP, Tmrt\text{-}Ta) + Ta$$

2.2 Previously related studies

Scientific literature has been assessed in order to establish a more accurate predictive framework for early design performance evaluations of large scale residential urban fabrics.

2.2.1. “Studying impact of infrastructure development on urban microclimate: Integrated multiparameter analysis using Open-FOAM”

This study adopts a compelling and meticulous method to analyzing the influence of infrastructure development on urban microclimates. The authors conducted comprehensive multiparameter research of the microclimate changes produced by infrastructure development using a numerical simulation tool (OpenFOAM). The study's findings are noteworthy as they provide important insights into the complicated links between urban infrastructure and microclimate. The authors proved the capability of modeling microclimate changes using the simulation capabilities of OpenFOAM and identified many important factors that impact microclimate in urban areas. The findings reveal that infrastructure development can influence air temperature, relative humidity, and wind velocity, as well as the urban heat island effect. The simplistic portrayal of urban geometry and the simulation's restricted scope are two of the study's limitations. The authors also highlighted the necessity for additional confirmation of the findings through field measurements.

2.2.2. “Assessing the impact of urban microclimate on building energy demand by coupling CFD and building performance simulation”

This study presents a novel technique to assessing the influence of urban microclimate on building energy consumption. The authors investigated the association between urban microclimate and building energy consumption using a combined technique of Computational Fluid Dynamics (CFD) and building performance simulation.

The findings of this study are notable as they offer significant insight into the complex links between urban microclimate and building energy consumption. The

authors have shown that the coupled technique is successful in properly predicting building energy demand and have identified numerous key variables that impact building energy demand in urban areas. The findings indicate that the urban microclimate has a substantial influence on building energy demand and that the building envelope and HVAC systems are critical in managing building energy demand.

The study's limitations include the reduced representation of urban morphology and building parameters, as well as the simulation's limited scope. The authors highlight the necessity for additional confirmation of the findings through field measurements.

2.2.3. "Detailed investigation of vegetation effects on microclimate by means of computational fluid dynamics (CFD) in a tropical urban environment"

In this thorough study the authors examine how greenery affects the microclimate in tropical urban areas using simulations of the environment both with and without greenery to measure its impact. The authors employed Computational Fluid Dynamics (CFD) for analysis.

This study's findings are noteworthy and give important insights into the function of greenery in determining the microclimate of tropical urban areas. The authors established the viability of utilizing CFD to simulate microclimate and greenery impacts, as well as identifying multiple important variables that influence microclimate in tropical urban areas. The findings indicate that vegetation has a considerable impact on air temperature, relative humidity, and wind velocity, as well as the urban heat island effect.

The simplified portrayal of urban geometry and vegetation factors, as well as the simulation's limited scope, are some of the study's limitations. The authors also highlight the necessity for additional confirmation of the findings through field measurements.

2.2.4. “Urban microclimate and energy consumption: A multi-objective parametric urban design approach for dense subtropical cities”

This study delivers a new angle of the relationship between urban microclimate and energy consumption in dense subtropical cities. The authors present a multi-objective parametric urban design technique that optimizes urban design based on the trade-off between microclimate and energy consumption.

The results of this research is ground-breaking as they offer important insights into the relationship between urban microclimate and energy consumption. The authors proved the efficacy of the multi-objective parametric urban design approach in optimizing urban design based on a trade-off between microclimate and energy usage. The findings reveal that urban design has a considerable impact on the microclimate and energy consumption of dense subtropical cities, and that an optimal urban design may efficiently manage the trade-off between the two objectives.

The simplified portrayal of urban geometry and the simulation's limited scope, are two of the study's limitations.

2.2.5. “Impact of urban morphology on urban microclimate and building energy loads.”

This study provides a thorough examination of the effects of urban morphology on urban microclimate and building energy loads. The authors assessed the influence of urban morphology on microclimate and building energy loads using computational fluid dynamics (CFD) simulations.

The authors have shown that CFD models may be used to examine the impact of urban morphology on microclimate and building energy loads, and they have identified many crucial elements that influence these interactions. The authors of this study stated the following parameters:

Building height and density: Building height and density may influence wind patterns and shading effects in the urban environment, affecting the microclimate and building energy loads.

Building orientation: The orientation of a building may alter the quantity of solar radiation it receives, which affects its energy loads.

Street geometry: The geometry of the street network, including street width and intersection design, can influence wind patterns and air movement in the urban environment, hence influencing microclimate and building energy loads.

Vegetation: The presence of greenery in the urban area may influence microclimate through shading, cooling, and affecting wind patterns, which in turn influences building energy loads.

Land use patterns: The distribution of residential, commercial, and industrial areas, for example, can have an influence on the microclimate and building energy loads in the urban environment.

However, there are certain limitations that must be recognized. To begin, the simulations' portrayal of urban geometry is simplified, which may impair the accuracy of the results. The simplified depiction of urban morphology may result in an oversimplification of the complexity of real-world urban environments, which may have an influence on the conclusions validity. Also, the simulation scope limits the generalizability of the results. To validate the findings, larger-scale investigations and more advanced models are required.

Furthermore, the authors emphasized the necessity for additional confirmation of the data using field measurements. To verify the correctness and validity of the results, CFD simulation results should be confirmed using real-world measurements.

2.2.6. "Analyzing impacts of urban morphological variables and density on outdoor microclimate for tropical cities: A review and a framework proposal for future research directions."

This paper provides a thorough examination of the effects of urban morphological variables and density on outdoor microclimate in tropical cities. The authors reviewed previous research and found critical elements that determine the link between urban morphological variables, density, and outdoor microclimate in tropical cities.

This study's findings are important for comprehending the intricacies of the interactions between urban morphological variables, density, and outdoor microclimate in tropical cities. The authors have provided a framework for future study that will examine particular urban morphological variables and their influence on outdoor microclimate in tropical cities.

The limitations of this study include the limited scope of the literature review to studies conducted in tropical cities, which may limit the generalizability of the results to other regions. Furthermore, the authors do not consider the influence of other critical factors, such as vegetation and land use patterns, on outdoor microclimate in tropical cities.

Ultimately, the authors have supplied useful information about the effects of urban morphological variables and density on outdoor microclimate in tropical cities. The approach established for future research provides a foundation for future studies that might expand on the current study's results and address its limitations. Researchers and urban planners are encouraged to explore the suggested framework and concentrate on specific urban morphological variables and their influence on outdoor microclimate in tropical cities.

2.2.7. "Impact of reflective materials on urban canyon albedo, outdoor and indoor microclimates."

The paper examines the effect of reflective materials on urban canyon albedo and urban microclimate by using numerical simulations. The findings suggest that using reflective materials in urban canyons may significantly increase albedo, reducing the urban heat island effect and improving the overall microclimate.

This study, however, has many limitations. The simulations employed idealized conditions that may not adequately reflect the intricacies of real-world urban areas. The authors also did not take into account the influence of different seasons or times of day, which might have a substantial impact on the results.

The study offers insight into the effects of reflective materials on urban canyon albedo and microclimate. The findings imply that using reflective materials might significantly enhance the microclimate of urban areas. Further study, however, is

required to better understand the intricacies of the interactions between reflecting materials, albedo, and microclimate in real-world urban environments.

2.2.8. “Assessing local heat stress and air quality with the use of remote sensing and pedestrian perception in urban microclimate simulations”

The influence of urban microclimate on local heat stress and air quality is examined in this study. The authors measure the microclimate in urban environments using a mix of remote sensing data and pedestrian perception.

The study's findings provided insight into the connections between urban microclimate, heat stress, and air quality. The study's utilization of remote sensing and pedestrian perception data allowed for a more complete comprehension of urban microclimates. The findings indicate that urban microclimate has a considerable influence on local heat stress and air quality, emphasizing the necessity of taking these elements into account when planning and designing cities.

However, the study has certain limitations. The authors simulated the microclimate using a simplified model, which may not adequately depict the complex interactions between the environment, buildings, and people in real-world urban contexts. Furthermore, the utilization of remote sensing and pedestrian perception data may be prone to measurement error and biases, affecting the accuracy of the results.

The authors present an approach for future studies to expand on the current study's findings and address its limitations. To fully comprehend the intricacies of the connections between urban microclimate, heat stress, and air quality in real-world urban environments additional research is required.

2.2.9. “Microclimate and human comfort considerations in planning a historic urban quarter”

The influence of urban microclimate on human comfort in a historic urban quarter is examined in this research. The authors provide a case study of a specific urban quarter, assessing the microclimate and its impact on human comfort through the use of several environmental factors such as temperature, wind, and sun radiation.

The study's findings highlight the significance of addressing microclimate in the planning and design of historic urban districts. The findings imply that microclimate has a substantial impact on human comfort in these environments, emphasizing the need of considering microclimate while preserving and revitalizing historic urban districts.

However, the study had limitations. The authors concentrated on a single case study, which may not adequately reflect the complexities of microclimate in other historic urban districts. Furthermore, the study relied on numerical models, which may not accurately represent the real-world microclimate and its impact on human comfort in historic urban districts.

The study highlights the significance of addressing microclimate in the planning and design of historic urban districts. The authors have offered an approach for future studies to expand on the current study's findings and address its limitations. Additional research is needed to fully comprehend the complexity of microclimate and its influence on human comfort in historic urban districts.

2.2.11. "Urban building energy and microclimate modeling – From 3D city generation to dynamic simulations."

This paper examines the link between urban building energy consumption and microclimate, as well as provides a methodology for modeling the intricate interplay between these factors. The authors investigate the impact of several 3D city models, as well as the use of dynamic simulations, on urban microclimate and consumption of energy.

The study provides a comprehensive assessment of prior research on the subject, emphasizing the limits and constraints of traditional building energy and microclimate models. To provide a more accurate and thorough assessment of urban microclimate and energy consumption, the authors present a novel technique that blends 3D city models, dynamic simulations, and building energy consumption models.

The study's findings indicate that the suggested framework may offer useful insights into the link between urban building energy consumption and microclimate, which can help guide urban planning and design decisions. The research also emphasizes the need of considering the dynamic character of urban landscapes, as well

as the need for multidisciplinary methods that incorporate numerous models and simulations.

However, the study's scope is restricted, and the findings need be confirmed in real-world case studies. Furthermore, the authors did not particularly address data collection and processing challenges, which may be a significant restriction in large-scale urban modeling and simulation initiatives.

The authors propose an effective framework for modeling urban building energy and microclimate that takes the intricacies and dynamics of urban environments into consideration. Future research should, however, focus on confirming the findings in real-world case studies and navigating data collection and processing challenges.

2.2.12. "Experimental Study of Urban Microclimate on Scaled Street Canyons with Various Aspect Ratios."

This study examines the link between urban microclimate and street canyon aspect ratios. A physical scale model was utilized in the study to examine the effects of aspect ratio on outdoor microclimate variables such as air temperature, relative humidity, and air velocity.

According to the study, street canyon aspect ratios have significant impacts on urban microclimate, with higher aspect ratios resulting in greater air temperatures, lower relative humidity, and higher air velocity. These findings emphasize the need of including aspect ratios into urban planning in order to improve outdoor microclimate conditions.

The use of a small-scale physical model, which may not adequately depict the entire spectrum of complexity and interactions in real-world urban environments, is one of the study's limitations. Furthermore, the study examined only a restricted set of microclimate variables and ignored additional factors that might influence urban microclimate, such as urban heat island effects and human activity.

The study offers important insights into the impact of street canyon aspect ratios on urban microclimate and emphasizes the need for additional research to better understand the intricate interplay between urban design and microclimate. Future

research should examine additional microclimate variables and apply the findings to real-world urban contexts, according to the authors.

2.3 Aim and Originality

The studies listed above show that there is a link between the morphology of urban settlements and regional microclimate conditions, as well as the amount of energy utilized. However, a study of various optimization scenarios and large scale outdoor urban performance would be a valuable addition to the existing information. The gaps in the literature that this topic covers are detailed below.

There have been no previous studies that have simulated different models of optimization within the same built environment morphological scene.

To date, there has been no scholarly investigation conducted on outdoor spaces of significant scale in residential areas that were designed in the early stages. Previous research, exemplified by Zhou et al. (2022), has conducted an examination and analysis of diverse neighborhoods with differing densities, built-to-unbuilt surface area, building heights, and other relevant factors. The study conducted by M et al. (2020) explores the effects of proposed morphology. However, rather than proposing alternative building shapes and arrangements, the study focuses on analyzing various H/W ratio factors. At the present time, there has been no academic study conducted on the effects of vertical or horizontal greenery in regions with a Mediterranean climate. There is a dearth of research on the effects of green facades on buildings in the Mediterranean climate, both in terms of morphology and on a larger scale. Consequently, the objective of this paper is to initiate a broader investigation into the assessment of early stage design, given the widespread adoption of greenery as a prevailing global phenomenon. The issue of population growth is a matter of global concern, and numerous urban studies have been conducted in countries that have been grappling with this challenge for a considerable period. In contrast, it is noteworthy that the issue of urban heat island effect has only emerged in developing nations like Albania and several Mediterranean climate countries in recent times. The primary objective of this research is to furnish planners with a comprehensive framework for selecting the optimal morphology layout and greening type that aligns with the specific climatic conditions prevalent in the region.

CHAPTER 3

METHODOLOGY

3.1 Overview

The microclimate and thermal comfort of a city are significantly impacted by high-rise constructions due to their nature. Given that these buildings have a significant influence on one another, their impact is significantly increased when taking into account whole communities containing these structures. This research's primary goal is to determine the effect of courtyard neighborhood morphology on outdoor thermal comfort. Figure 1 provides an illustration of the approach framework employed in this investigation. Selecting a residential urban area is the first stage in the procedure, after which it will be computer-modeled and simulated. The data will then be analyzed and evaluated in order to provide a set of recommendations for future planners on how to consider the impact of urban residential areas mixed with courtyard morphological designs on outdoor thermal comfort.

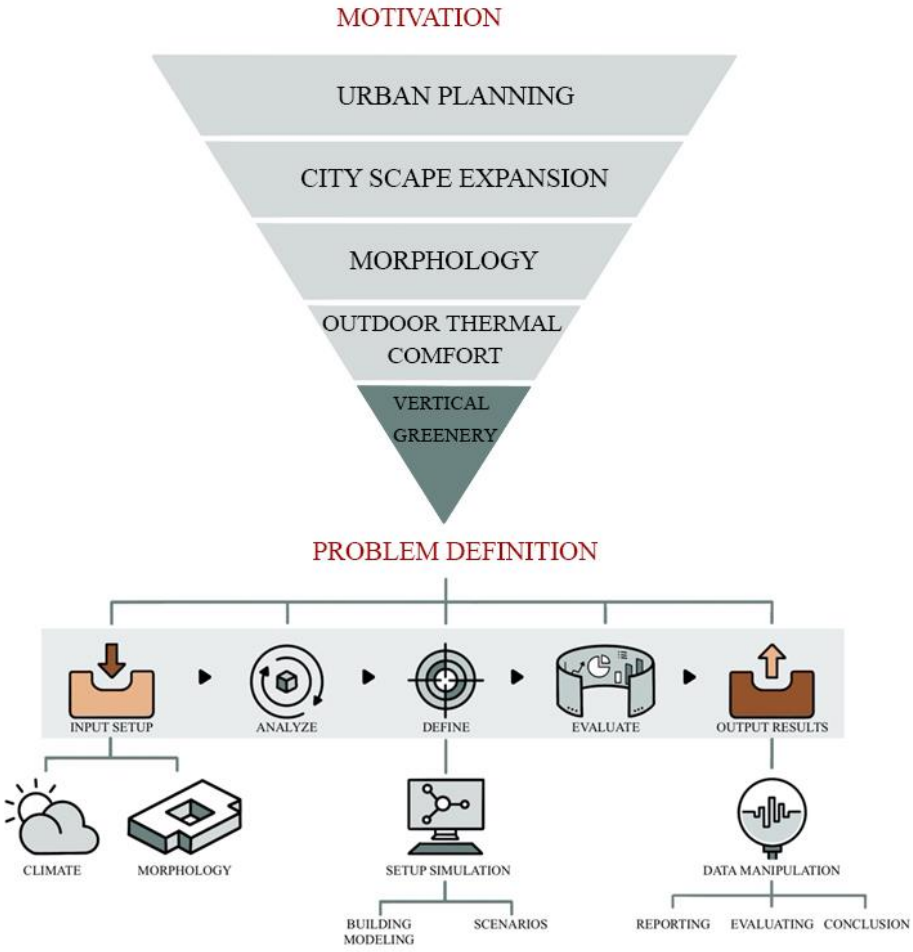

Figure 1. Methodology framework of the research

3.2 Climatic context

Comprehending the pivotal function of microclimate in the performance of buildings and the broader built environment is of utmost significance. The term microclimate pertains to the specific climatic conditions that are present in a restricted geographical region, such as a building or a city block. The environmental factors that can affect the well-being and satisfaction of individuals within a building may encompass variables such as temperature, humidity, wind, and other related conditions. The incorporation of microclimate analysis is a crucial aspect in the design of buildings and urban environments, as it plays a pivotal role in ensuring optimal levels of comfort, health, and energy efficiency.

The evaluation of thermal comfort in both outdoor and indoor environments can be effectively conducted by considering the correlation between microclimate and Universal Thermal Climate Index (UTCI). This correlation holds considerable significance in this regard. The Universal Thermal Climate Index (UTCI) is a comprehensive metric utilized for evaluating the effects of weather and environmental factors on the thermal comfort of human beings. The Unified Thermal Climate Index (UTCI) is utilized by architects and building designers to forecast and assess the thermal conditions in various microclimates by gauging the collective impact of air temperature, humidity, wind speed, and radiation on the human body. This data can be utilized to create architectural structures that offer maximum thermal satisfaction to inhabitants, while simultaneously curbing energy usage and mitigating ecological repercussions.

It is essential to comprehend microclimate and how it relates to UTCI when developing healthy and sustainable structures and urban settings. Architects and designers may construct pleasant, energy-efficient, and ecologically friendly buildings by taking into account microclimate considerations. Architects may also make sure that the structures they create will suit the demands of the people who will inhabit them, enhancing their quality of life and general wellbeing. This is done by employing UTCI to assess thermal comfort.

The capital of Albania, Tirana, has hot, dry summers and cold, rainy winters due to its Mediterranean climate. Compared to other coastal cities, the city is 110 meters above sea level, which results in milder temperatures and lower humidity (Pervazi, Krçiku, & Mahmutaj, 2021). The World Meteorological Organization reports that the average annual air temperature in Tirana is 16.2°C, with July being the hottest month and January being the coldest (World Meteorological Organization, n.d.). In the summer, temperatures may rise as high as 35°C, while in the winter, they can fall as low as 0°C.

Tirana's relative humidity is typically approximately 75%, with winter months seeing the greatest levels because of more precipitation (Krçiku, Pervazi, & Mahmutaj, 2021). The city gets 1,148 mm of precipitation on average every year, with July being the driest month with just 32 mm of precipitation and December being the wettest with 202 mm (World Meteorological Organization, n.d.).

A thermal inversion is produced by the city's valley position and mountainous surroundings, which may trap air pollutants and worsen the city's air quality (EPA, n.d.). In addition, because to its location in a seismic zone, the city is vulnerable to earthquakes. Buildings in Tirana need to be built to resist earthquakes since this might affect how well they conduct heat and how efficiently they use energy (Rugova & Brahaj, 2020).

In conclusion, Tirana's microclimate characteristics provide particular difficulties for urban designers and architects. In order to design structures and urban settings that are safe, pleasant, and sustainable, it is crucial to comprehend the numerical data relating to air temperature, humidity, precipitation, and seismic activity.

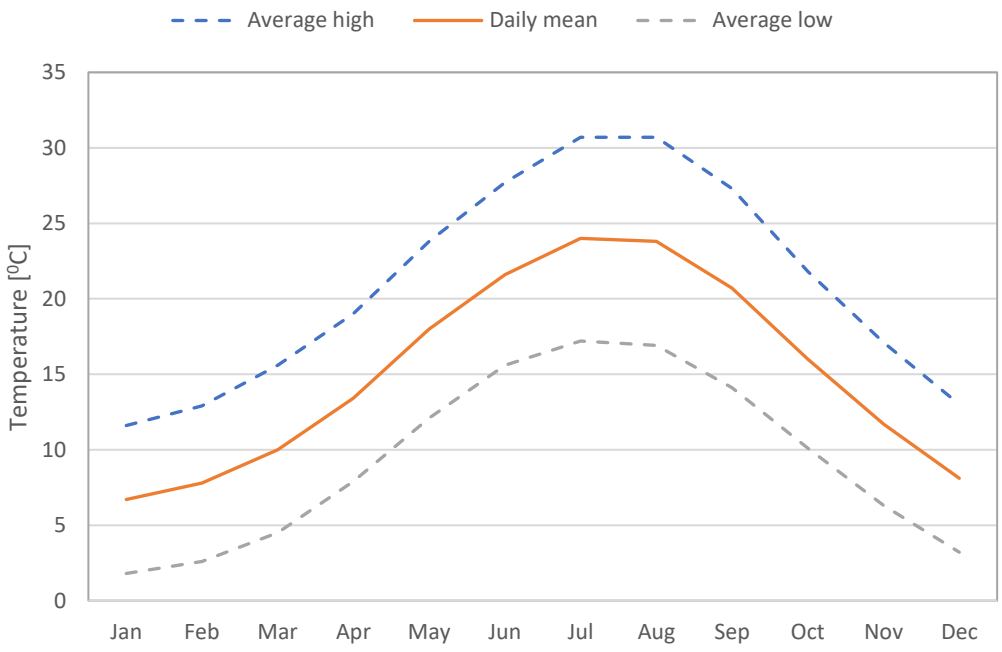

Figure 2. Tirana's annual temperatures

3.3 Case study selection

In order to perform any relevant analysis regarding urban thermal comfort and urban thermal performance the case study selection had to be performed in depth. During this phase a number of potential case studies came up but only the recently built, affordable residential, large urban fabric of "Mangalem 21" stood out.

3.3.1 Site selection

The chosen site is placed in a recently developed area of Tirana, Albania. The aim is to evaluate the effects of morphology, greenery, orientation, depth, and façade finishing of recently developed urban residential areas. To better understand the effects of the contributors above in the urban outdoor environment and their impact on Universal thermal comfort indicator.

Figure 3. Site location

3.3.2 Site description

Mangalem 21, designed by OMA Studio, is a mixed-use development located in the historic district of Mangalem in Tirana, Albania. The project was designed by the Dutch architect Rem Koolhaas and his team with the aim of creating a contemporary intervention within the historic fabric of the city while celebrating the area's rich cultural heritage. The design was inspired by the traditional architecture of the Mangalem district, which features narrow streets and closely-packed buildings.

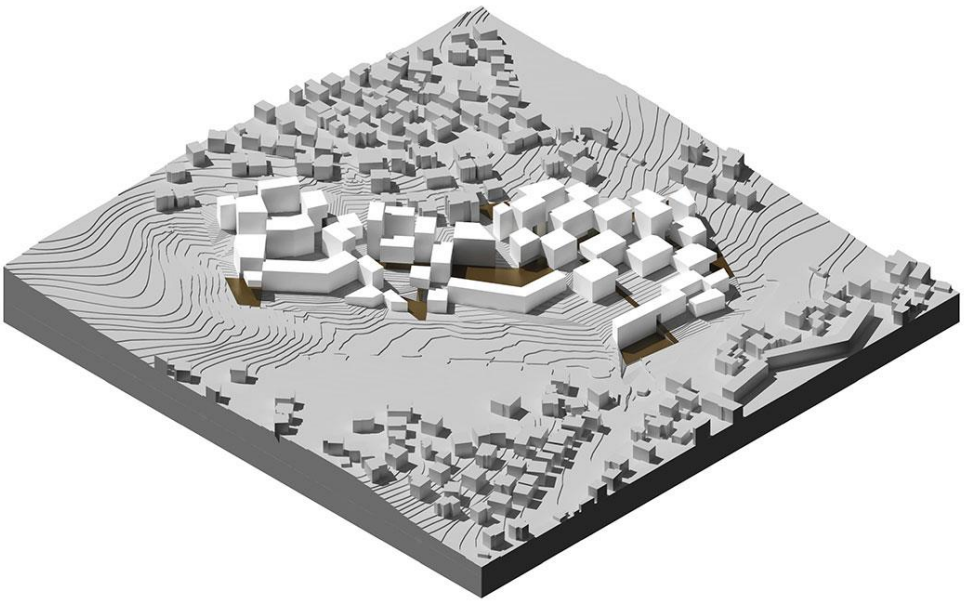

Figure 4. Mangalem 21 urban area site

The Mangalem 21 concept is described as a collection of several linked structures, each with an own personality, grouped around a number of core courtyards. The structures are designed to create outside areas. Residential units and certain commercial areas are included in the specified space division. The site's entire built-up area is more than 108,000 m2. This area is separated between a residential, retail/commercial, and an underground parking space. (Illustrated in *Table 1*.)

Table 1. Functional area distributions on site

Residential tot. area	**97601m²**
Commercial tot. area	**11084m²**
Underground parking tot. area	**10140m²**

The outdoor area of this site is vast and very diverse. Mangalem 21's outdoor area consists of thirty-three different courtyards as illustrated on *Figure 5*.

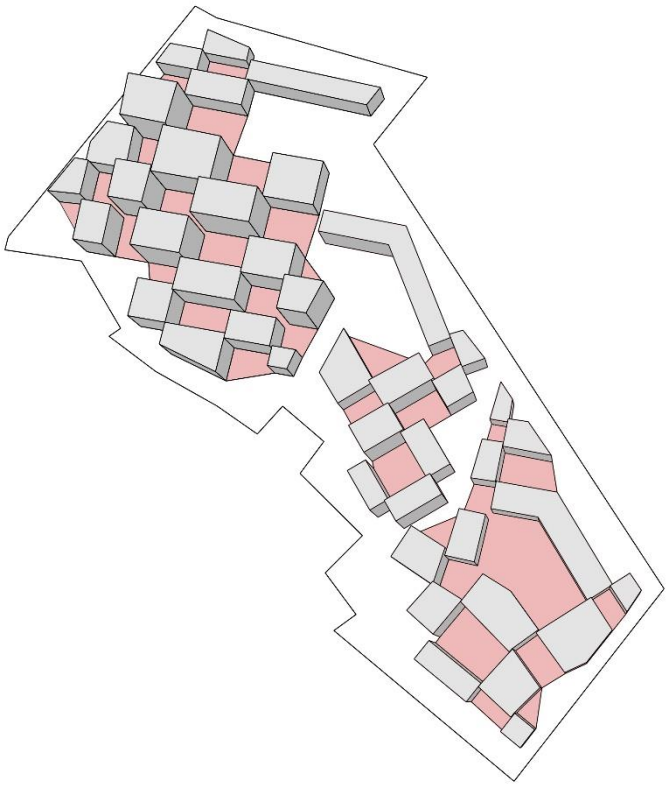

Figure 5. Mangalem 21's outdoor areas/ courtyards

These courtyards show a variety of differences in morphological indicators but the primary characteristic we have focused on when conducting the division of this

research is enclosure. The courtyards are divided into two tables as seen below where the enclosed courtyards are shown on *Table 2* and the non-enclosed one are shown on *Table 4.*

Table 2. Fully enclosed courtyard visualization (Plane, Axo, Section)

C01	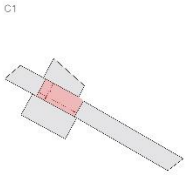	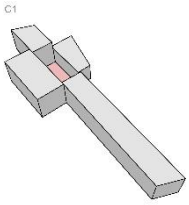	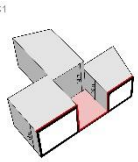
C04	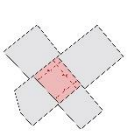	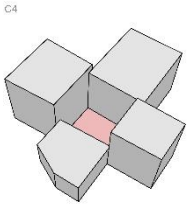	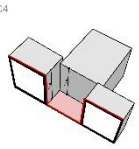
C06	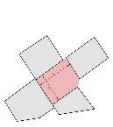	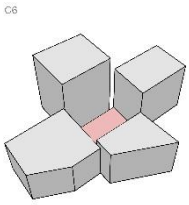	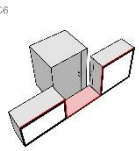
C07	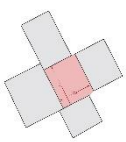	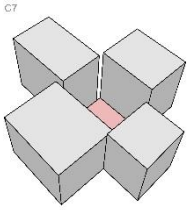	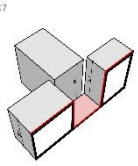

C11

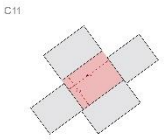

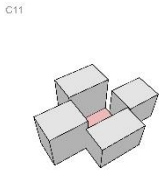

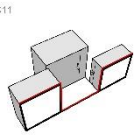

C14

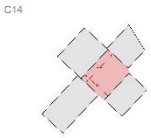

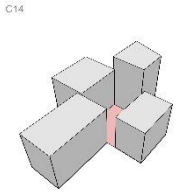

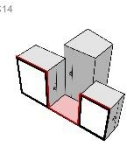

C17

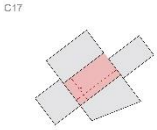

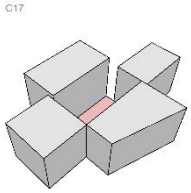

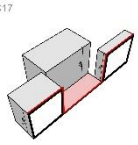

C23

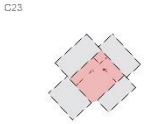

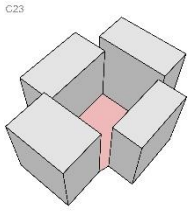

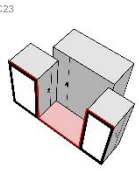

C27

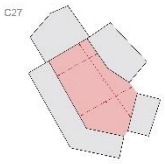

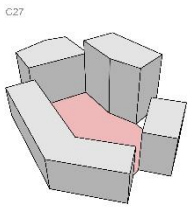

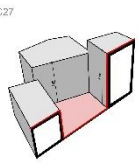

C28	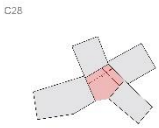	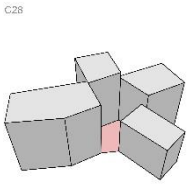	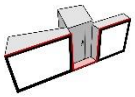
C29	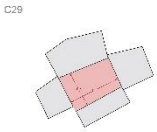	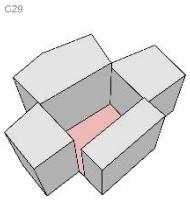	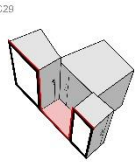

To perform a detailed analysis on the morphology of the built environment where these courtyards are situated some morphology indicators were calculated as shown on *Table 3.*

Table 3. Courtyards morphology indicators

	x(m)	y(m)	Avg. h (m)	Courtyard area (m²)	Façade area (m²)
C01	19	11	14.8	209	754
C04	19	20	21.3	380	1797
C06	21	21	19.0	441	942
C07	21	21	27.3	441	2371
C11	21	21	25.8	462	2189
C14	22	22	23.8	352	1551

C17	22	22	20.5	352	1716
C23	22	18	26.3	396	2221
C27	40	40	22.3	1080	3064
C28	13	13	26.8	208	1481
C29	24	24	28.8	432	2415

To distinguish and relate the performance of all outdoor area within the site, semi open and open courtyards morphological indicators are taken into consideration. An example of some of the semi open and fully open courtyards is illustrated on *Table 4.*

Table 4. Non-enclosed Courtyards illustrations (Plane, Axo, Section)

C02	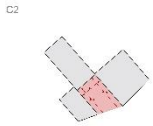	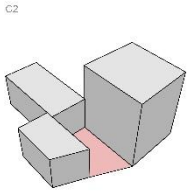	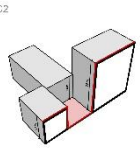
C03	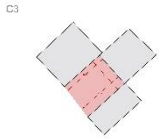	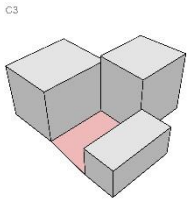	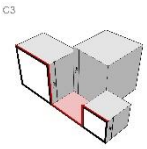

C05	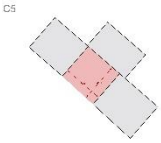	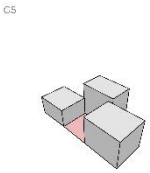	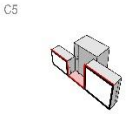
C08	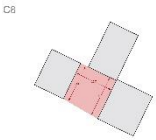	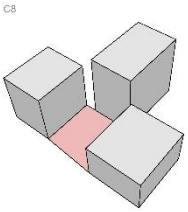	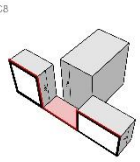
C09	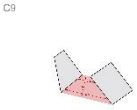	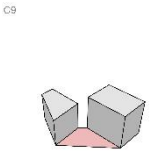	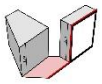
C10	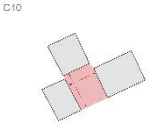	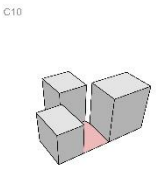	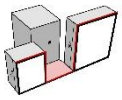
C12	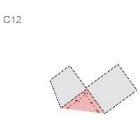	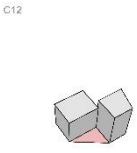	

C13	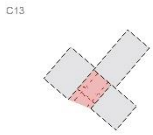	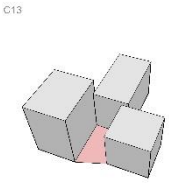	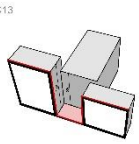
C15	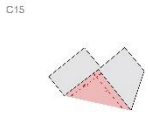	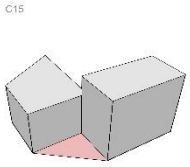	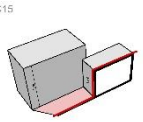
C16	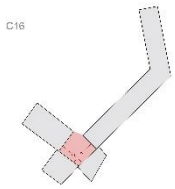	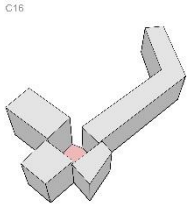	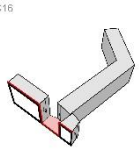
C18	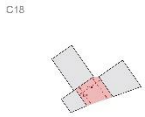	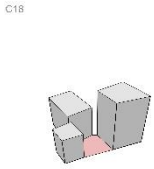	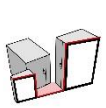
C19	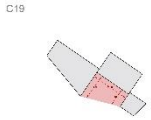	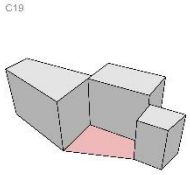	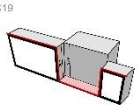

C20	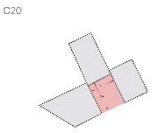	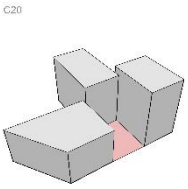	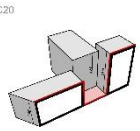
C21	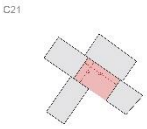	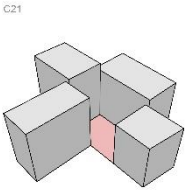	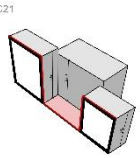
C22	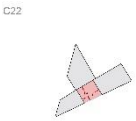	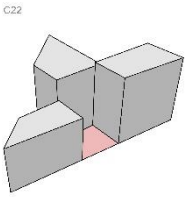	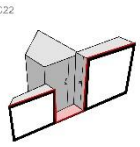
C24	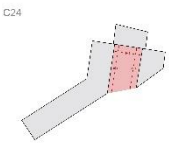	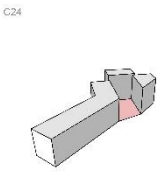	
C25	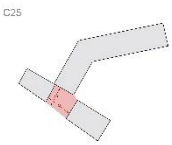	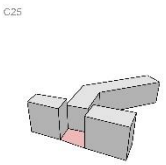	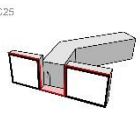

C26	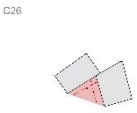	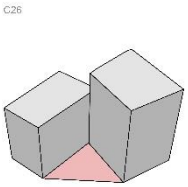	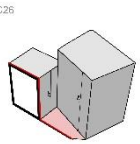
C30	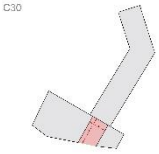	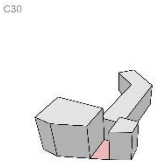	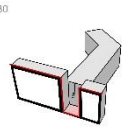
C31	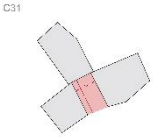	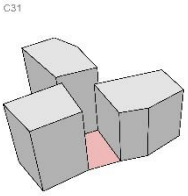	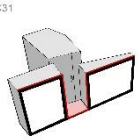
C33	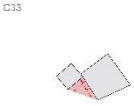	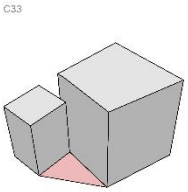	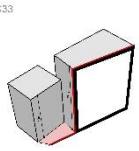

Table 5. Non-enclosed Courtyards morphology indicators

	x(m)	y(m)	Avg. h (m)	Courtyard area (m²)	Façade area (m²)
C02	26	17	16.0	442	1220
C03	25	22	20.0	550	1384
C05	20	22	23.3	440	1498
C08	22	22	22.7	462	1597
C09	13	13	18.0	169	556
C10	19	23	25.0	437	1384
C12	12	22	26.5	264	822
C13	22	16	23.7	352	1276
C15	22	25	19.5	550	1074
C16	18	16	19.5	288	1330
C18	9	17	22.0	153	936
C19	18	10	18.7	180	923
C20	22	16	21.7	352	1224
C21	8	22	23.3	176	1333
C22	6	12	17.3	72	431
C24	28	16	18.3	448	1202
C25	9	16	18.7	144	700

C26	14	24	23.5	336	811
C30	16	16	19.7	256	921
C31	24	16	26.7	384	1368
C32	20	11	24.7	220	894
C33	15	8	23.0	120	574

The courtyards are individually analyzed and the whole urban fabric is computer modeled and simulated via ENVI-met simulation software.

3.4 Computational simulation

3.4.1. Software description

For the purpose of forecasting air temperature, humidity, and the Universal Thermal Climate Index (UTCI), Envi Met is a piece of software. The program simulates the intricate connections between environmental parameters using cutting-edge algorithms and modeling approaches, enabling precise forecasting of how changes in climate or land use can affect these variables. The program has a simple interface that makes it simple to enter environmental data and is user-friendly and simple to use. For environmental scientists trying to understand how climate change and other environmental factors are affecting these vital variables, it can provide very precise forecasts of air temperature, humidity, and UTCI at various places and periods. For environmental scientists who want to make wise choices and advance their work significantly, Envi Met is an essential tool. It has strong visualization features that make it possible to analyze complicated data sets quickly and easily and spot patterns and trends. Envi Met can assist in forecasting air temperature, humidity, and UTCI, which is useful for researching the effects of climate change on regional ecosystems, evaluating the efficacy of land use regulations, or trying to better understand the intricate connections between environmental parameters. Envi Met simulations produce data

through the use of a complex grid-based modeling system that takes into account a wide range of environmental factors. The software divides the modeling area into a grid of cells, each of which represents a specific location in the modeled environment.

Each cell is characterized by a set of environmental parameters, such as topography, land cover, and meteorological data. These parameters are used to simulate the interactions between various environmental factors, including solar radiation, atmospheric conditions, and moisture content.

The accuracy of Envi Met's simulations is due in part to the software's ability to take into account the unique characteristics of each individual cell. By modeling each cell as a discrete entity, Envi Met is able to accurately simulate the complex interactions between different environmental factors at a fine scale, resulting in highly detailed and accurate predictions of air temperature, humidity, and UTCI.

The complexity of Envi Met's modeling system also allows for the simulation of a wide range of environmental scenarios. By inputting different environmental parameters and land use scenarios, researchers can simulate the impacts of climate change, urbanization, and other environmental factors on air temperature, humidity, and UTCI.

The Envi Met simulation software simulation Scenario is illustrated in *Figure 6.* Where the buildings, the topography and site characteristics are inputted.

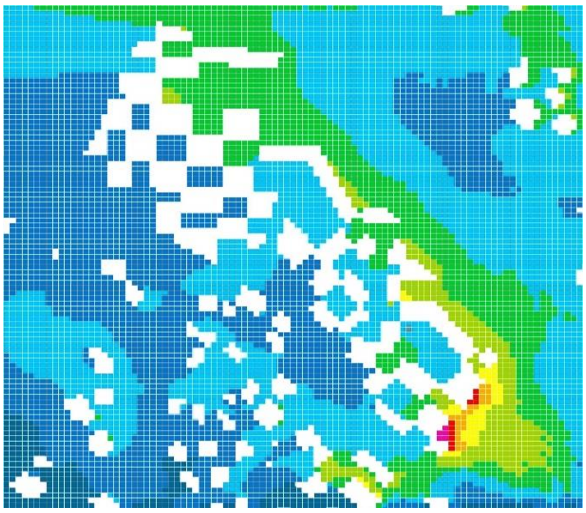

Figure 6. Illustrates the site buildings, and the cell like structure of the model

3.4.2. Software data input

In order to perform the simulation through Envi Met, a set of input data is required. The built environment part of the site is modeled within “Space” which is part of Envi Met. Since the chosen site is positioned in a sloppy terrain area, the topography of the site is imported through “Monde”, another part of the Envi Met Software package.

After completing these steps, the simulation package requires a set of weather input parameters. These parameters were generated through “Metero-lab”. Within “Envi-guide” the microclimate and weather parameters are combined together with the completed model into a SIMX-file where the specific forcing for the simulation is chosen as well as the specific date. As mentioned above, in order to analyze the thermal performance and Universal thermal comfort index the date chosen for the simulation is the hottest day of the year 2022 in Tirana Albania, respectively the seventeenth of July 2022.

3.4.3. Software data output

After the simulation is completed the outputs of the simulation can be read and visualized through “Leonardo”, another integrated part of Envi Met. Even though the output data is easily visualized through “Leonardo”, given that the site area is very large and our interest lays on the outdoor areas within the recently constructed Mangalem 21 neighborhood, the output data is run through a python script in order to calculate average values of UTCI for every courtyard during every hour of the day. An example of the python script can be seen below on *Figure 7.*

```
from shapely.geometry import Point, Polygon

import csv

fileName = "New Simulation 23.00.01 13.07.csv"  #duhet ndryshuar sipas file qe deshiron te analizosh (file duhet bere upload me pare)

file = open(fileName, "r")

data = list(csv.reader(file, delimiter=","))

file.close()

#listen me poshte e ndryshon sipas deshires, mjafton qe koordinatat e kulmeve te poligonit te jepen ne menyre ciklike

C1 = [(112, 34), (124, 340), (124, 42), (112, 42)]

C2 = [(100, 46), (88, 46), (80, 50), (100, 50)]

C3 = [(112, 62), (128, 62), (112, 74), (124, 74)]

C4 = [(92, 82), (96, 82), (96, 94), (92, 94)]

C5 = [(132, 98), (144, 98), (144, 86), (132, 78)]

C6 = [(76, 102), (80, 102), (80, 118), (76, 118)]

C7 = [(108, 102), (124, 104), (124, 118), (108, 118)]

C8 = [(152, 122), (172, 122), (172, 106), (152, 106)]

C9 = [(60, 118), (72, 118), (72, 138)]

C10 = [(92, 138), (100, 138), (100, 122), (94, 122)]

C11 = [(128, 126), (148, 126), (148, 138), (128, 138)]

C12 = [(172, 126), (172, 142), (184, 142)]

C13 = [(108, 146), (120, 146), (120, 150), (108, 150)]

C14 = [(152, 150), (164, 150), (164, 162), (152, 162)]

C15 = [(192, 162), (204, 174), (208, 178), (208, 182), (216, 182), (224, 174), (228, 170), (228, 166), (224, 162)]

C16 = [(236, 166), (232, 170), (232, 178), (236, 182), (240, 166)]

C17 = [(124, 170), (144, 170), (144, 162), (124, 162)]

C18 = [(168, 166), (180, 166), (176, 174), (168, 174)]

C19 = [(148, 182), (148, 198), (164, 186), (164, 182)]

C20 = [(196, 206), (208, 194), (212, 198), (212, 202), (208, 206), (208, 210)]

C21 = [(232, 190), (236, 190), (236, 194), (240, 198), (232, 202), (224, 202), (224, 198)]

C22 = [(260, 202), (264, 202), (264, 206), (260, 206)]

C23 = [(224, 218), (228, 218), (228, 222), (236, 230), (236, 234), (228, 242), (220, 234), (220, 222)]

C24 = [(268, 214), (288, 214), (288, 226), (268, 226)]

C25 = [(260, 230), (264, 230), (264, 242), (256, 242)]

C26 = [(252, 246), (236, 254), (244, 254), (244, 258), (252, 258)]

C27 = [(268, 246), (284, 246), (296, 258), (296, 262), (304, 262), (304, 282), (296, 290), (292, 290), (276, 274), (268, 270)]

C28 = [(252, 270), (264, 270), (264, 278), (260, 282), (256, 282), (252, 278)]

C29 = [(264, 290), (280, 306), (280, 310), (276, 314), (276, 318), (268, 318), (252, 302)]

C30 = [(316, 278), (320, 278), (324, 282), (324, 290), (320, 286), (316, 282)]

C31 = [(288, 298), (292, 298), (308, 314), (296, 314), (288, 306)]

C32 = [(268, 334), (276, 326), (284, 334), (284, 338), (280, 306)]

C33 = [(292, 330), (292, 334), (300, 334), (300, 322)]

#lista e shapes (me poshte) duhet te jete ne perputhje me listen e poligoneve percaktuar me lart

shapes = [C1, C2, C3, C4, C5, C6, C7, C8, C9, C10, C11, C12, C13, C14, C15, C16, C17, C18, C19, C20, C21, C22, C23, C24, C25, C26, C27,
C28, C29, C30, C31, C32, C33]

#lista e shapeNames duhet te jete ne perputhje me listen e poligoneve me lart (emrat vihen sipas deshires)

shapeNames = ["C1","C2", "C3", "C4", "C5", "C6", "C7", "C8", "C9", "C10", "C11", "C12", "C13", "C14", "C15", "C16", "C17", "C18",
"C19", "C20", "C21", "C22", "C23", "C24", "C25", "C26", "C27", "C28", "C29", "C30", "C31", "C32", "C33"]

polygons = [Polygon(sh) for sh in shapes]

sums = [0 for sh in shapes]

counts = [0 for sh in shapes]
```

```
countsIrregular = [0 for sh in shapes]
irregularPoints = [[] for sh in shapes]
totalPoints = [0 for sh in shapes]
for lineNum, item in enumerate(data[1:]):
  for i, p in enumerate(polygons):
    if p.covers(Point(float(item[2]),float(item[3]))):
      totalPoints[i] += 1
      if float(item[4]) > -100:
        sums[i] += float(item[4])
        counts[i] += 1
      else:
        irregularPoints[i].append((lineNum,item))
        countsIrregular[i] += 1
averages = [s/c if c != 0 else 0 for s,c in zip(sums,counts)]
outputFileName = "Results-" +fileName[:-4]+".txt";
outputFile = open(outputFileName, "w")
outputFile.write("Shape".ljust(15)+"Average".ljust(25)+"Total Points".ljust(25)+"Regular Points (used for evaluation)\n")
outputFile.write(100*"-"+"\n")
for n, avg, total, count in zip(shapeNames, averages, totalPoints, counts):
  outputFile.write(n.ljust(15)+str(avg).ljust(25)+str(total).ljust(25)+str(count) + "\n")
outputFile.write("\n\n")
for n, irr in zip(shapeNames, irregularPoints):
  outputFile.write("Irregular points for shape "+n+ "("+ str(len(irr))+" points) \n")
  for item in irr:
    outputFile.write(str(item)+"\n")
  outputFile.write("\n\n")
outputFile.close()
print("OUTPUT FILE '"+outputFileName+"' IS SUCCESSFULLY GENERATED.")
print("CHECK THE FOLDER SECTION IN THE LEFT.")
```

Figure 7. Illustrates the site python script used to obtain average values within courtyards

Each courtyard is identified as “Cn” and the coordinates of the outmost outer cells of each courtyard are integrated within the python script. This script then outputs average UTCI data regarding each courtyard on every hour of the day.

CHAPTER 4

RESULTS AND

DISCUSSIONS

4.1 Overview

In this rubric, the UTCI values of every outdoor area illustrated and evaluated on a micro and macro scale.

Since UTCI is a value obtained by a formula that combines air temperature, relative humidity, wind speed and mean radiant temperature all together, physiological comfort of the human body is the factor of evaluation.

$$UTCI = f(Ta, Vs, VP, Tmrt-Ta) + Ta \qquad \text{(Equation 1)}$$

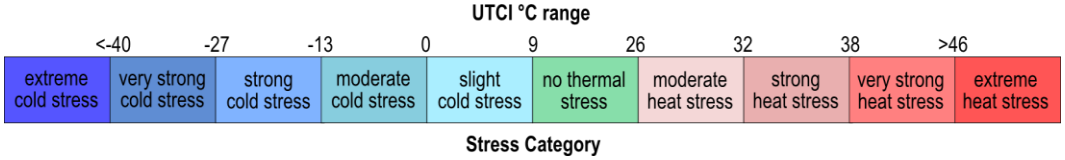

Figure 8. UTCI thermal stress categorization

The thermal stress classification is displayed in *Figure 48*, where the ideal zone with no thermal stress is shown between 9 ˚C and 26 ˚C.

4.2 Micro scale

Providing an understanding of the overall universal thermal comfort indicator by regarding the whole outdoor area as one big outdoor space would provide a skewed opinion on influencing factors within each courtyard's UTCI performance. To avoid this a deeper and more in detail analysis is provided in the form of a micro scale examination.

4.2.1 Courtyard 01

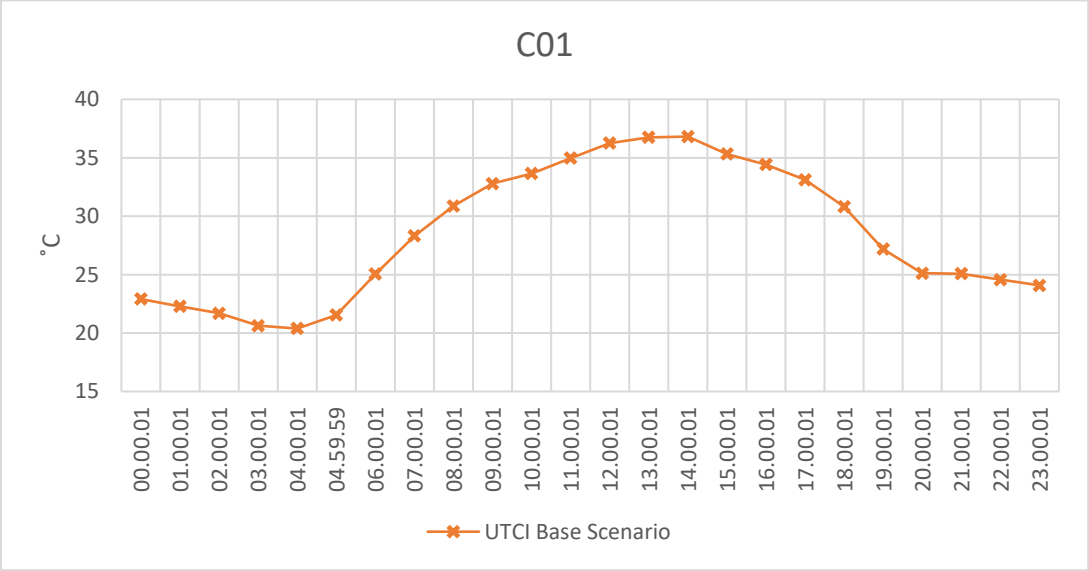

Figure 9. Graphical illustration of UTCI performance of Courtyard 01

Figure 9 illustrates the values of UTCI through the 24 hours of the simulation. It is clear that the hottest perceived temperatures occur during 13:00 and 14:00. The graph on *Figure 9* also shows a consistent decrease in UTCI from 16:00 until 20:00.

4.2.2 Courtyard 02

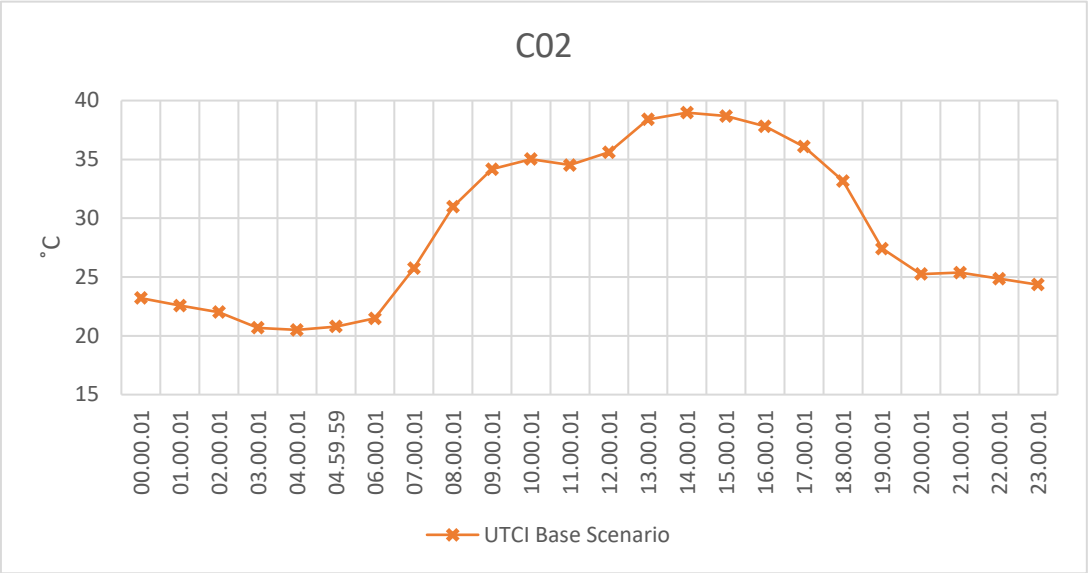

Figure 10. Graphical illustration of UTCI performance of Courtyard 02

Figure 10 illustrates the values of UTCI through the 24 hours of the simulation within courtyard "C02". It is clear that the hottest perceived temperatures occur during 13:00, 14:00, and 15:00. The graph on *Figure 10* also shows a consistent decrease in UTCI from 17:00 until 20:00.

The value of UTCI remains almost steady at 35˚C during the morning hours from 09:00 until 11:00.

4.2.3 Courtyard 03

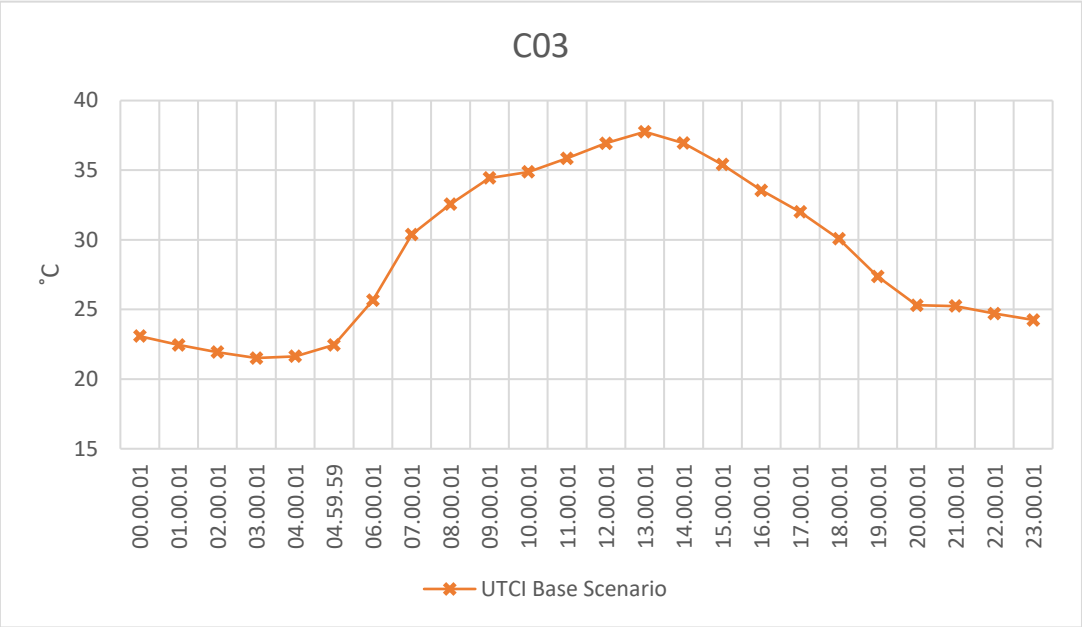

Figure 11. Graphical illustration of UTCI performance of Courtyard 03

Figure 11 illustrates the values of UTCI through the 24 hours of the simulation within courtyard "C03". It is clear that the hottest perceived temperatures occurs during 13:00. The graph on *Figure 11* also shows a consistent decrease in UTCI from 14:00 until 20:00.

The maximum value of UTCI of this Courtyard is 37.7˚C and this courtyard achieves this value only at 13:00.

4.2.4 Courtyard 04

Figure 12 illustrates the values of UTCI through the 24 hours of the simulation within courtyard "C04".This courtyard displays low values of UTCI during the first hours of the day, respectively from 00:00 until 06:00 where the values of UTCI begin a steady increase reaching the maximum value of 39.5˚C. The graph on *Figure 12* also shows a consistent decrease in UTCI from 14:00 until 21:00 where UTCI values drop to 24.7 ˚C.

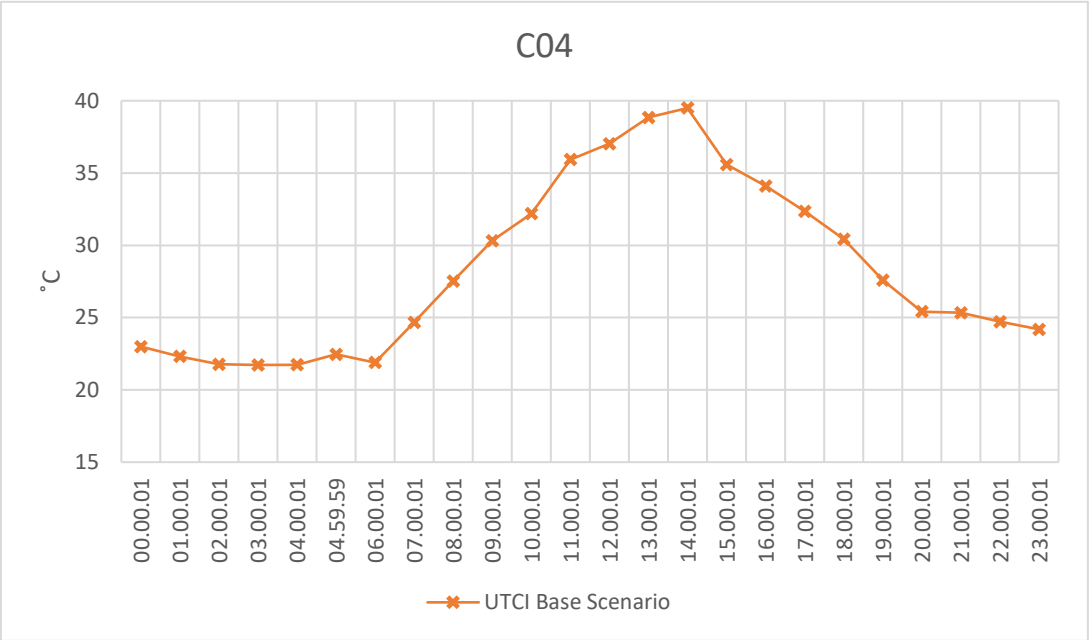

Figure 12. Graphical illustration of UTCI performance of Courtyard 04

4.2.5 Courtyard 05

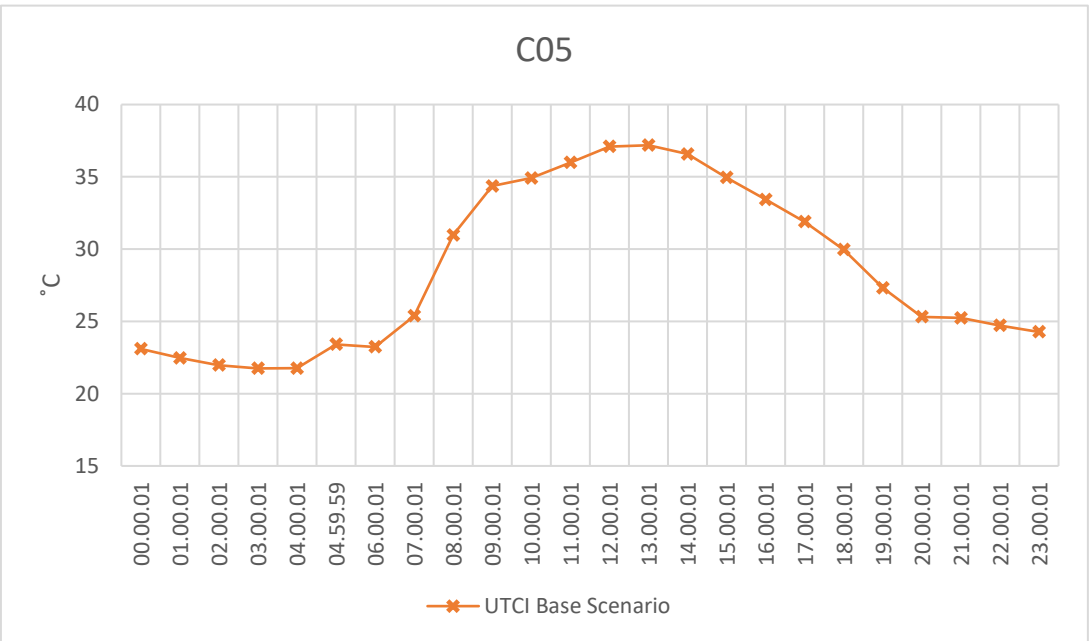

Figure 13. Graphical illustration of UTCI performance of Courtyard 05

This courtyard displays similarities with "C03". *Figure 13* illustrates a constant UTCI performance from 00:00 until 04:00 where the UTCI increases by 2˚C. From

07:00 until 09:00 values of Universal thermal comfort index show a constant increase, reaching average temperatures of 34.8˚C at 09:00.

The highest values within this courtyard are obtained during 12:00, 13:00 and 14:00 where UTCI reaches a maximum value of 37.2˚C.

4.2.6 Courtyard 06

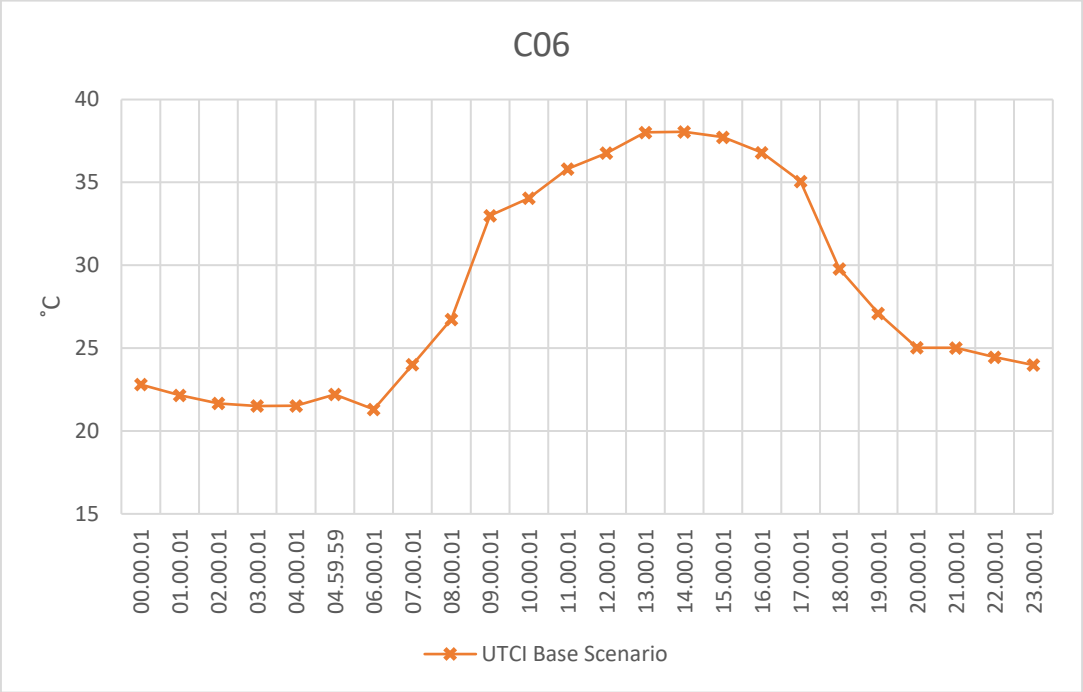

Figure 14. Graphical illustration of UTCI performance of Courtyard 06

Within courtyard “C06” UTCI values vary from a minimum of 21.3˚C to a maximum of 38.1˚C. The maximum values of Universal thermal comfort index are obtained from 12:00 until 16:00. The average UTCI average value throughout this day of “C06” is 28.4˚C.

4.2.7 Courtyard 07

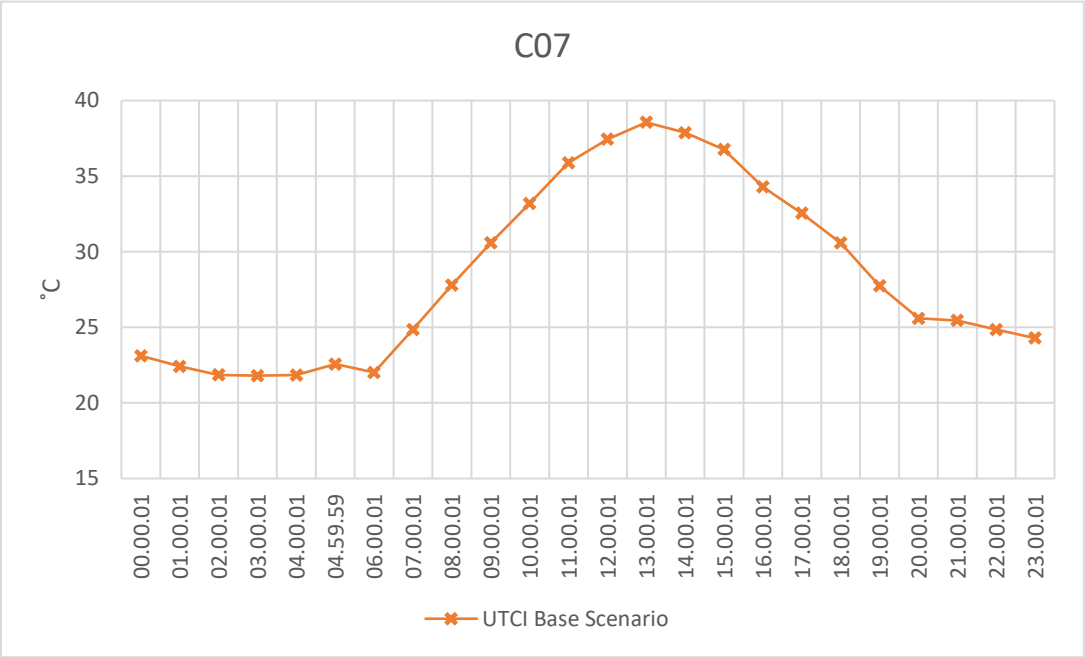

Figure 15. Graphical illustration of UTCI performance of Courtyard 07

Figure 15 illustrates the values of UTCI through the 24 hours of the simulation within courtyard "C07".This courtyard displays low values of UTCI during the first hours of the day, respectively from 00:00 until 06:00 where the values of UTCI begin a steady increase reaching the maximum value of 38.6˚C at 13:00 hour. The graph on *Figure 15* also shows a consistent decrease in UTCI from 15:00 until 20:00 where UTCI values drop to 25.6 ˚C.

This courtyard displays a maximum UTCI value of 38.6 ˚C with the hottest hour being 13:00 and an average of 28.5 ˚C throughout this day.

4.2.8 Courtyard 08

Figure 16 illustrates the values of UTCI through the 24 hours of the simulation within courtyard "C08".This courtyard displays low values of UTCI during the first hours of the day, respectively from 00:00 until 04:00 where the values of UTCI begin a steady increase reaching the maximum value of 37.6˚C. The graph on *Figure 16* also

shows a consistent decrease in UTCI from 14:00 until 20:00 where UTCI values drop to 24.8 ˚C.

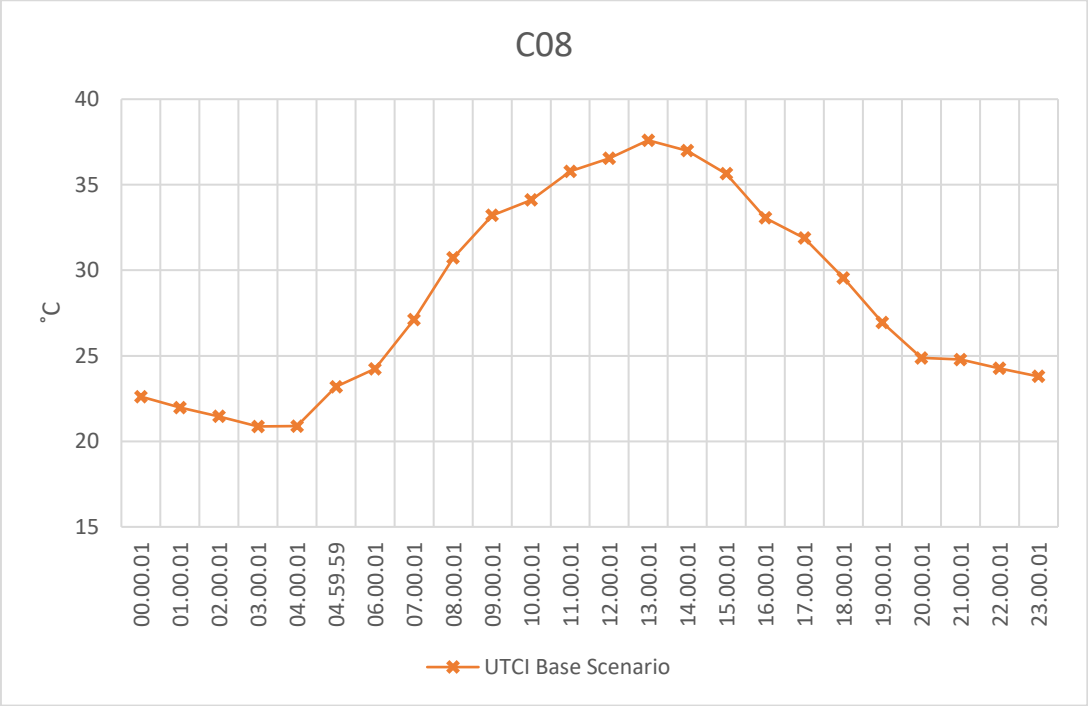

Figure 16. Graphical illustration of UTCI performance of Courtyard 08

This courtyard registers the highest UTCI value at 13:00 hour with a respective value of 37.6 ˚C. The average UTCI value within this courtyard throughout the day is 28.4 ˚C.

4.2.9 Courtyard 09

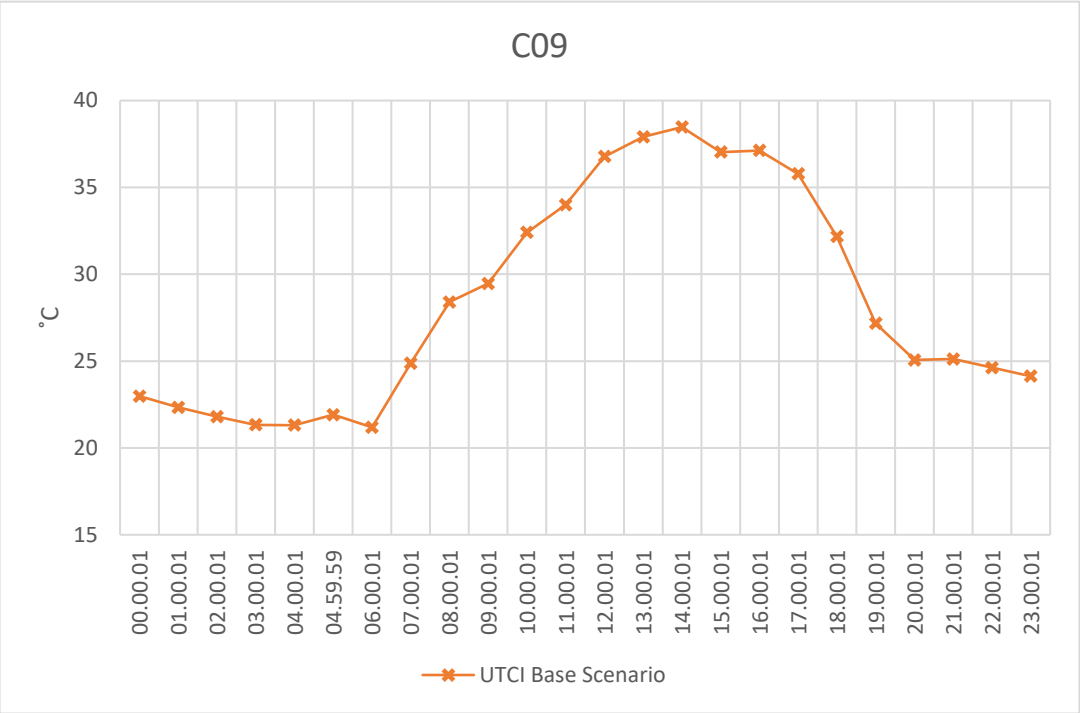

Figure 17. Graphical illustration of UTCI performance of Courtyard 09

This courtyard displays similarities with "C06". *Figure 17* illustrates a constant UTCI performance from 00:00 until 04:00 where the UTCI increases by 1.5˚C. From 07:00 until 12:00 values of Universal thermal comfort index show a constant increase, reaching average temperatures of 37.1˚C at 12:00.

The highest values within this courtyard are obtained during 12:00 and 13:00 where UTCI reaches a maximum value of 38.5 ˚C. "C09" UTCI values display an average of 28.4 ˚C throughout this day.

4.2.10 Courtyard 10

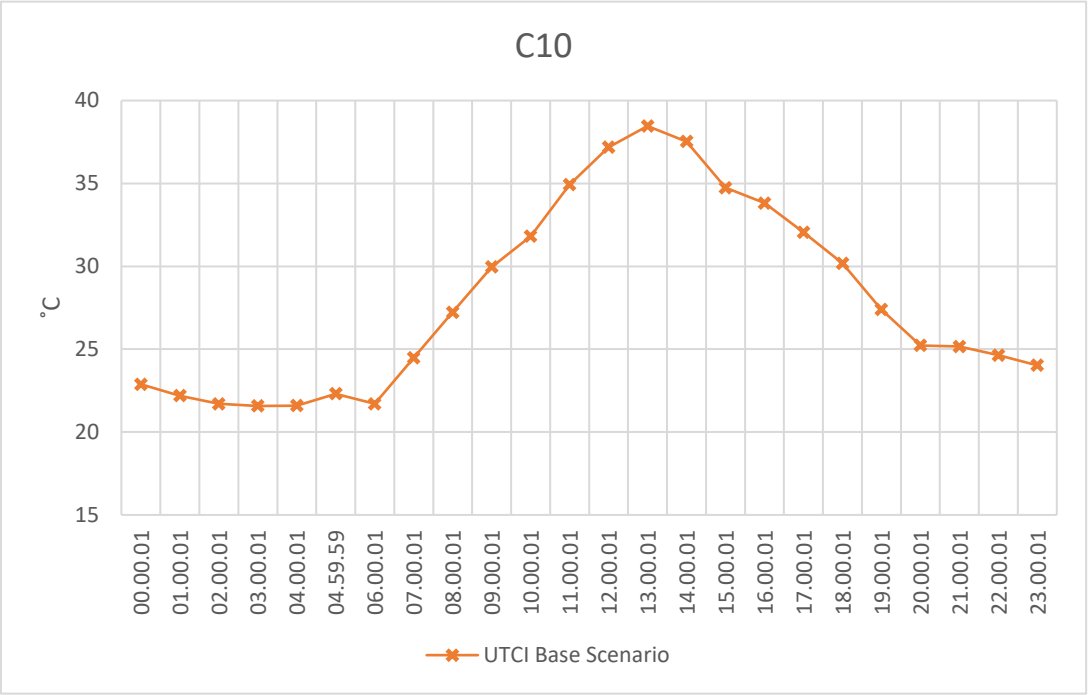

Figure 18. Graphical illustration of UTCI performance of Courtyard 10

Figure 18 illustrates the values of UTCI through the 24 hours of the simulation within courtyard "C10".This courtyard displays low values of UTCI during the first hours of the day, respectively from 00:00 until 06:00 where the values of UTCI begin a steady increase reaching the maximum value of 38.4˚C at 13:00 hour. The graph on *Figure 18* also shows a consistent decrease in UTCI from 13:00 until 20:00 where UTCI values drop to 25.2 ˚C.

This courtyard displays a maximum UTCI value of 38.4 ˚C with the hottest hour being 13:00 and an average of 28.0 ˚C throughout this day.

4.2.11 Courtyard 11

This courtyard displays similarities with "C08". *Figure 19* illustrates a constant UTCI performance from 00:00 until 05:00 where the UTCI increases by 1.8˚C. From 06:00 until 09:00 values of Universal thermal comfort index show a constant increase, reaching average temperatures of 32.7˚C at 09:00. In *Figure 19* the graph shows a steady

decrease in UTCI from 15:00 to 20:00 where UTCI values drop from 36.8 ˚C to 25.2 ˚C.

The highest values within this courtyard are obtained during 13:00 hour where UTCI reaches a maximum value of 38.7 ˚C. “C11” UTCI values display an average of 28.4 ˚C throughout this day.

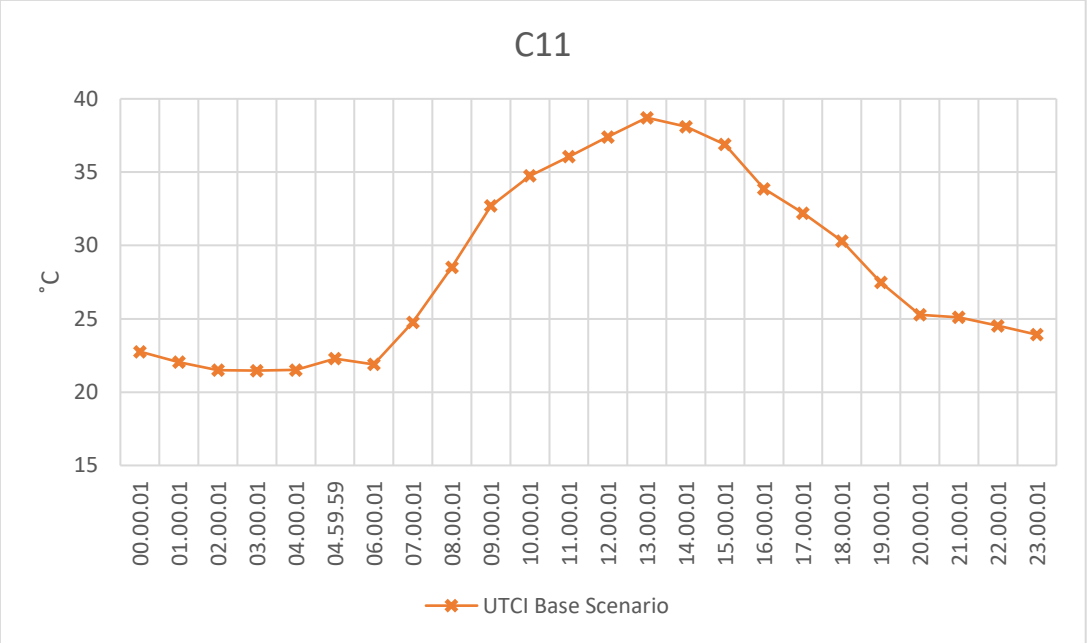

Figure 19. Graphical illustration of UTCI performance of Courtyard 11

4.2.12 Courtyard 12

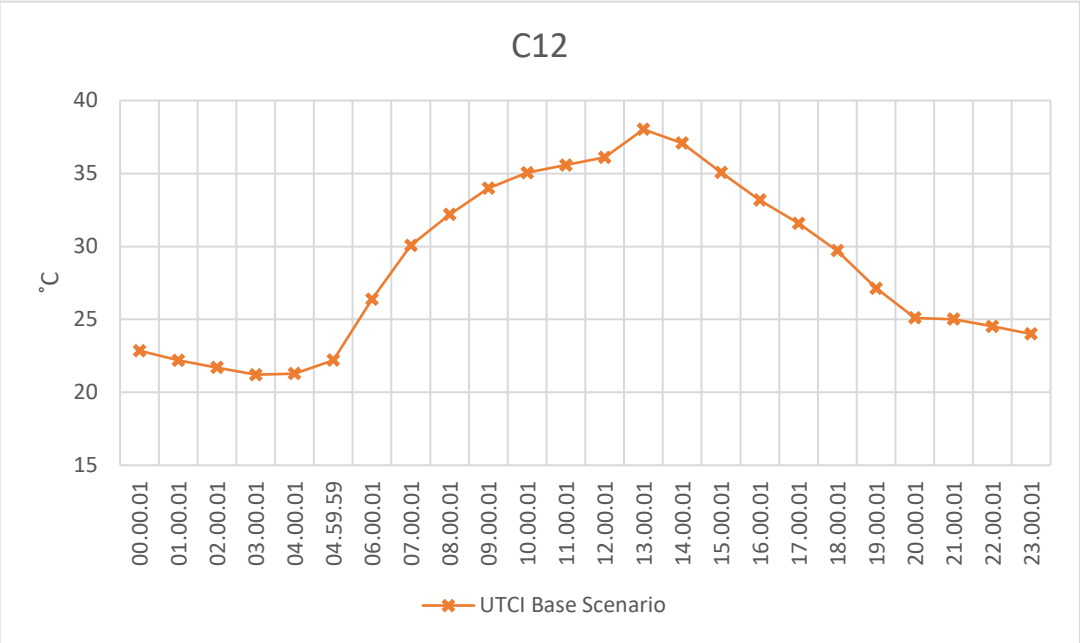

Figure 20. Graphical illustration of UTCI performance of Courtyard 12

Figure 20 illustrates the values of UTCI through the 24 hours of the simulation within courtyard "C12".This courtyard displays low values of UTCI during the first hours of the day, respectively from 00:00 until 04:00 where the values of UTCI begin a steady increase reaching the maximum value of 38.0˚C at 13:00 hour. The graph on *Figure 20* also shows a consistent decrease in UTCI from 13:00 until 20:00 where UTCI values drop to 25.1 ˚C.

This courtyard displays a maximum UTCI value of 38.0 ˚C with the hottest hour being 13:00 and an average of 28.5 ˚C throughout this day.

4.2.13 Courtyard 13

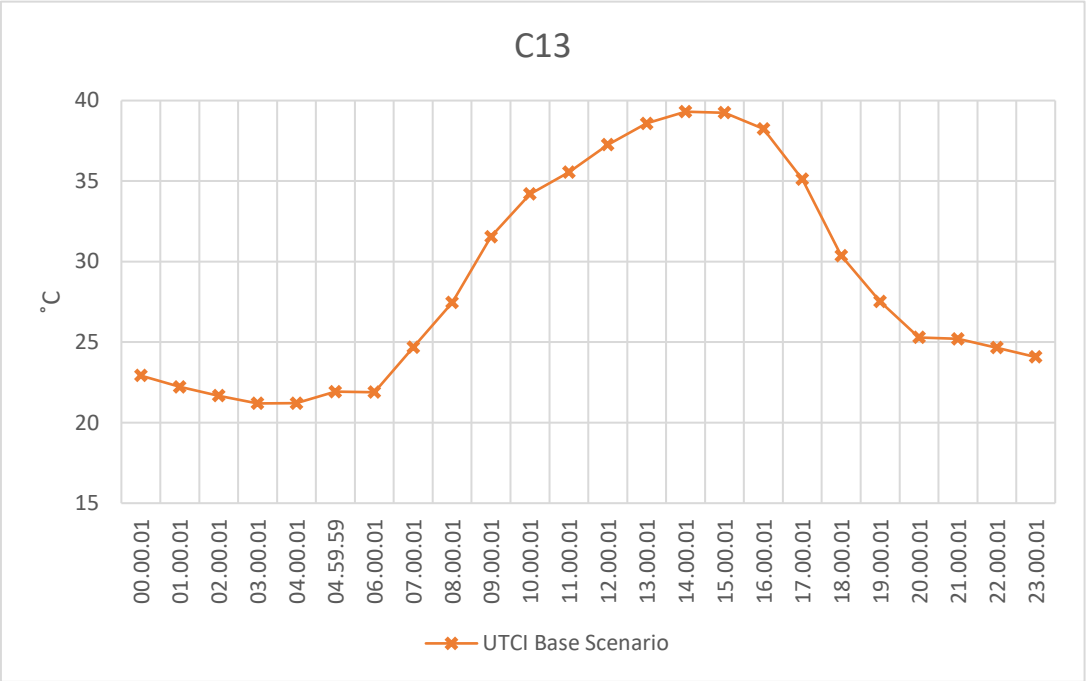

Figure 21. Graphical illustration of UTCI performance of Courtyard 13

Figure 21 illustrates the values of UTCI through the 24 hours of the simulation within courtyard "C13".This courtyard displays low values of UTCI during the first hours of the day, respectively from 00:00 until 05:00 where the values of UTCI begin a steady increase reaching the maximum value of 39.3˚C at 14:00 and 15:00 hour. The graph on *Figure 21* also shows a consistent decrease in UTCI from 16:00 until 20:00 where UTCI values drop to 25.3 ˚C.

This courtyard displays a maximum UTCI value of 39.3 ˚C with the hottest hour being 13:00 and an average of 28.8 ˚C throughout this day.

4.2.14 Courtyard 14

Figure 22 illustrates the values of UTCI through the 24 hours of the simulation within courtyard "C14".This courtyard displays low values of UTCI during the first hours of the day, respectively from 00:00 until 06:00 where the values of UTCI begin a steady increase reaching the maximum value of 38.6˚C at 13:00 hour and 14:00. The

graph on *Figure 22* also shows a consistent decrease in UTCI from 14:00 until 20:00 where UTCI values drop to 25.3 ˚C.

This courtyard displays a maximum UTCI value of 38.6 ˚C with the hottest hour being 14:00 and an average of 28.3 ˚C throughout this day.

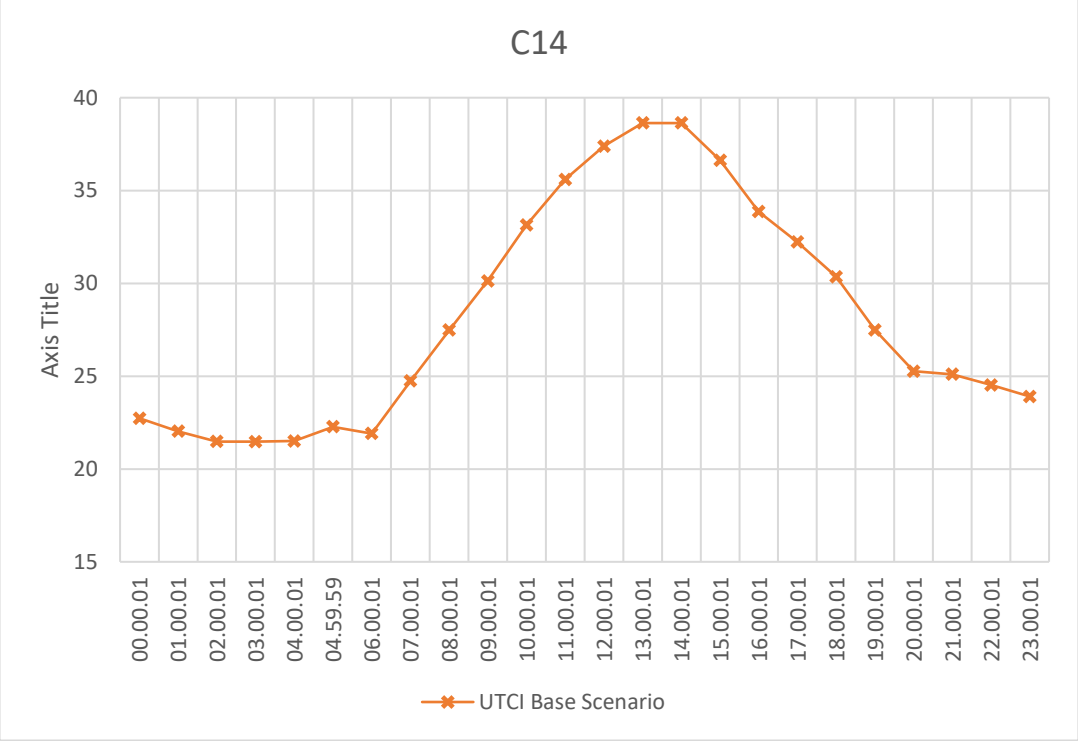

Figure 22. Graphical illustration of UTCI performance of Courtyard 14

4.2.15 Courtyard 15

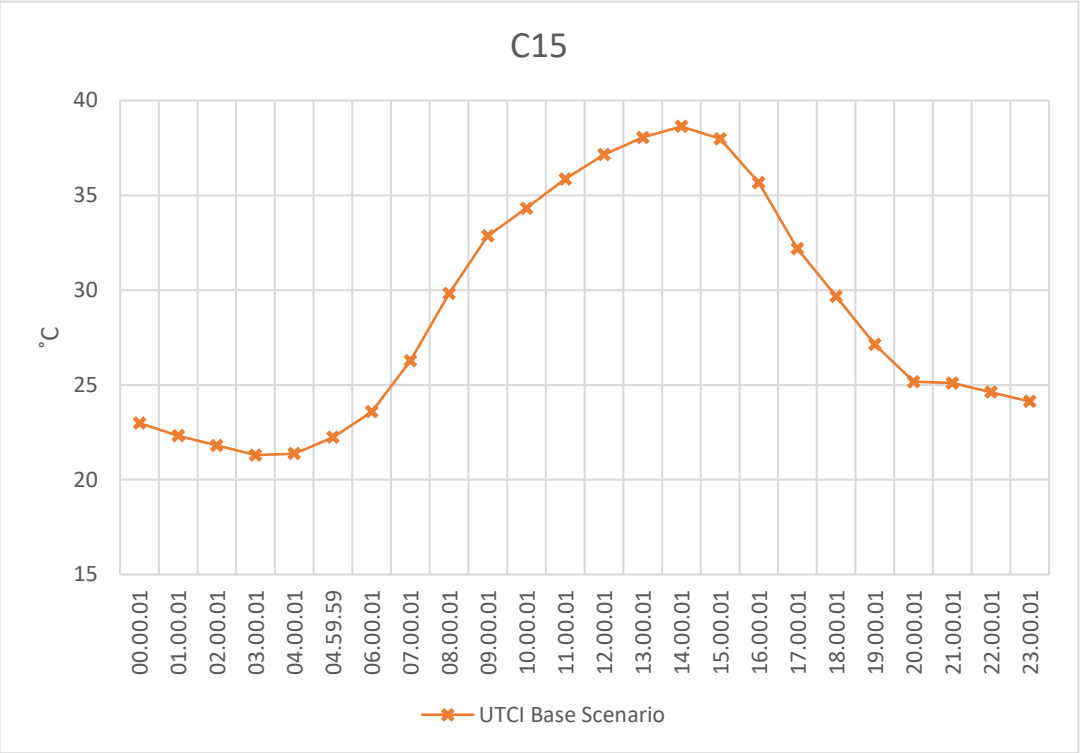

Figure 23. Graphical illustration of UTCI performance of Courtyard 15

Within courtyard "C15" UTCI values vary from a minimum of 21.3˚C to a maximum of 38.6˚C as displayed on *Figure 23*. The maximum values of Universal thermal comfort index are obtained at 12:00. The average UTCI average value throughout this day of "C06" is 28.7˚C.

4.2.16 Courtyard 16

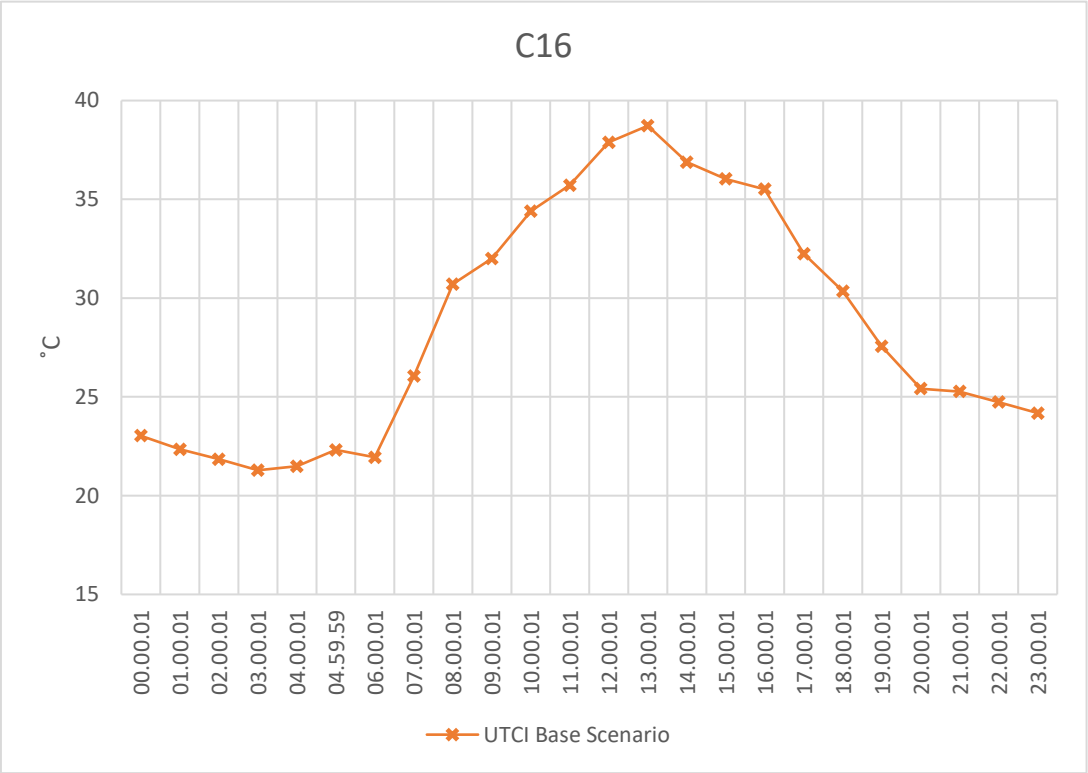

Figure 24. Graphical illustration of UTCI performance of Courtyard 16

Courtyard "C16" displays a very distinguished UTCI average value variance through this day. *Figure 24* illustrates a decreasing pattern in UTCI values from hour 00:00 until 04:00 where the first change of index is visible with an increase of 1.2 ˚C.

From 06:00 the average UTCI values of this courtyard display a steady increase until 09:00. The highest value of UTCI within this courtyard is 38.7 ˚C, marking 13:00 as the hottest hour within the simulated day. From 13:00 onwards there is a decrease in UTCI, the most significant being the one from 16:00 to 17:00.

Within the simulated day courtyard "C16" shows the highest UTCI value at hour 13:00 and the lowest UTCI value at 03:00. The average Universal thermal comfort index through the simulated day for "C16" is 28.2 ˚C.

4.2.17 Courtyard 17

Within courtyard "C17" UTCI values vary from a minimum of 21.5˚C to a maximum of 38.8˚C as displayed on *Figure 25*. The maximum values of Universal thermal comfort index are obtained at 14:00. The average UTCI average value throughout this day of "C17" is 28.8˚C.

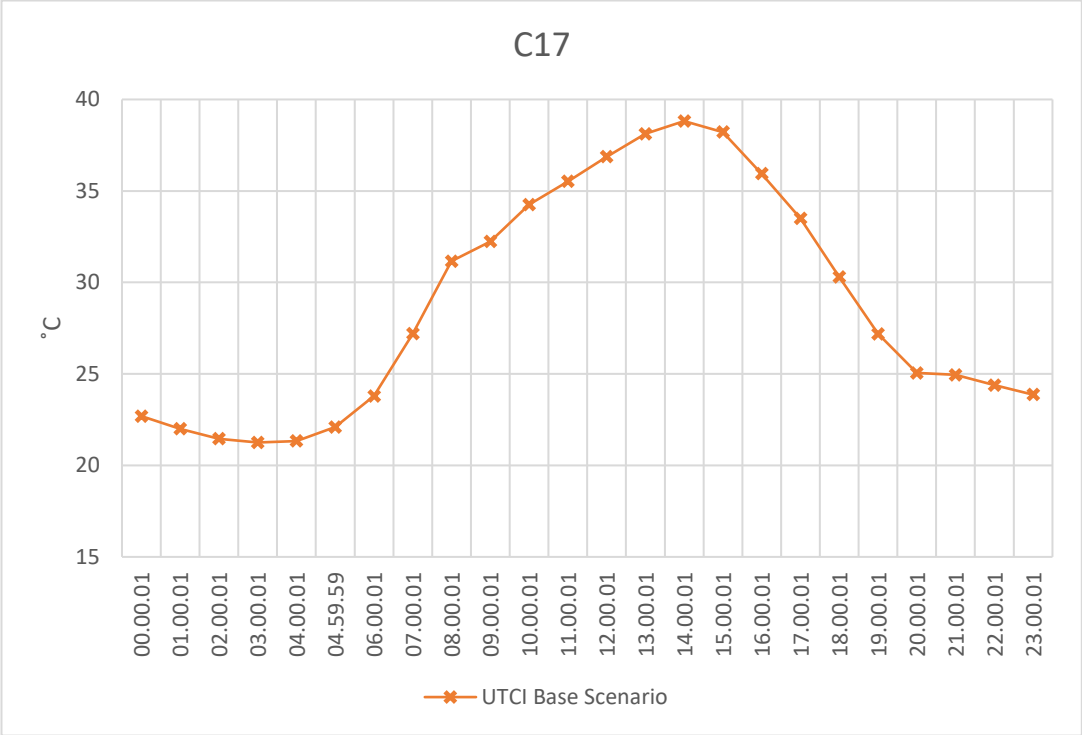

Figure 25. Graphical illustration of UTCI performance of Courtyard 17

4.2.18 Courtyard 18

This courtyard displays similarities with "C15". *Figure 26* illustrates a constant UTCI performance from 00:00 until 04:00 where the UTCI increases by 1.8˚C. From 04:00 until 07:00 values of Universal thermal comfort index show a constant increase, reaching average temperatures of 30.2˚C at 07:00. In *Figure 26* the graph shows a steady decrease in UTCI from 15:00 to 20:00 where UTCI values drop from 38.2 ˚C to 25.1 ˚C.

The highest values within this courtyard are obtained during 13:00 hour where UTCI reaches a maximum value of 38.3 ˚C. “C18” UTCI values display an average of 29.1 ˚C throughout this day.

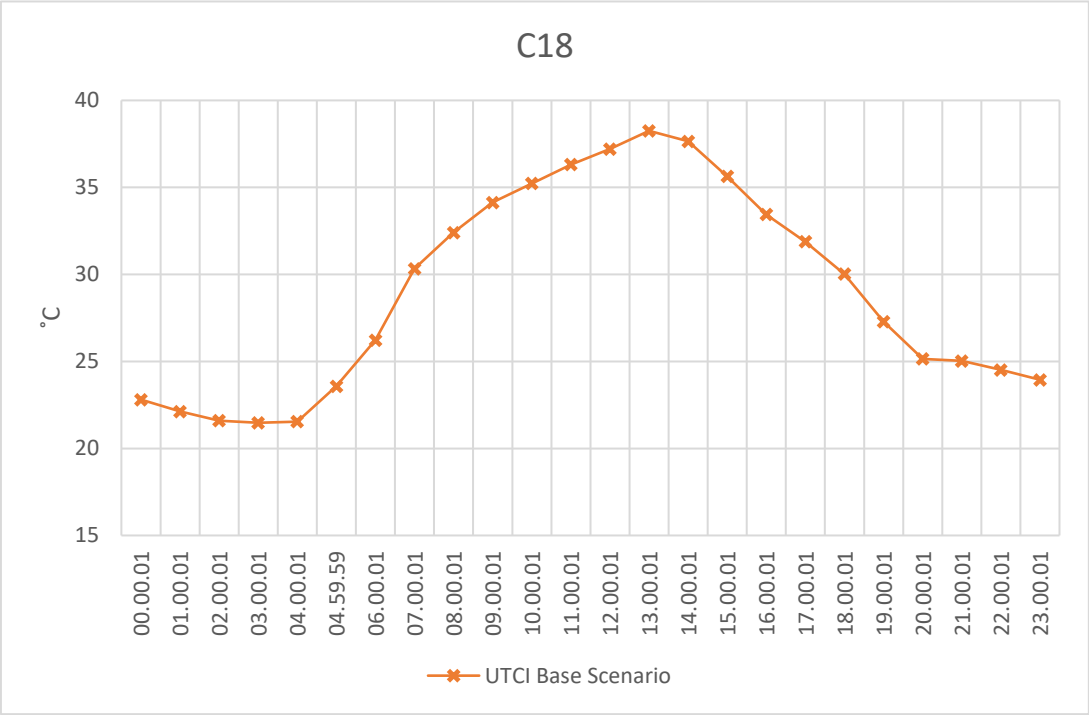

Figure 26. Graphical illustration of UTCI performance of Courtyard 18

4.2.19 Courtyard 19

Figure 27 illustrates the values of UTCI through the 24 hours of the simulation within courtyard “C19”.This courtyard displays low values of UTCI during the first hours of the day, respectively from 00:00 until 04:00 where the values of UTCI begin a steady increase reaching the maximum value of 37.8˚C at 14:00. The graph on *Figure 27* also shows a consistent decrease in UTCI from 17:00 until 20:00 where UTCI values drop to 25.1 ˚C.

This courtyard displays a maximum UTCI value of 37.8 ˚C with the hottest hour being 14:00 and an average of 28.9 ˚C throughout this day.

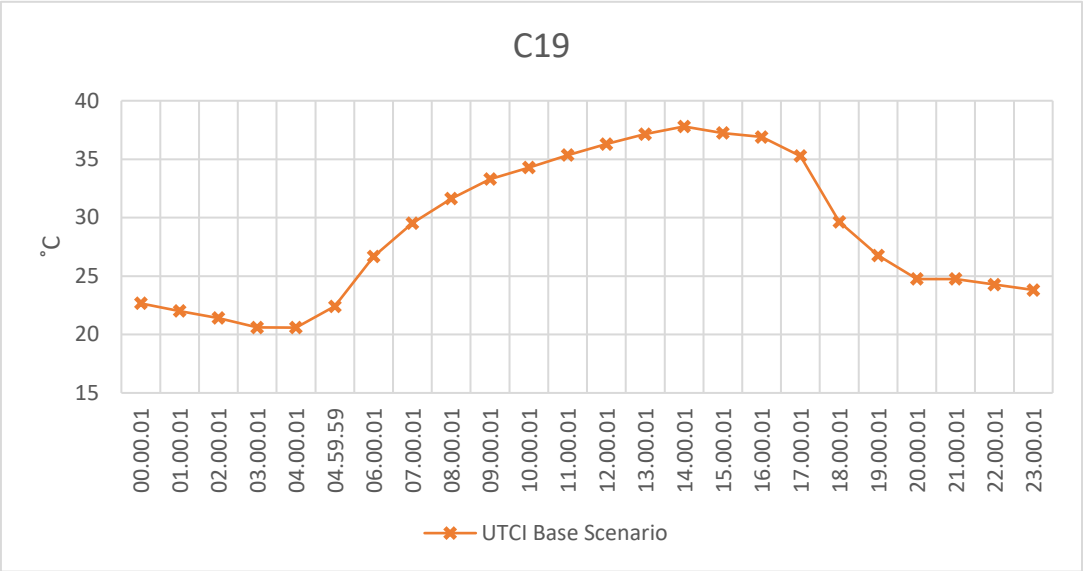

Figure 27. Graphical illustration of UTCI performance of Courtyard 19

4.2.20 Courtyard 20

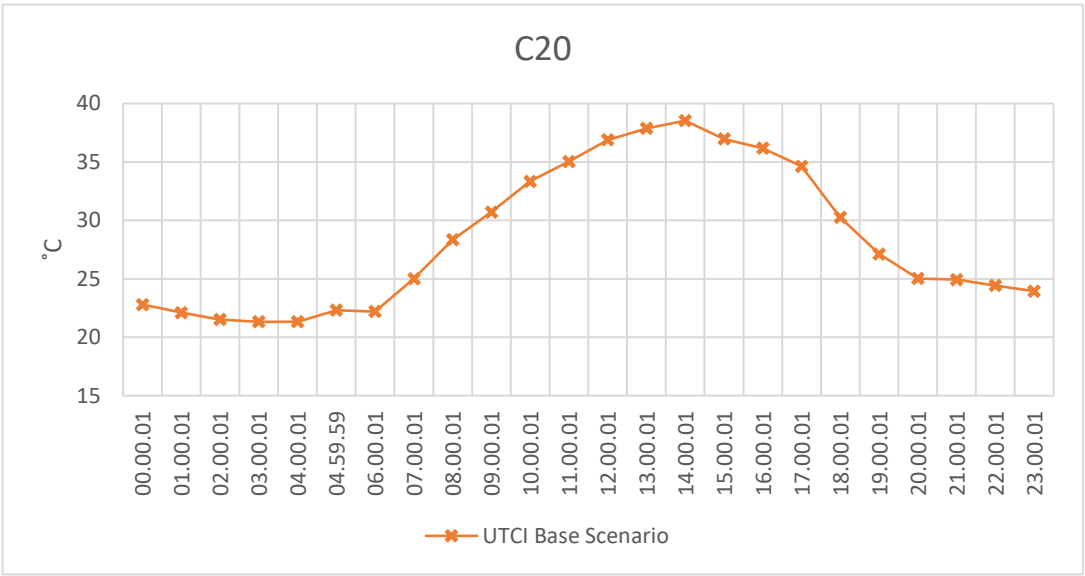

Figure 28. Graphical illustration of UTCI performance of Courtyard 20

Figure 28 illustrates the values of UTCI through the 24 hours of the simulation within courtyard "C20".This courtyard displays low values of UTCI during the first hours of the day, respectively from 00:00 until 06:00 where the values of UTCI begin a

steady increase reaching the maximum value of 38.5˚C at 14:00 hour. The graph on *Figure 28* also shows a consistent decrease in UTCI from 17:00 until 20:00 where UTCI values drop to 25.2 ˚C.

This courtyard displays a maximum UTCI value of 38.5 ˚C with the hottest hour being 14:00 and an average of 28.5 ˚C throughout this day.

4.2.21 Courtyard 21

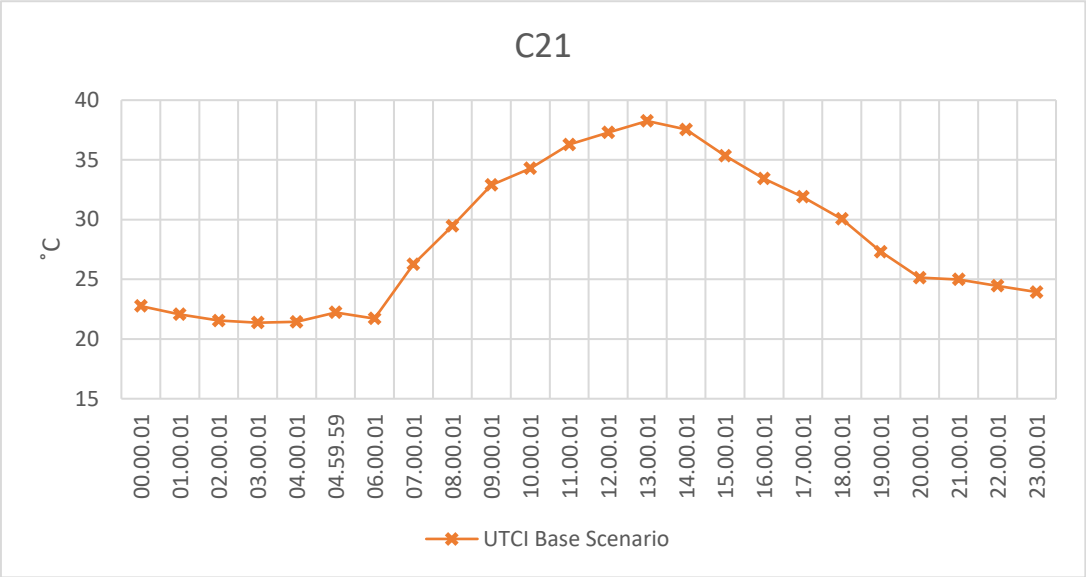

Figure 29. Graphical illustration of UTCI performance of Courtyard 21

This courtyard displays similarities with “C11”. *Figure 29* illustrates a constant UTCI performance from 00:00 until 05:00 where the UTCI increases by 1.1˚C. From 06:00 until 09:00 values of Universal thermal comfort index show a constant increase, reaching average temperatures of 32.9˚C at 09:00. In *Figure 29* the graph shows a steady decrease in UTCI from 15:00 to 20:00 where UTCI values drop from 36.8 ˚C to 25.2 ˚C.

The highest values within this courtyard are obtained during 13:00 hour where UTCI reaches a maximum value of 38.3 ˚C. “C21” UTCI values display an average of 28.4 ˚C throughout this day.

4.2.22 Courtyard 22

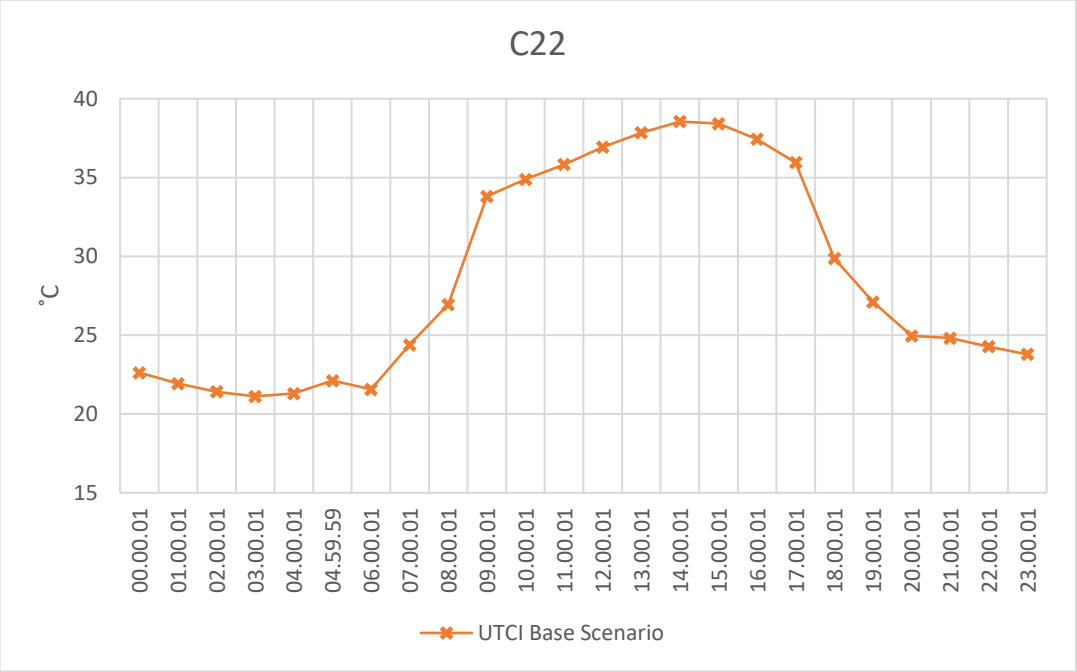

Figure 30. Graphical illustration of UTCI performance of Courtyard 22

Within courtyard "C22" UTCI values vary from a minimum of 21.1˚C to a maximum of 38.3˚C as displayed in *Figure 30*. The maximum values of Universal thermal comfort index are obtained from 14:00 until 16:00. The average UTCI average value throughout this day of "C06" is 28.4˚C.

4.2.23 Courtyard 23

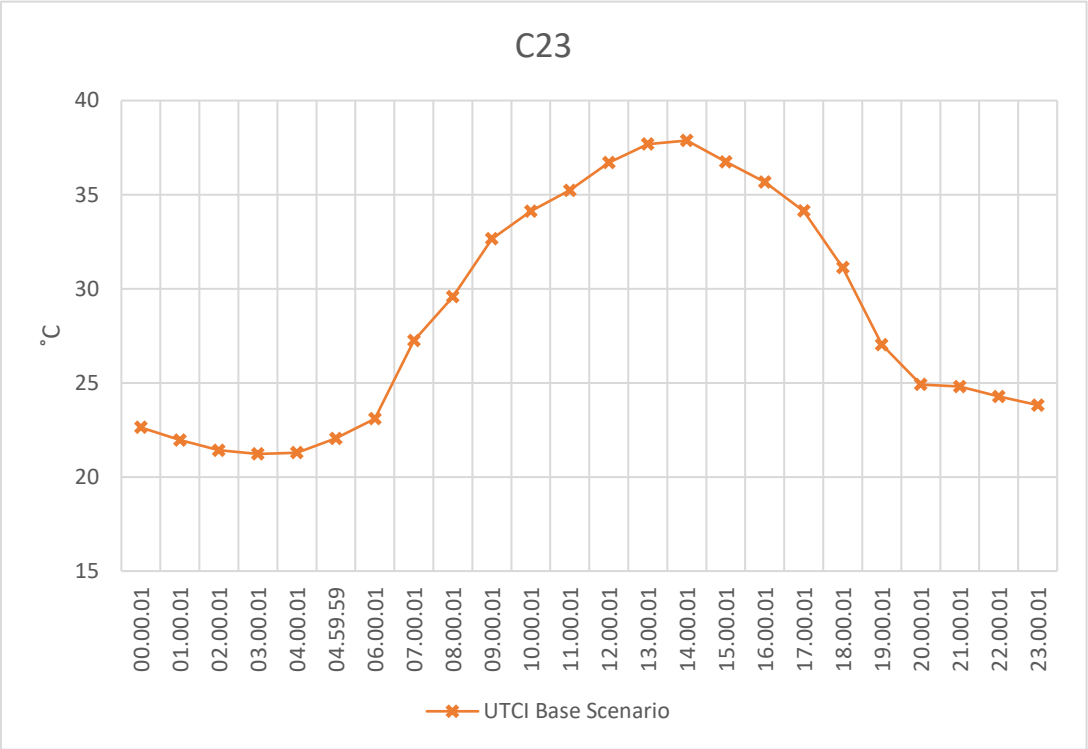

Figure 31. Graphical illustration of UTCI performance of Courtyard 23

This courtyard displays similarities with "C21". *Figure 31* illustrates a constant UTCI performance from 00:00 until 05:00 where the UTCI increases by 1.1˚C. From 06:00 until 09:00 values of Universal thermal comfort index show a constant increase, reaching average temperatures of 29.8˚C at 09:00. In *Figure 31* the graph shows a steady decrease in UTCI from 16:00 to 20:00 where UTCI values drop from 31.8 ˚C to 24.9 ˚C.

The highest values within this courtyard are obtained during 14:00 hour where UTCI reaches a maximum value of 37.8 ˚C. "C23" UTCI values display an average of 28.6 ˚C throughout this day.

4.2.24 Courtyard 24

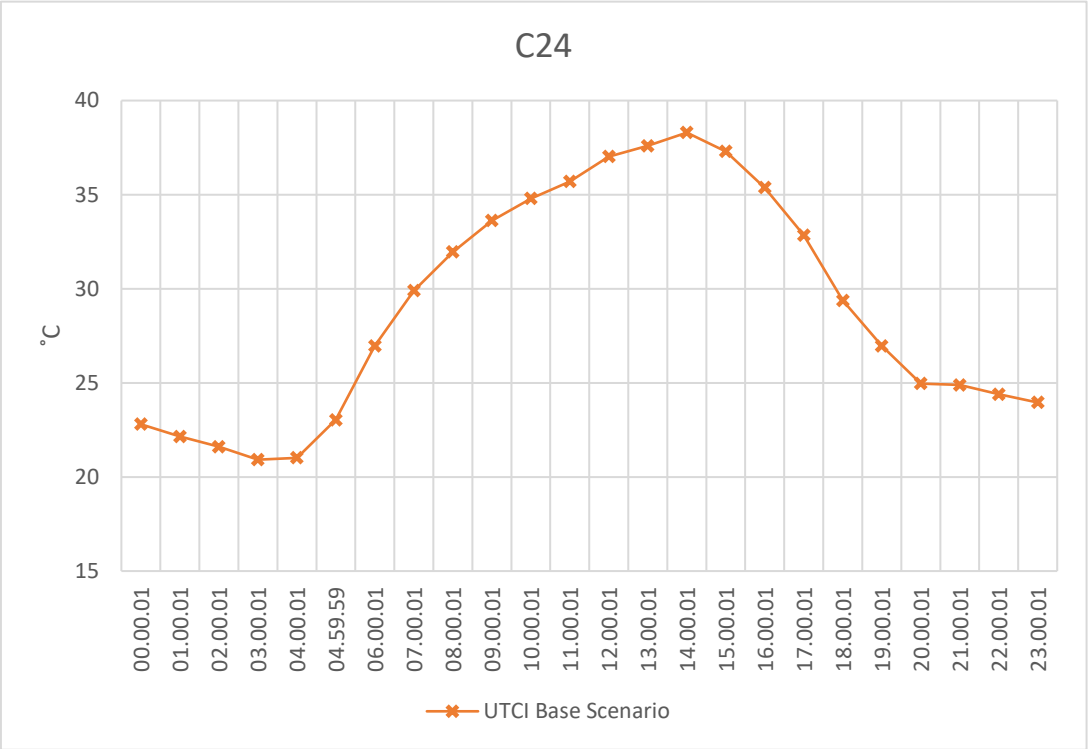

Figure 32. Graphical illustration of UTCI performance of Courtyard 24

Within courtyard "C24" UTCI values vary from a minimum of 20.9˚C to a maximum of 38.3˚C as displayed on *Figure 32*. The maximum values of Universal thermal comfort index are obtained at 14:00. The average UTCI average value throughout this day of "C24" is 29.1˚C.

4.2.25 Courtyard 25

Courtyard "C25" displays a very distinguished UTCI average value variance through this day. *Figure 33* illustrates a decreasing pattern in UTCI values from hour 00:00 until 04:00. From 05:00 the average UTCI values of this courtyard display a steady increase until 11:00. The highest value of UTCI within this courtyard is 38.1 ˚C, marking 14:00 as the hottest hour within the simulated day. From 15:00 onwards there is a decrease in UTCI, the most significant being the one from 18:00 to 19:00.

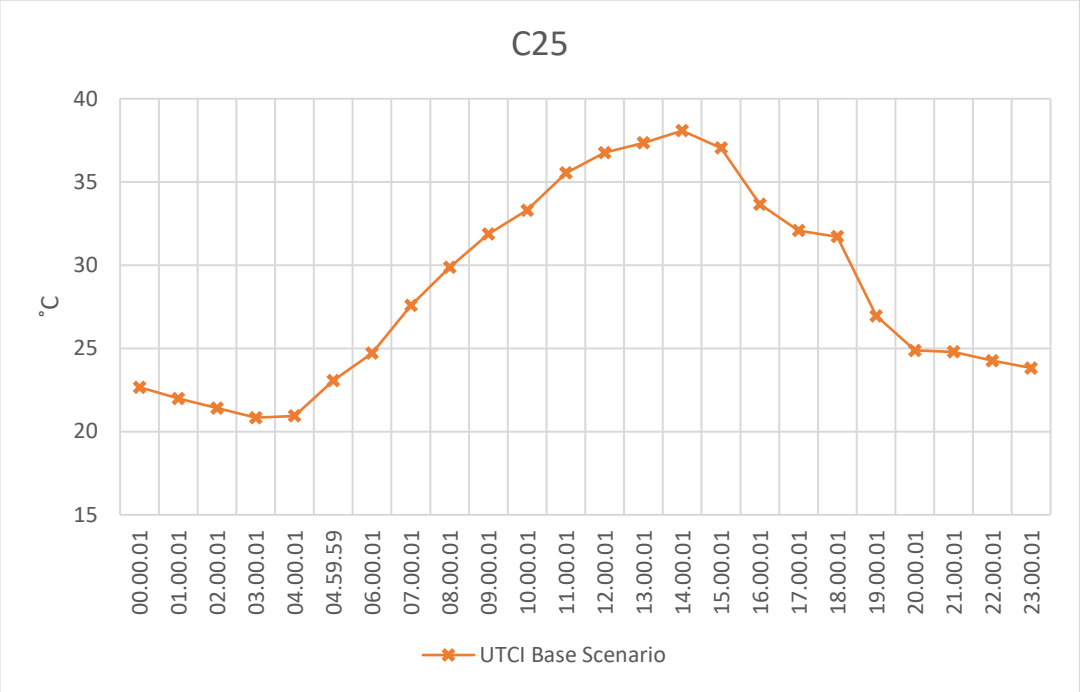

Figure 33. Graphical illustration of UTCI performance of Courtyard 25

Within the simulated day courtyard "C25" shows the highest UTCI value at hour 14:00 and the lowest UTCI value at 03:00. The average Universal thermal comfort index through the simulated day for "C25" is 28.6 ˚C.

4.2.26 Courtyard 26

This courtyard displays similarities with "C15" and "C18". *Figure 34* illustrates a constant UTCI performance from 00:00 until 04:00 where the UTCI increases by 1.8˚C. From 04:00 until 09:00 values of Universal thermal comfort index show a constant increase, reaching average temperatures of 29.9˚C at 09:00. In *Figure 34* the graph shows a steady decrease in UTCI from 14:00 to 20:00 where UTCI values drop from 38.2 ˚C to 25.1 ˚C.

The highest values within this courtyard are obtained during 13:00 hour where UTCI reaches a maximum value of 38.1 ˚C. "C26" UTCI values display an average of 28.5 ˚C throughout this day.

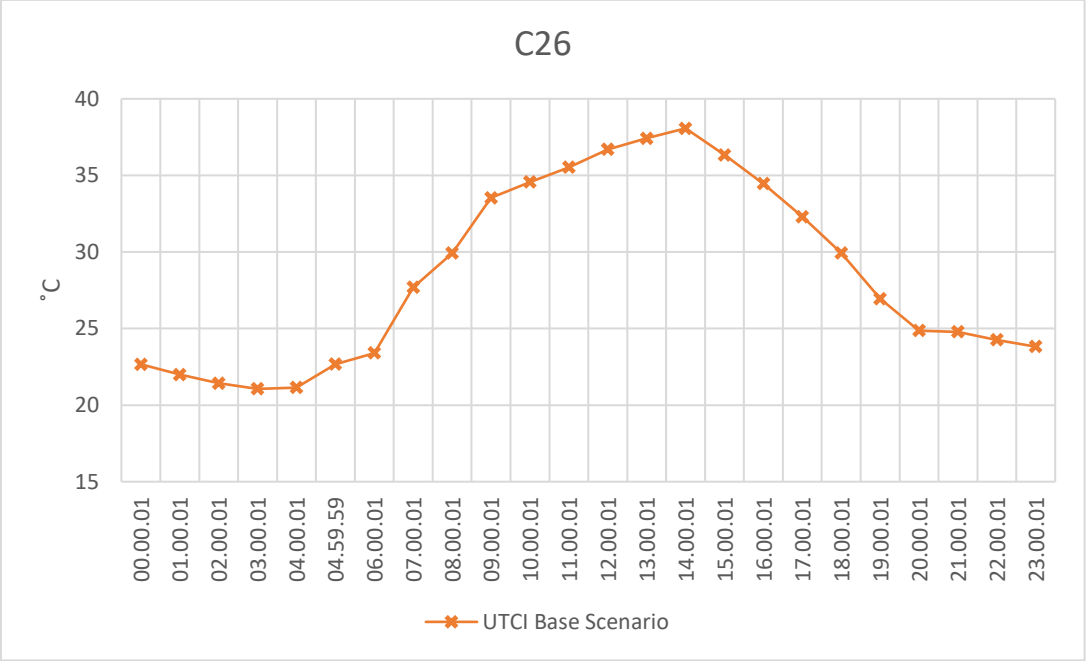

Figure 34. Graphical illustration of UTCI performance of Courtyard 26

4.2.27 Courtyard 27

Within courtyard "C15" UTCI values vary from a minimum of 21.3˚C to a maximum of 38.6˚C as displayed on *Figure 35*. The maximum values of Universal thermal comfort index are obtained at 12:00. The average UTCI average value throughout this day of "C06" is 28.7˚C.

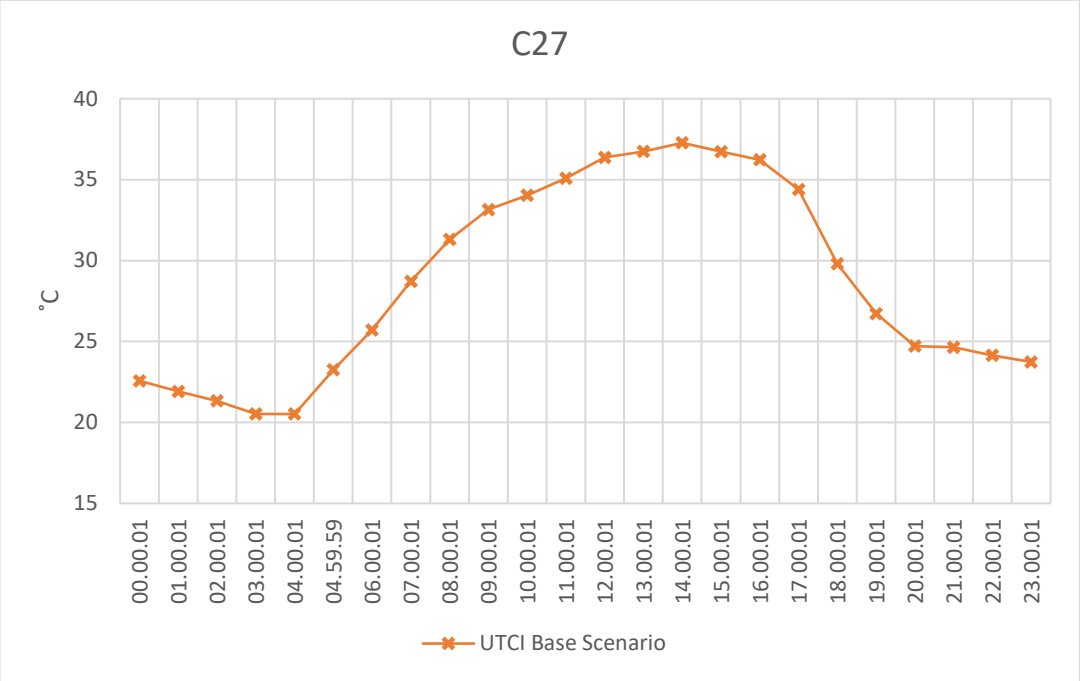

Figure 35. Graphical illustration of UTCI performance of Courtyard 27

4.2.28 Courtyard 28

This courtyard displays similarities with "C09". *Figure 36* illustrates a constant UTCI performance from 00:00 until 04:00 where the UTCI increases by 2.2˚C. From 06:00 until 12:00 values of Universal thermal comfort index show a constant increase, reaching average temperatures of 36.1˚C at 13:00.

The highest values within this courtyard are obtained during 13:00 where UTCI reaches a maximum value of 37.5 ˚C. "C09" UTCI values display an average of 28.6 ˚C throughout this day.

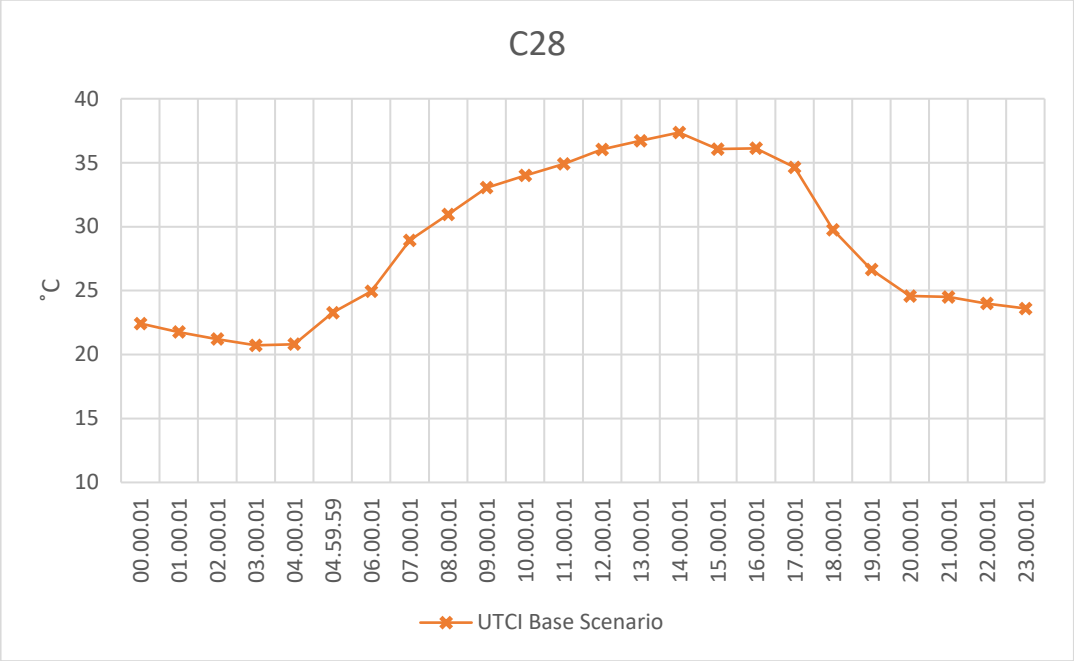

Figure 36. Graphical illustration of UTCI performance of Courtyard 28

4.2.29 Courtyard 29

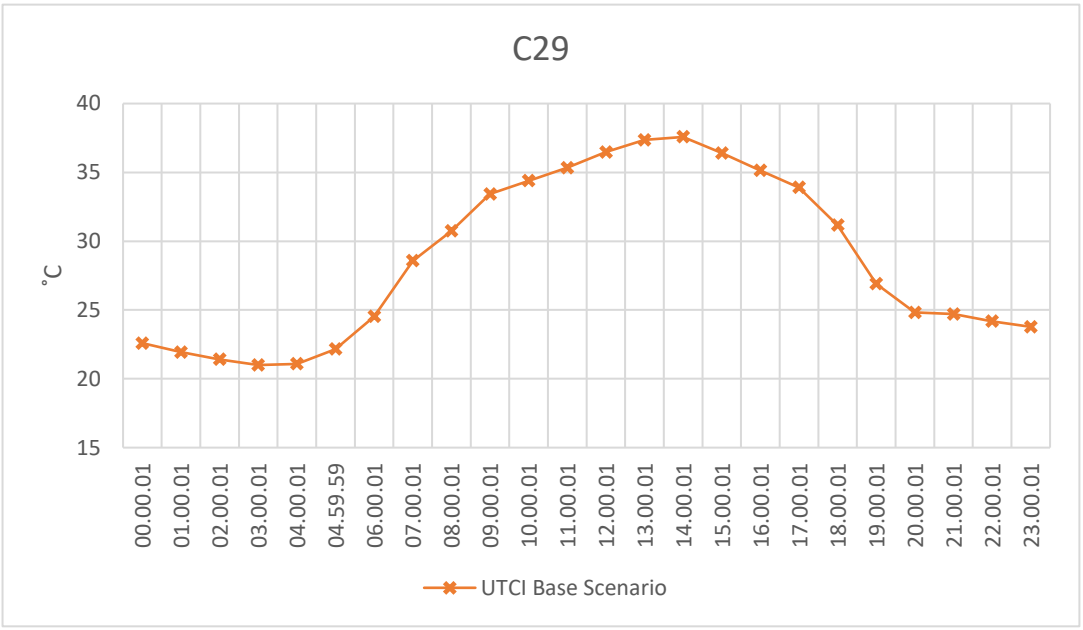

Figure 37. Graphical illustration of UTCI performance of Courtyard 29

Figure 37 illustrates the values of UTCI through the 24 hours of the simulation within courtyard “C29”. It is clear that the hottest perceived temperatures occur during 13:00 and 14:00. The graph on *Figure 37* also shows a consistent decrease in UTCI from 16:00 until 20:00.

The highest values within this courtyard are obtained during 14:00 where UTCI reaches a maximum value of 37.6 ˚C. “C09” UTCI values display an average of 28.7 ˚C throughout this day.

4.2.30 Courtyard 30

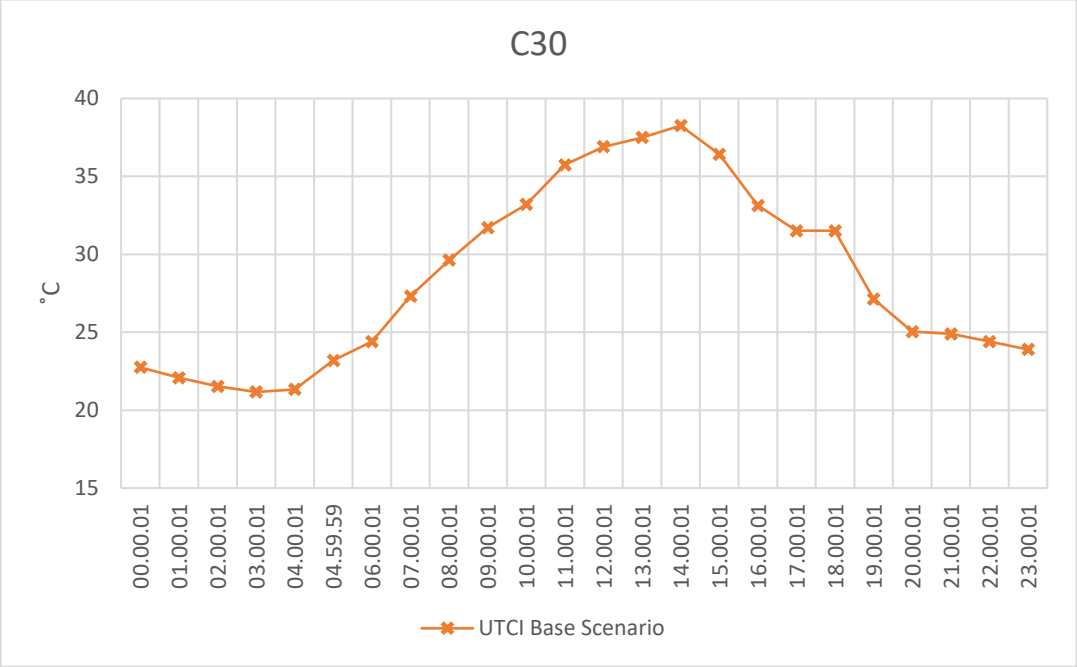

Figure 38. Graphical illustration of UTCI performance of Courtyard 30

Courtyard “C30” displays a very distinguished UTCI average value variance through this day. *Figure 38* illustrates a decreasing pattern in UTCI values from hour 00:00 until 04:00. From 04:00 the average UTCI values of this courtyard display a steady increase until 11:00. The highest value of UTCI within this courtyard is 38.3 ˚C, marking 14:00 as the hottest hour within the simulated day. From 15:00 onwards there is a decrease in UTCI, the most significant being the one from 18:00 to 19:00.

Within the simulated day courtyard “C30” shows the highest UTCI value at hour 14:00 and the lowest UTCI value at 03:00. The average Universal thermal comfort index through the simulated day for “C30” is 28.5 ˚C.

4.2.31 Courtyard 31

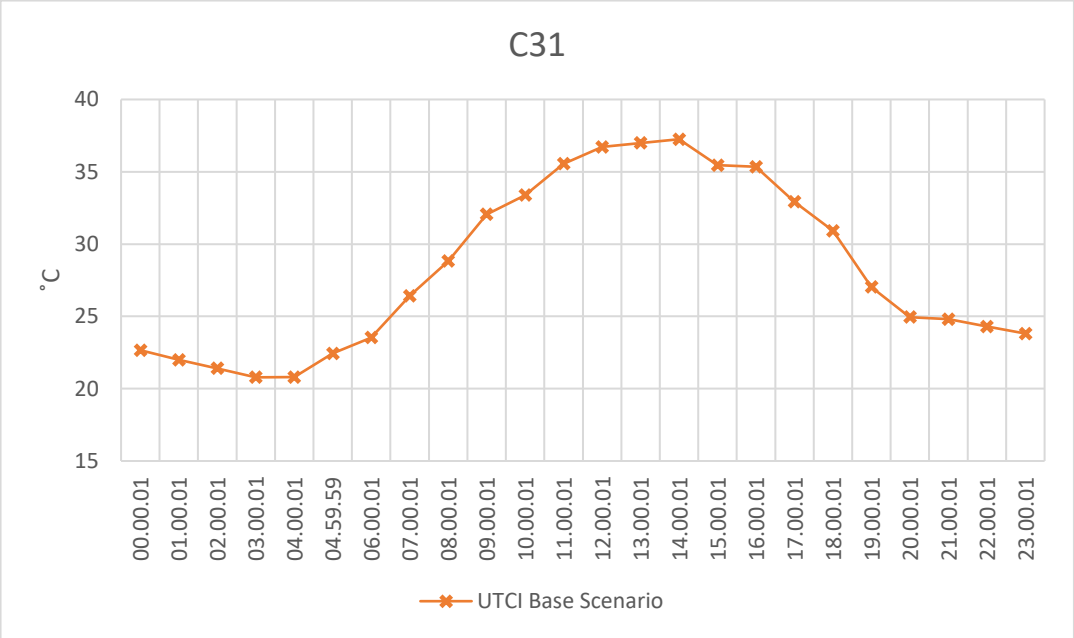

Figure 39. Graphical illustration of UTCI performance of Courtyard 31

Figure 39 illustrates the values of UTCI through the 24 hours of the simulation within courtyard “C31”.This courtyard displays low values of UTCI during the first hours of the day, respectively from 00:00 until 04:00 where the values of UTCI begin a steady increase reaching the maximum value of 37.3˚C. The graph on *Figure 39* also shows a consistent decrease in UTCI from 16:00 until 20:00 where UTCI values drop to 24.9 ˚C.

This courtyard registers the highest UTCI value at 14:00 hour with a respective value of 37.3 ˚C. The average UTCI value within this courtyard throughout the day is 28.3 ˚C.

4.2.32 Courtyard 32

Within courtyard "C32" UTCI values vary from a minimum of 21.2˚C to a maximum of 36.6˚C. The maximum values of Universal thermal comfort index are obtained from 12:00 until 15:00 as illustrated on *Figure 40*. The average UTCI average value throughout this day of "C32" is 28.1˚C.

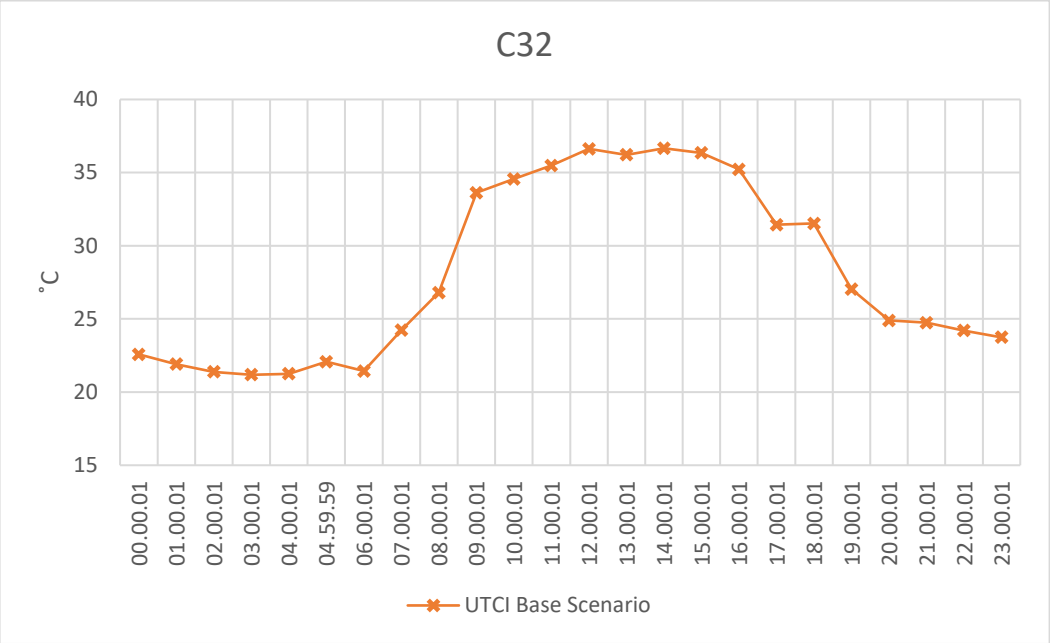

Figure 40. Graphical illustration of UTCI performance of Courtyard 32

4.2.33 Courtyard 33

Courtyard “C33” UTCI values vary from a minimum of 20.4˚C to a maximum of 36.4˚C. The maximum values of Universal thermal comfort index are obtained from 12:00 until 15:00 as illustrated on *Figure 41*. The average UTCI average value throughout this day of “C33” is 28.4˚C.

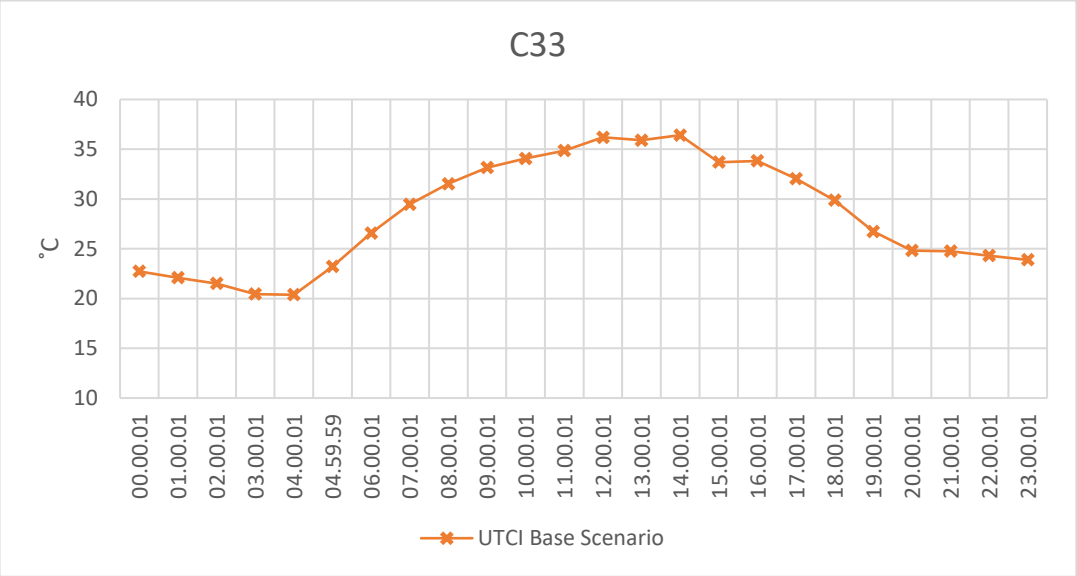

Figure 41. Graphical illustration of UTCI performance of Courtyard 33

4.3 Macroscale

In order to provide a better understanding of the data output visualized above where every courtyard's UTCI values are visualized through graph a general overview is needed.

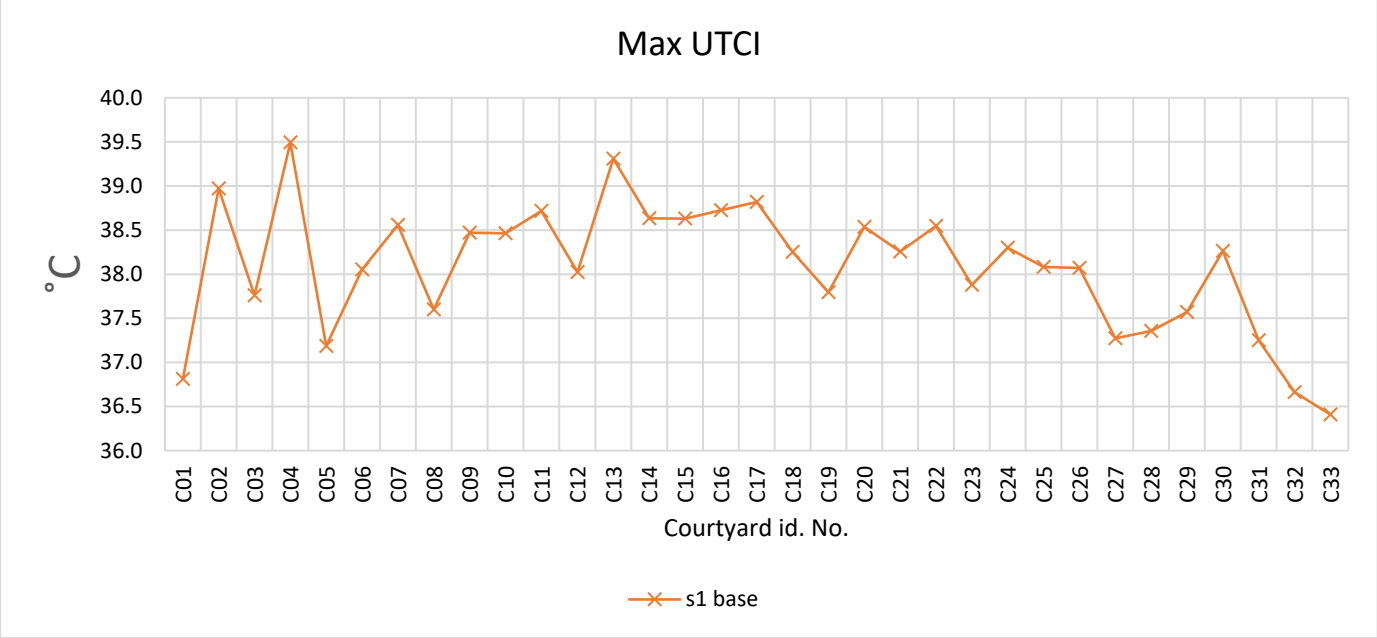

Figure 42. Graphical illustration of max UTCI performance of all courtyards

Figure 42 illustrates the differences between maximum values of UTCI within all courtyards. As it is shown, UTCI values range from 36.8 ˚C to 39.5 ˚C.

In order to distinguish a correlation between courtyard's UTCI values and the built area morphology, some of the morphological indicators are observed as showcased below.

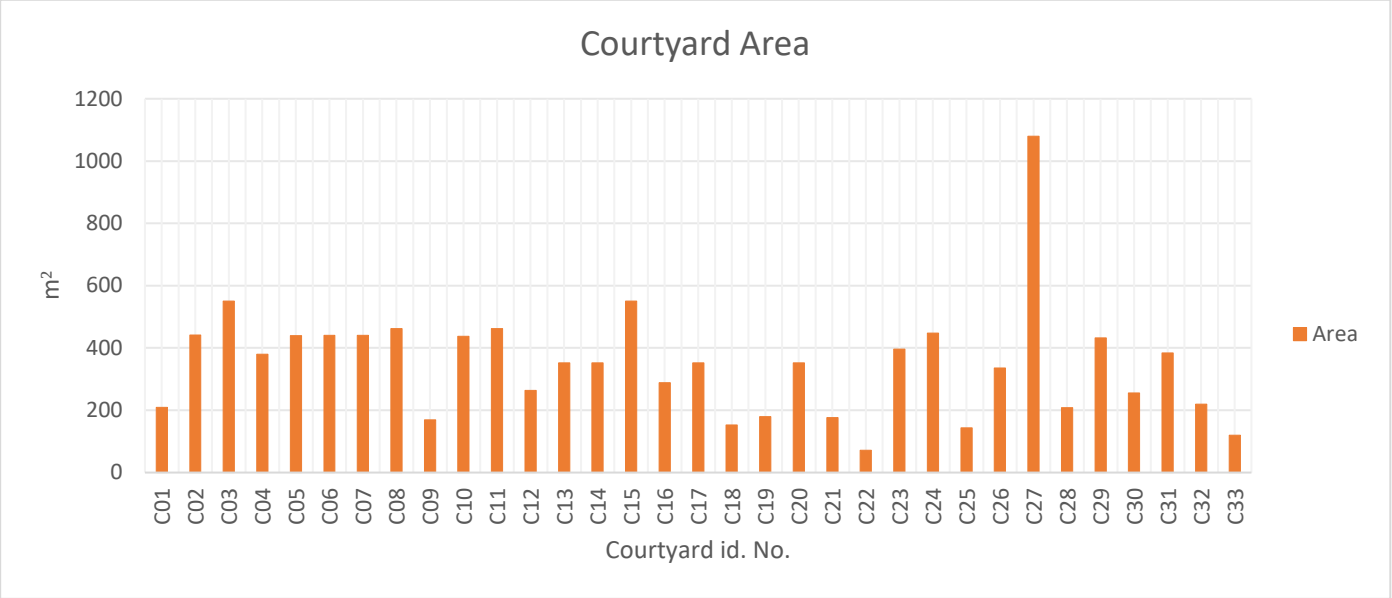

Figure 43. Graphical illustration of surface area morphological indicator

Figure 43 shows the visual representation of all courtyards areas and through observations it is clear that there is no evident correlation between courtyard area and UTCI.

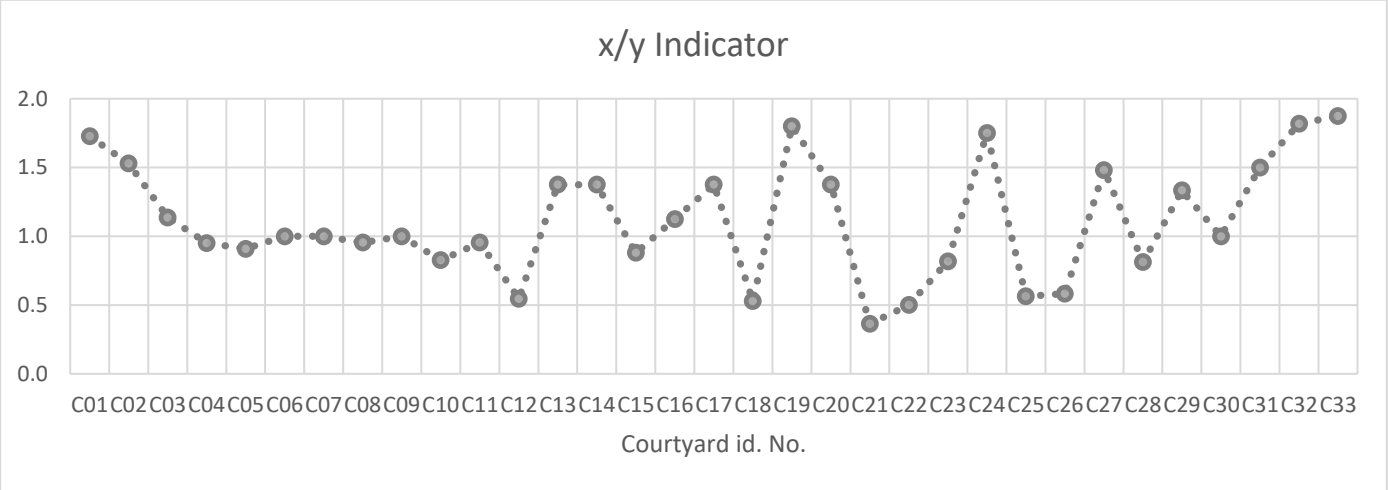

Figure 44. Graphical illustration of courtyard width over length morphological indicator

Figure 44 shows a visual representation in line-graph form of the width over length morphological indicator. It is visible that there is no direct correlation between the UTCI and the width over length morphological indicator.

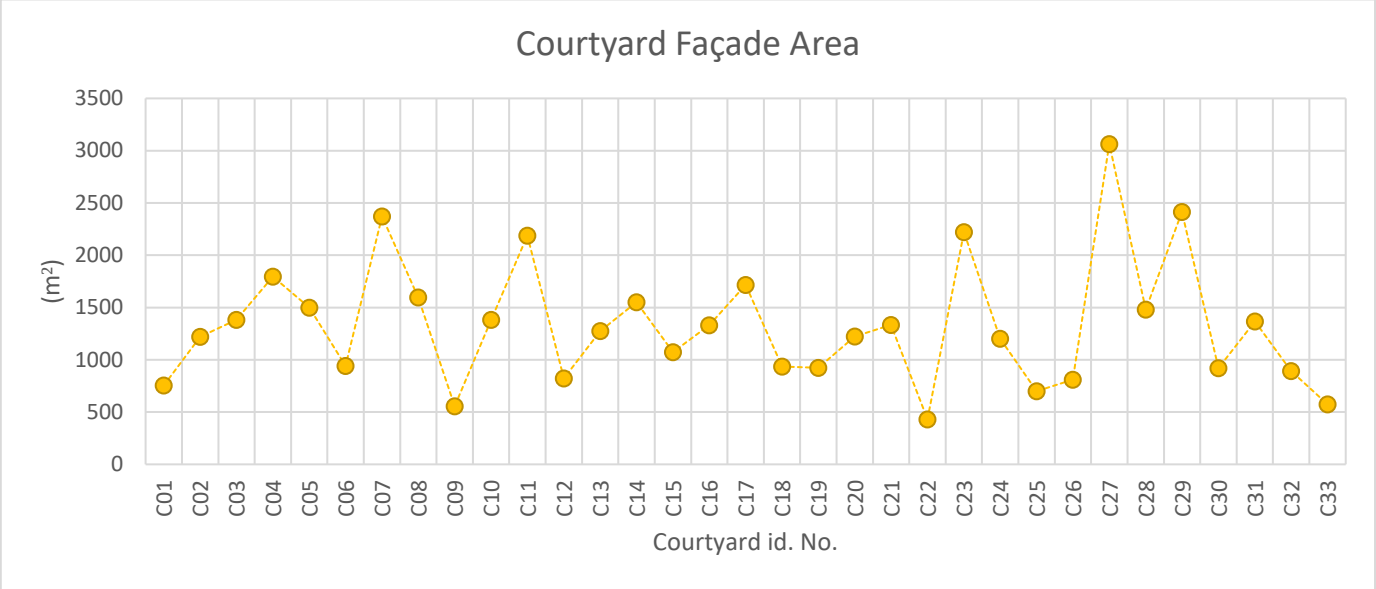

Figure 45. Graphical illustration of courtyard façade area morphological indicator

Figure 45 shows a visual representation in line-graph form of the façade area morphological indicator. It is visible that there is a partial correlation between the fully enclosed courtyards façade area to the respective UTCI values. This correlations is visible through courtyards “C04”, “C06”, “C07”, “C11”, “C14”, “C17”, “C21”, “C23”, “C27” and “C29”.

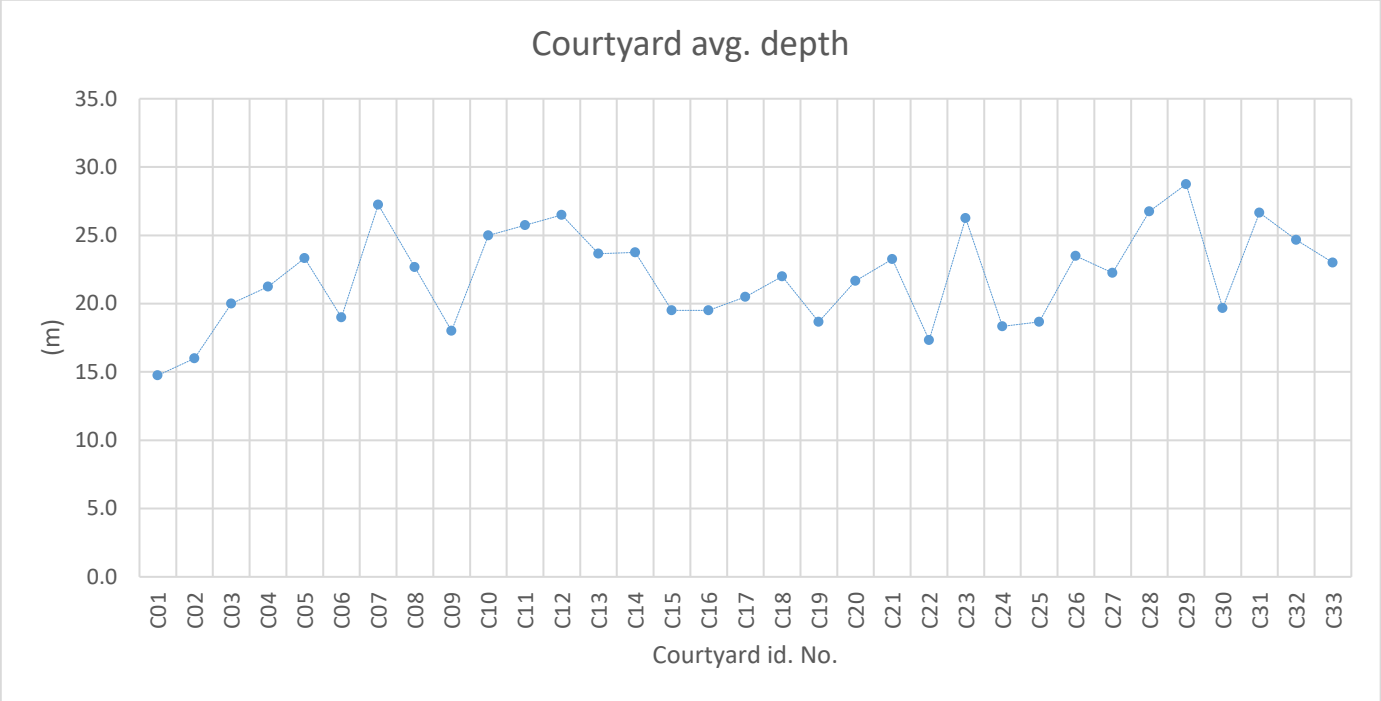

Figure 46. Graphical illustration of courtyard average depth morphological indicator

Figure 46 shows a visual representation in line-graph form of the façade area morphological indicator. It is visible that there is a correlation between the courtyards average depth to the respective UTCI values. This correlations is visible throughout all courtyards.

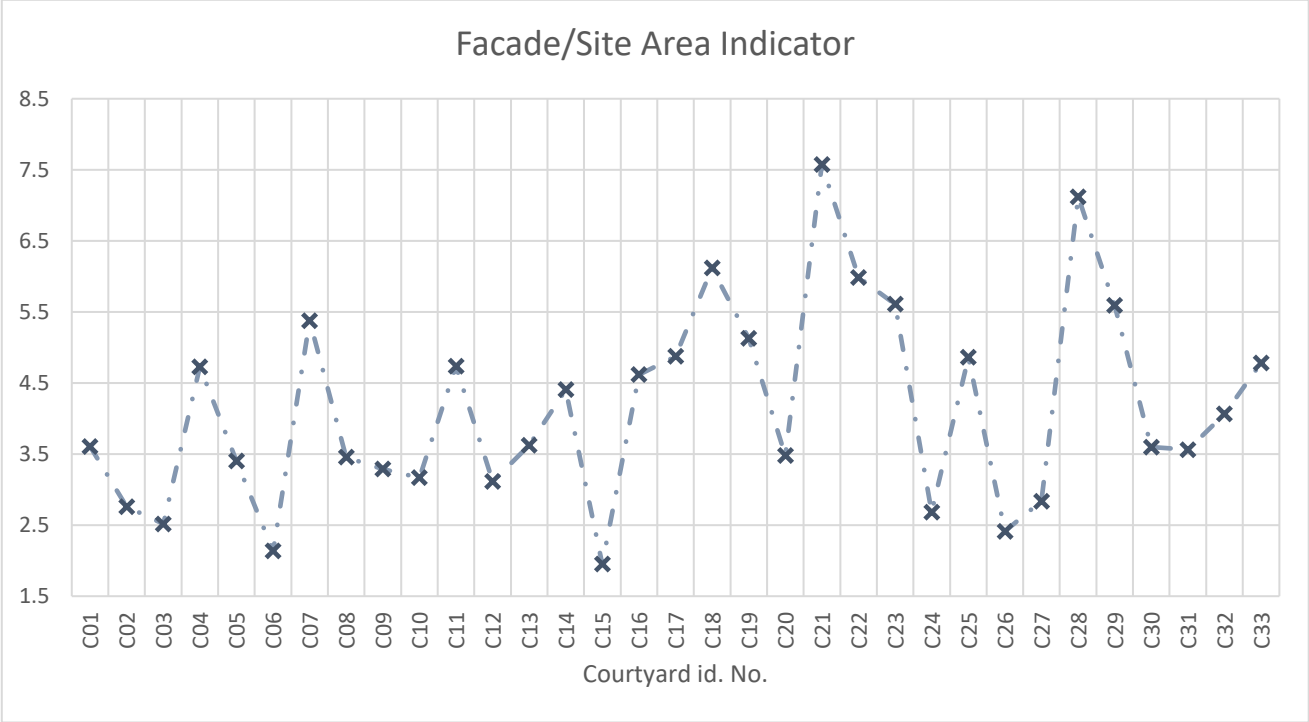

Figure 47. Graphical illustration of courtyard façade area over site area morphological indicator

Figure 47 shows a visual representation of the façade area over site area morphological indicator. It is visible that there is a correlation between the courtyards average depth to the respective UTCI values. This correlations is visible throughout all courtyards. This correlation is visible throughout all fully enclosed courtyards.

On a macro scale it is important to evaluate the overall performance in UTCI of every outdoor area on the maximum obtained values and on an average during the day.

As it is evident on *Figure 42* the maximum values of UTCI throughout all of the outdoor areas within the site fluctuate between 35 ˚C and 39.5 ˚C. This means that the thermal stress varies between moderate heat stress to strong heat stress.

Figure 49 on the other hand illustrates the average UTCI performance of all outdoor areas of the site. It is evident that throughout this day the average value of UTCI within Mangalem 21, varies between 28 ˚C and 29 ˚C. When referring to UTCI thermal stress categorization it is evident that throughout the simulated day the average sized human would experience on average moderate or higher heat stress during all times of the day.

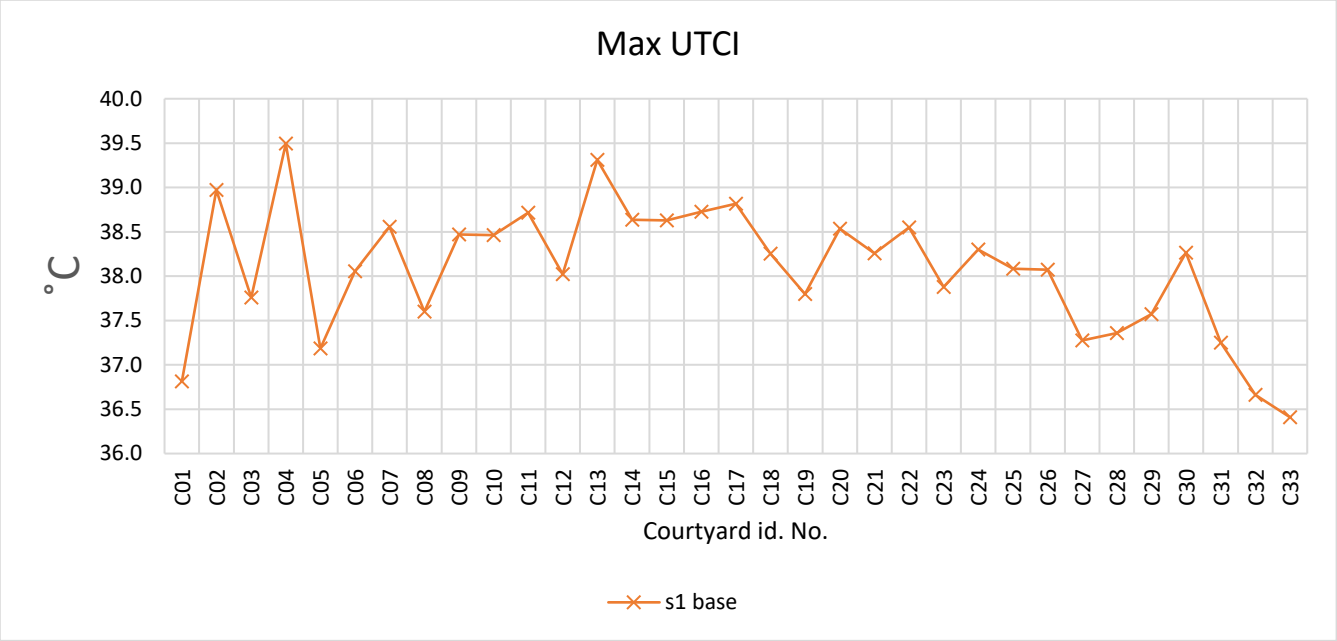

Figure 48. Graphical illustration of max. UTCI performance of all courtyards

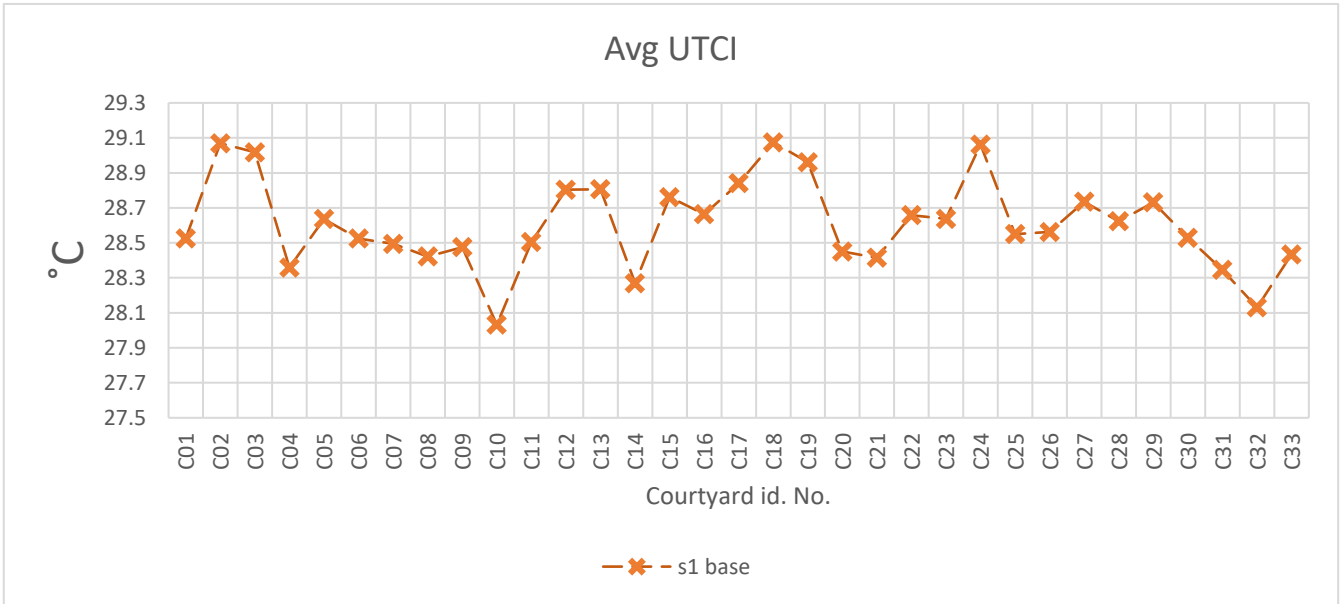

Figure 49. Graphical illustration of average UTCI performance of all courtyards

CHAPTER 5

OPTIMIZATION

5.1 Overview

To provide a better performing outdoor space, the UTCI of the analyzed outdoor spaces should fall within the rage of "no thermal stress", meaning that there is a need for the maximum and average values of UTCI to be lower. Hence this need, two different optimization scenarios are proposed and evaluated.

Both optimization scenarios do not interfere with the building morphology or the site's morphological attributes. The first proposed and evaluated scenario consists of installing façade greenery. The second scenario consists of implementation of a green roof along every building roof within the site as illustrated on *Figure 50*.

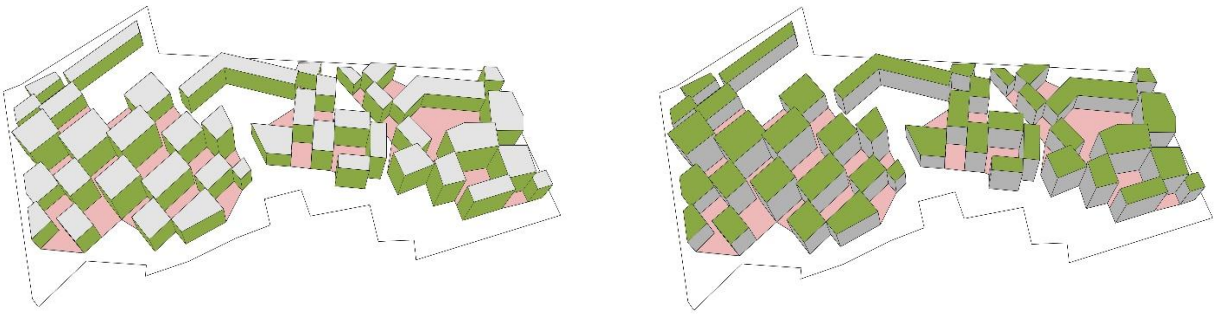

Figure 50. Graphical illustration of optimization scenarios

These two scenarios were modeled and simulated in the same way the base scenario was and the data obtained by these two simulations went through the same collection and extrapolation process as the initial simulation data.

To obtain a better understanding of the change in UTCI levels on both optimization cases, the results are examined in a micro scale and a macro scale.

5.2 Microscale

The UTCI values are examined regarding each courtyard individually to acquire a better understanding on the differences in performance of each optimization scenario. Courtyards are labeled as “Cn” for the purpose of evaluation and optimization scenarios are labeled as “s2 optimized” for the green façade scenario and “s3 optimized” for the green roof scenario.

5.2.1 Courtyard 01

Table 6. UTCI performance differences between optimization scenarios on “C01”

Name	Image	Difference (˚C)
C01 s2 optimized	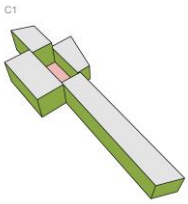	Avg. UTCI diff. = 2.66 ˚C Max. UTCI diff. = 2.41 ˚C
C01 s3 optimized	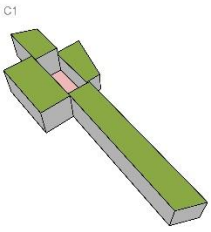	Avg. UTCI diff. = 0.11 ˚C Max. UTCI diff. = 1.17 ˚C

Table 6 and *Figure 51* illustrate the comparison of both optimization scenarios within courtyard “C01”. As it is shown above the difference in UTCI from the base model during the hottest hour of the day on the green façade “s2 optimized” is 2.41 ˚C, while the difference of average UTCI from the base/current state model is 2.66 ˚C.

The other optimization scenario displays a difference in UTCI during the hottest hour of the day of 1.17 ˚C and a difference on avg. UTCI of 0.11 ˚C. These differences in UTCI can be better observed on *Figure 51*.

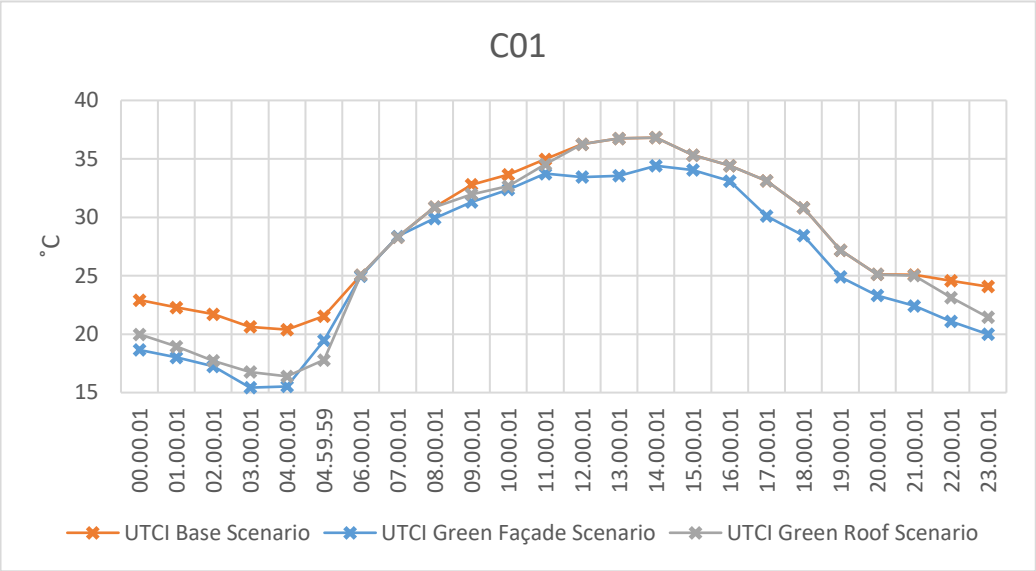

Figure 51. Graphical illustration of optimization UTCI performance of "C01"\

5.2.2 Courtyard 02

Table 7. UTCI performance differences between optimization scenarios on "C02"

Name	Image	Difference (˚C)
C02 s2 optimized	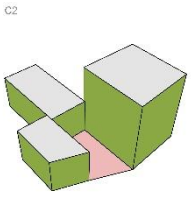	Avg. UTCI diff. = 2.06 ˚C Max. UTCI diff. = 1.63 ˚C

C02 s3 optimized	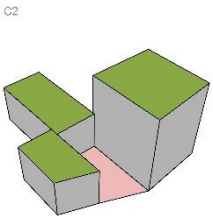	Avg. UTCI diff. = 0.04 ˚C Max. UTCI diff. = 1.41 ˚C

Table 7 and *Figure 52* illustrate the comparison of both optimization scenarios within courtyard “C02”. The data mentioned above indicates that the UTCI deviation from the baseline model on the green façade "s2 optimized" is 1.63 ˚C during the peak hour of the day, whereas the average UTCI deviation from the current state model is 2.06 ˚C. The alternative optimization scenario exhibits a variation in UTCI of 1.41 ˚C during the hour of highest temperature, and an average difference in UTCI of 0.04 ˚C. These differences in UTCI can be better observed on *Figure 52.*

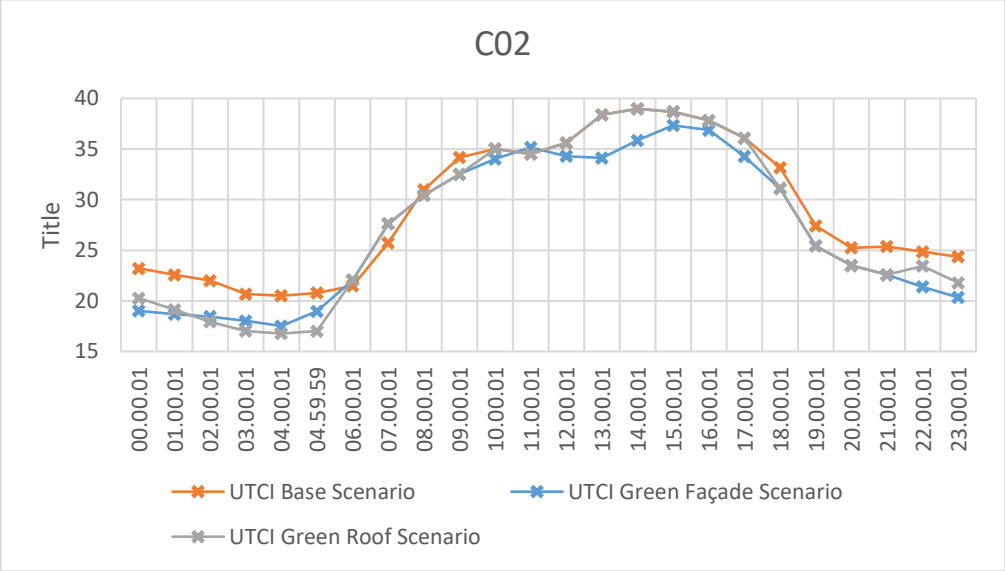

Figure 52. Graphical illustration of optimization UTCI performance of “C02”

5.2.3 Courtyard 03

Table 8. UTCI performance differences between optimization scenarios on "C03"

Name	Image	Difference (˚C)
C03 s2 optimized	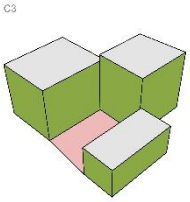	Avg. UTCI diff. = 2.09 ˚C Max. UTCI diff. = 1.78 ˚C
C03 s3 optimized	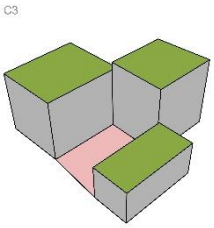	Avg. UTCI diff. = 0.02 ˚C Max. UTCI diff. = 1.18 ˚C

Table 8 and *Figure 53* illustrate the comparison of both optimization scenarios within courtyard "C03". As it is shown above the difference in UTCI from the base model during the hottest hour of the day on the green façade "s2 optimized" is 1.78 ˚C, while the difference of average UTCI from the base/current state model is 2.09 ˚C. The second optimization scenario exhibits a disparity in UTCI values during the peak hour of the day amounting to 1.18 ˚C, and an average UTCI difference of 0.02 ˚C. These differences in UTCI can be better observed on *Figure 53.*

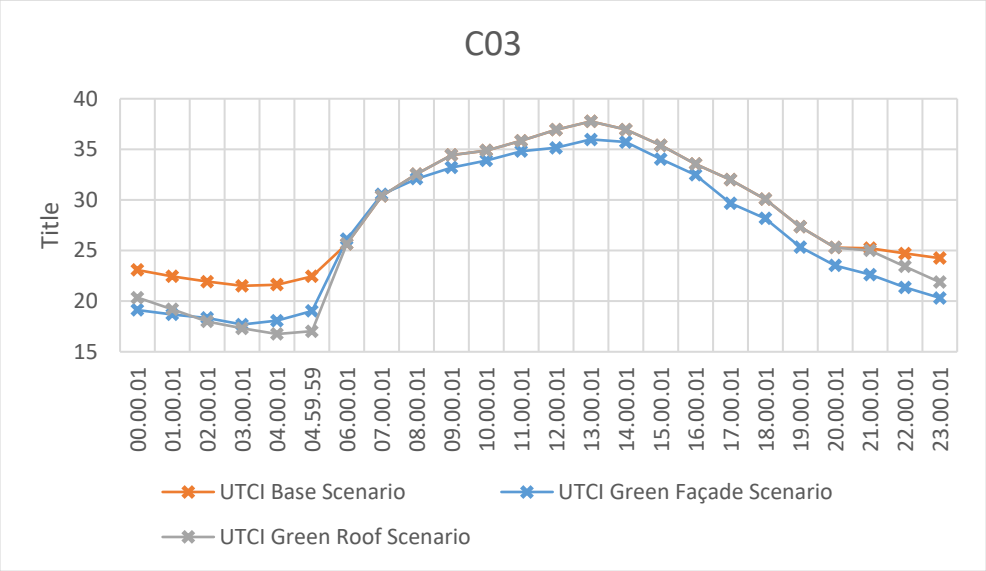

Figure 53. Graphical illustration of optimization UTCI performance of "C03"

5.2.4 Courtyard 04

Table 9. UTCI performance differences between optimization scenarios on "C04"

Name	Image	Difference (˚C)
C04 s2 optimized	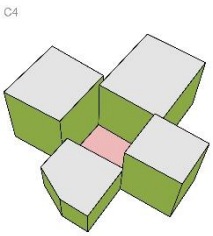	Avg. UTCI diff. = 1.77 ˚C Max. UTCI diff. = 2.01 ˚C

C04 s3 optimized	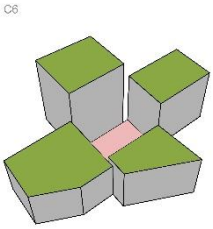	Avg. UTCI diff. = 1.31 ˚C Max. UTCI diff. = 0.61 ˚C

Table 9 and Figure 54 depict a comparison between two optimization scenarios in courtyard "C04". As it is shown above the difference in UTCI from the base model during the hottest hour of the day on the green façade “s2 optimized” is 2.01 ˚C, while the difference of average UTCI from the base/current state model is 1.77 ˚C. The alternative optimization scenario exhibits a variation in UTCI of 0.61 ˚C during the peak hour of the day and an average UTCI difference of 1.31 ˚C. These differences in UTCI can be better observed on *Figure 54.*

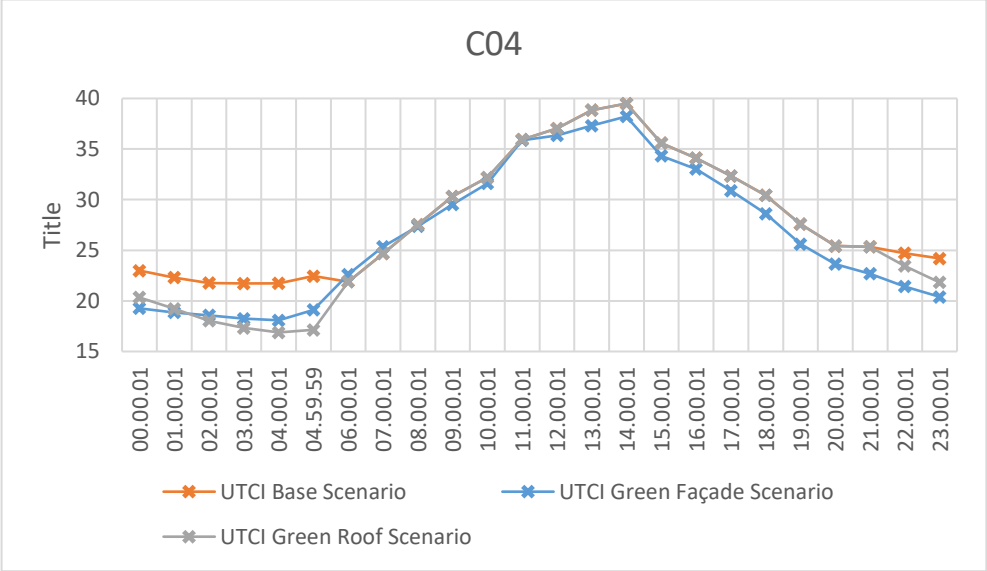

Figure 54. Graphical illustration of optimization UTCI performance of “C04”

5.2.5 Courtyard 05

Table 10. UTCI performance differences between optimization scenarios on "C05"

Name	Image	Difference (˚C)
C05 s2 optimized	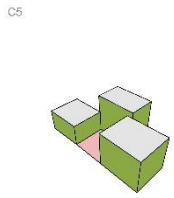	Avg. UTCI diff. = 1.51 ˚C Max. UTCI diff. = 2.05 ˚C
C05 s3 optimized	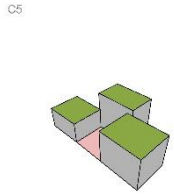	Avg. UTCI diff. = 1.31 ˚C Max. UTCI diff. = 0.61˚C

Table 10 and *Figure 55* illustrate the comparison of both optimization scenarios within courtyard "C05". As it is shown above the difference in UTCI from the base model during the hottest hour of the day on the green façade "s2 optimized" is 2.05 ˚C, while the difference of average UTCI from the base/current state model is 1.51 ˚C. The other optimization scenario displays a difference in UTCI during the hottest hour of the day of 0.61 ˚C and a difference on avg. UTCI of 1.31 ˚C. These differences in UTCI can be better observed on *Figure 55.*

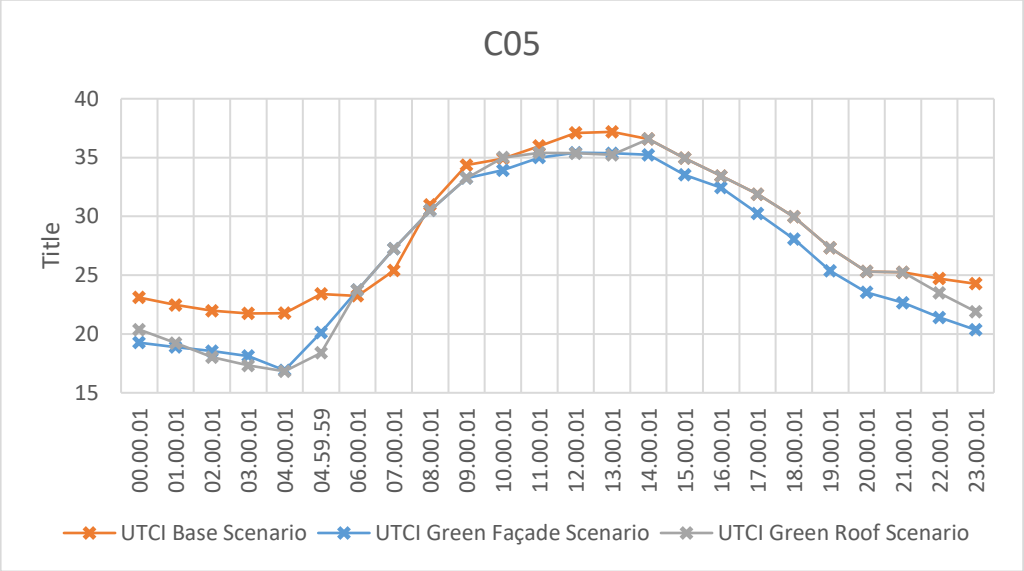

Figure 55. Graphical illustration of optimization UTCI performance of "C05"

5.2.6 Courtyard 06

Table 11. UTCI performance differences between optimization scenarios on "C06"

Name	Image	Difference (˚C)
C06 s2 optimized	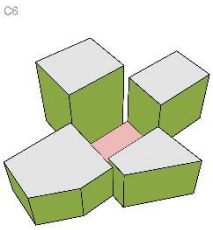	Avg. UTCI diff. = 2.05 ˚C Max. UTCI diff. = 1.51 ˚C
C06 s3 optimized	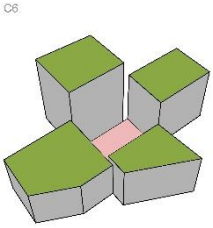	Avg. UTCI diff. = 0.66 ˚C Max. UTCI diff. = 0.01 ˚C

Table 11 and *Figure 56* illustrate the comparison of both optimization scenarios within courtyard “C06”. The aforementioned data illustrates that the UTCI deviation from the base model on the green façade "s2 optimized" is 2.05 ˚C at the peak hour of the day, whereas the average UTCI deviation from the current state model is 1.51 ˚C. The alternative optimization scenario exhibits a marginal variation of 0.01 ˚C in UTCI during the peak hour of the day and an average difference of 0.66 ˚C in UTCI. These differences in UTCI can be better observed on *Figure 56.*

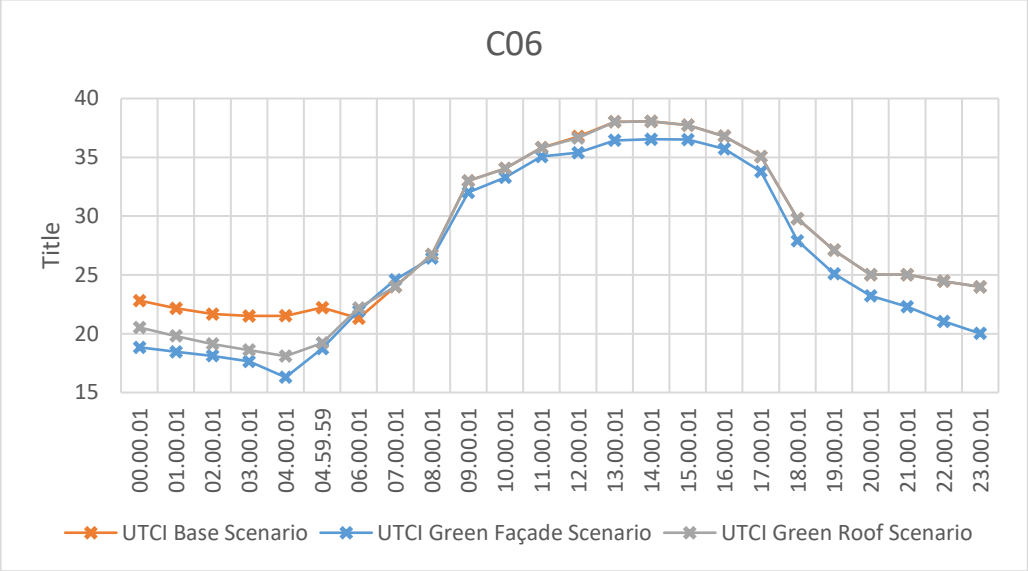

Figure 56. Graphical illustration of optimization UTCI performance of “C06”

5.2.7 Courtyard 07

Table 12. UTCI performance differences between optimization scenarios on “C07”

Name	Image	Difference (˚C)

C07 s2 optimized

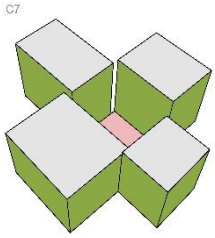

Avg. UTCI diff. = 1.83 ˚C

Max. UTCI diff. = 1.56 ˚C

C07 s3 optimized

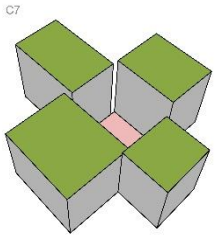

Avg. UTCI diff. = 0.77 ˚C

Max. UTCI diff. = 0.02 ˚C

Table 12 and *Figure 57* illustrate the comparison of both optimization scenarios within courtyard “C07”. As it is shown above the difference in UTCI from the base model during the hottest hour of the day on the green façade “s2 optimized” is 1.56 ˚C, while the difference of average UTCI from the base/current state model is 1.83 ˚C. The other optimization scenario displays a difference in UTCI during the hottest hour of the day of 0.02 ˚C and a difference on avg. UTCI of 0.77 ˚C. These differences in UTCI can be better observed on *Figure 57.*

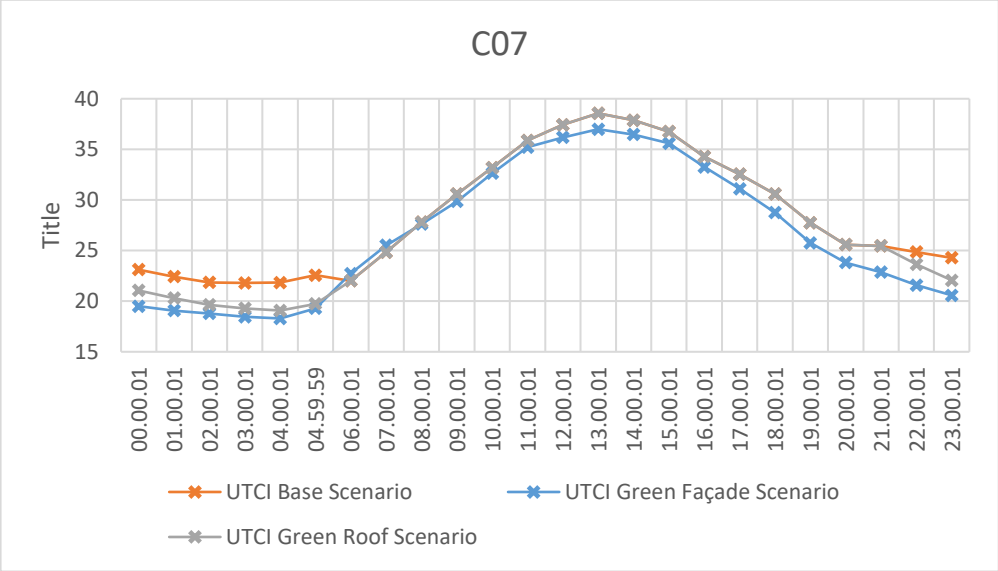

Figure 57. Graphical illustration of optimization UTCI performance of "C07"

5.2.8 Courtyard 08

Table 13. UTCI performance differences between optimization scenarios on "C08"

Name	Image	Difference (˚C)
C08 s2 optimized	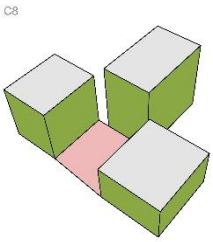	Avg. UTCI diff. = 2.24 ˚C Max. UTCI diff. = 2.11 ˚C
C08 s3 optimized	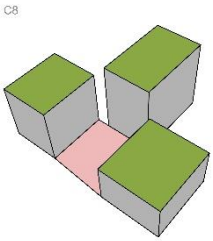	Avg. UTCI diff. = 0.34 ˚C Max. UTCI diff. = 0.01 ˚C

Table 13 and *Figure 58* illustrate the comparison of both optimization scenarios within courtyard "C08". As it is shown above the difference in UTCI from the base model during the hottest hour of the day on the green façade "s2 optimized" is 2.11˚C, while the difference of average UTCI from the base/current state model is 2.24 ˚C. The other optimization scenario displays a difference in UTCI during the hottest hour of the day of 0.01 ˚C and a difference on avg. UTCI of 0.34 ˚C. These differences in UTCI can be better observed on *Figure 58.*

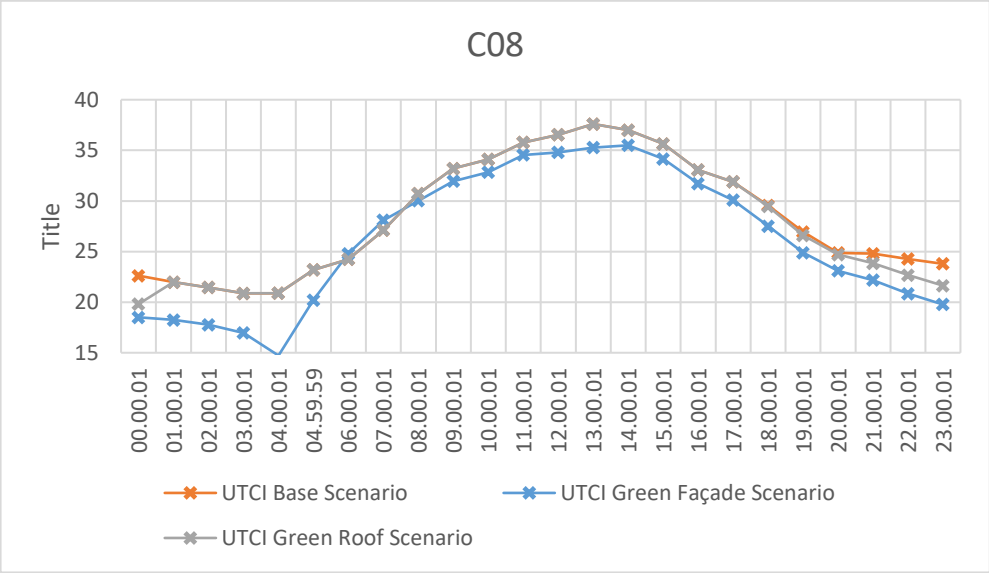

Figure 58. Graphical illustration of optimization UTCI performance of "C08"

5.2.9 Courtyard 09

Table 14. UTCI performance differences between optimization scenarios on "C09"

Name	Image	Difference (˚C)

C09 s2 optimized	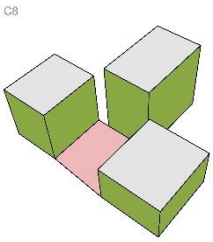	Avg. UTCI diff. = 1.61 ˚C Max. UTCI diff. = 2.15 ˚C
C09 s3 optimized	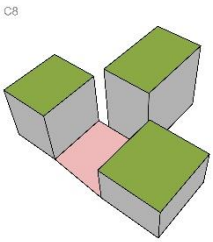	Avg. UTCI diff. = 0.21 ˚C Max. UTCI diff. = 0.01 ˚C

Table 14 and *Figure 59* illustrate the comparison of both optimization scenarios within courtyard “C09”. As it is shown above the difference in UTCI from the base model during the hottest hour of the day on the green façade “s2 optimized” is 2.15˚C, while the difference of average UTCI from the base/current state model is 1.61 ˚C. The other optimization scenario displays a difference in UTCI during the hottest hour of the day of 0.01 ˚C and a difference on avg. UTCI of 0.21 ˚C. These differences in UTCI can be better observed on *Figure 59.*

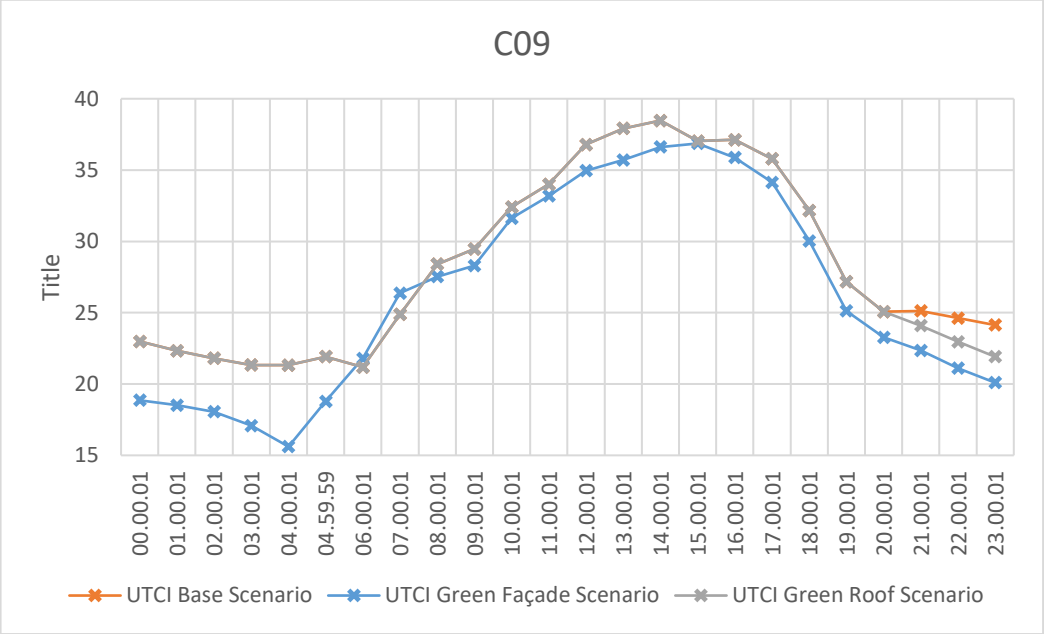

Figure 59. Graphical illustration of optimization UTCI performance of "C09"

5.2.10 Courtyard 10

Table 15 and *Figure 60* illustrate the comparison of both optimization scenarios within courtyard "C10". As it is shown above the difference in UTCI from the base model during the hottest hour of the day on the green façade "s2 optimized" is 1.65 ˚C, while the difference of average UTCI from the base/current state model is 2.02 ˚C. The other optimization scenario displays a difference in UTCI during the hottest hour of the day of 0.01 ˚C and a difference on avg. UTCI of 0.82 ˚C. These differences in UTCI can be better observed on *Figure 60.*

Table 15. UTCI performance differences between optimization scenarios on "C10"

Name	Image	Difference (˚C)

C10 s2 optimized	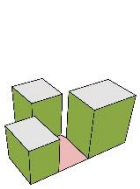	Avg. UTCI diff. = 2.02 ˚C Max. UTCI diff. = 1.65 ˚C
C10 s3 optimized	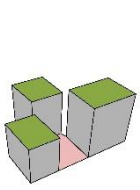	Avg. UTCI diff. = 0.82 ˚C Max. UTCI diff. = 0.01 ˚C

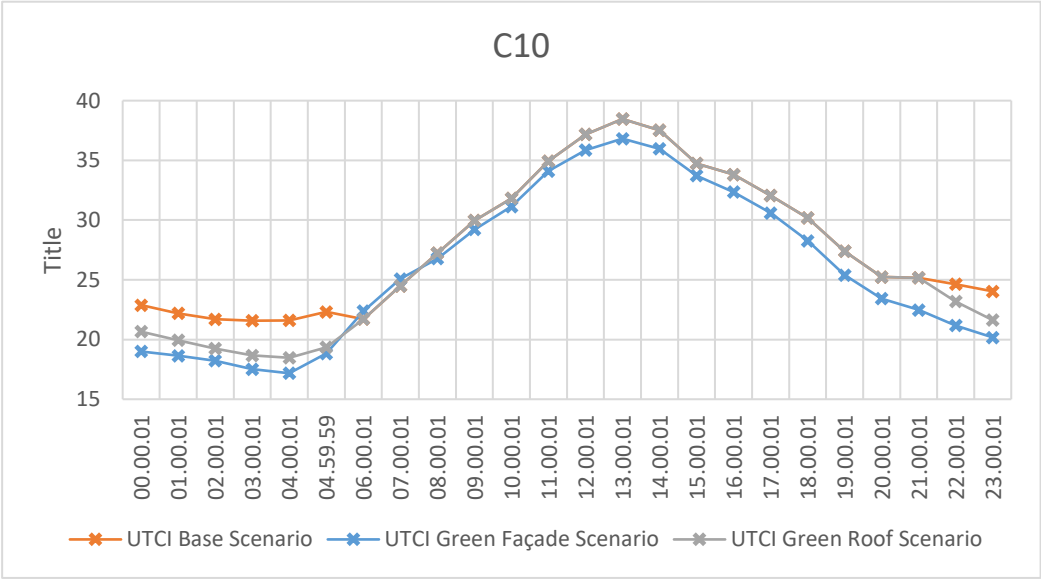

Figure 60. Graphical illustration of optimization UTCI performance of "C10"

5.2.11 Courtyard 11

Table 16 and *Figure 61* depict a comparative analysis of the two optimization scenarios in courtyard "C11". The results indicate that the UTCI differential between

the base model and the green façade "s2 optimized" during the hottest hour of the day is 1.69 ˚C. Moreover, the average UTCI differential between the base/current state model and the aforementioned green façade is 1.9 ˚C. The alternative optimization scenario exhibits a marginal variation of 0.01 ˚C in UTCI during the peak hour of the day, and an average difference of 0.57 ˚C in UTCI. These differences in UTCI can be better observed on *Figure 61*.

Table 16. UTCI performance differences between optimization scenarios on "C11"

Name	Image	Difference (˚C)
C11 s2 optimized	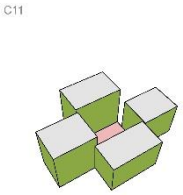	Avg. UTCI diff. = 1.9 ˚C Max. UTCI diff. = 1.69 ˚C
C11 s3 optimized	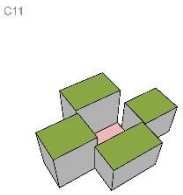	Avg. UTCI diff. = 0.57 ˚C Max. UTCI diff. = 0.01 ˚C

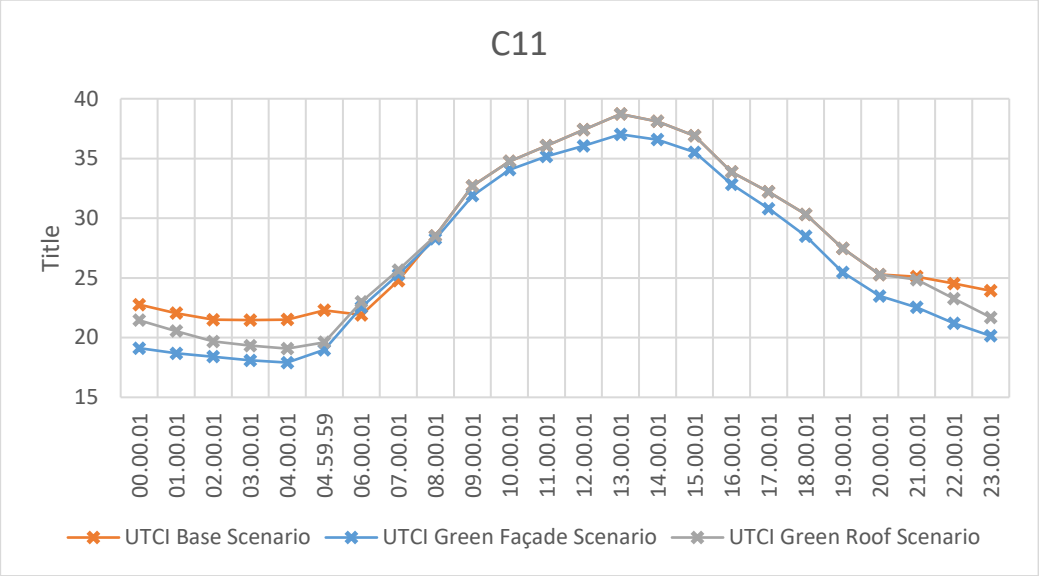

Figure 61. Graphical illustration of optimization UTCI performance of "C10"

5.2.12 Courtyard 12

Table 17. UTCI performance differences between optimization scenarios on "C12"

Name	Image	Difference (˚C)
C12 s2 optimized		Avg. UTCI diff. = 1.61 ˚C Max. UTCI diff. = 2.15 ˚C
C12 s3 optimized	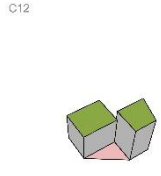	Avg. UTCI diff. = 0.21 ˚C Max. UTCI diff. = 0.01 ˚C

Table 17 and *Figure 62* illustrate the comparison of both optimization scenarios within courtyard "C12". As it is shown above the difference in UTCI from the base model during the hottest hour of the day on the green façade "s2 optimized" is 2.15˚C, while the difference of average UTCI from the base/current state model is 1.61 ˚C. The other optimization scenario displays a difference in UTCI during the hottest hour of the day of 0.01 ˚C and a difference on avg. UTCI of 0.21 ˚C. These differences in UTCI can be better observed on *Figure 62.*

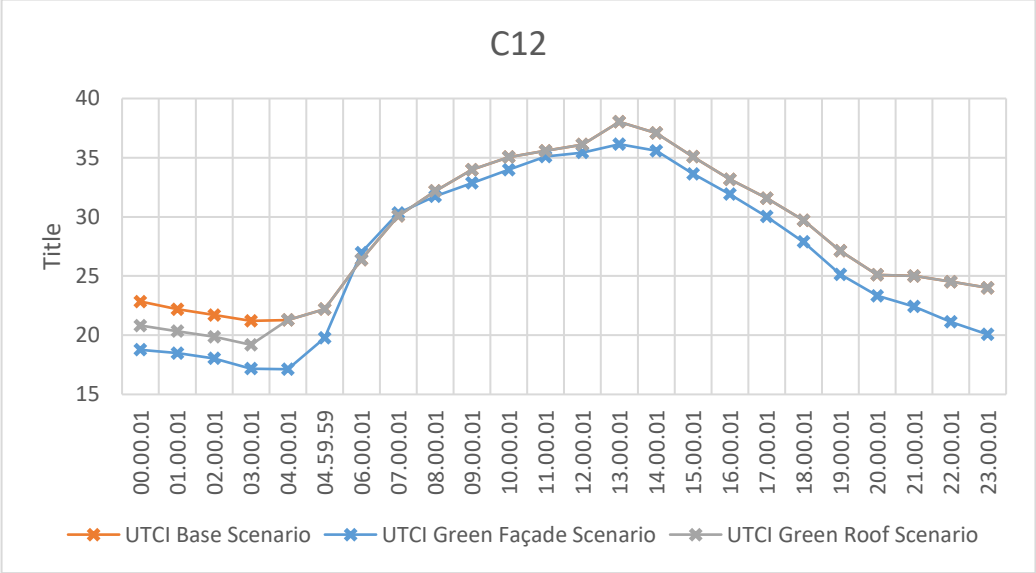

Figure 62. Graphical illustration of optimization UTCI performance of "C12"

5.2.13 Courtyard 13

Table 18. UTCI performance differences between optimization scenarios on "C13"

Name	Image	Difference (˚C)

C13 s2 optimized	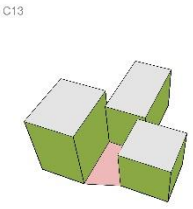	Avg. UTCI diff. = 1.93 ˚C Max. UTCI diff. = 1.29 ˚C
C13 s3 optimized	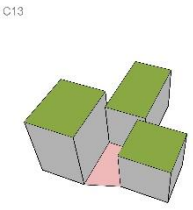	Avg. UTCI diff. = 0.67 ˚C Max. UTCI diff. = 0.01 ˚C

Table 18 and *Figure 63* illustrate the comparison of both optimization scenarios within courtyard “C13”. As it is shown above the difference in UTCI from the base model during the hottest hour of the day on the green façade “s2 optimized” is 1.29˚C, while the difference of average UTCI from the base/current state model is 1.93 ˚C. The other optimization scenario displays a difference in UTCI during the hottest hour of the day of 0.01 ˚C and a difference on avg. UTCI of 0.67 ˚C. These differences in UTCI can be better observed on *Figure 63.*

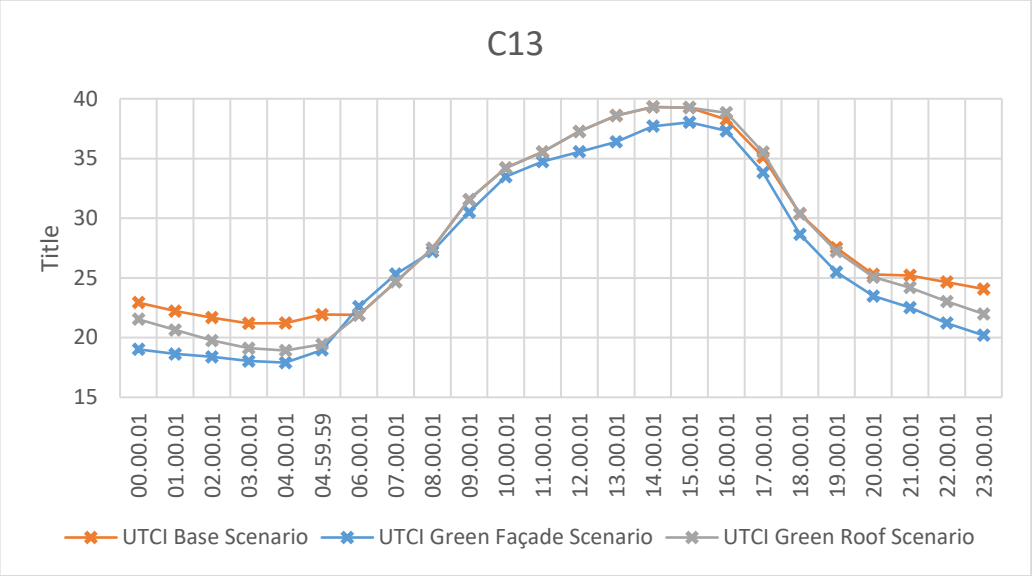

Figure 63. Graphical illustration of optimization UTCI performance of "C13"

5.2.14 Courtyard 14

Table 19. UTCI performance differences between optimization scenarios on "C14"

Name	Image	Difference (˚C)
C14 s2 optimized	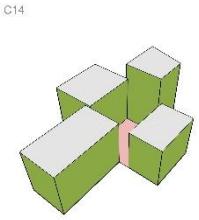	Avg. UTCI diff. = 1.89 ˚C Max. UTCI diff. = 1.43 ˚C

C14 s3 optimized

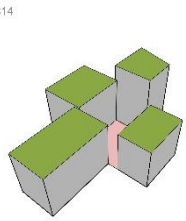

Avg. UTCI diff. = 0.96 ˚C

Max. UTCI diff. = 0.72 ˚C

Table 19 and *Figure 64* illustrate the comparison of both optimization scenarios within courtyard "C14". As it is shown above the difference in UTCI from the base model during the hottest hour of the day on the green façade "s2 optimized" is 1.43˚C, while the difference of average UTCI from the base/current state model is 1.89 ˚C. The other optimization scenario displays a difference in UTCI during the hottest hour of the day of 0.72 ˚C and a difference on avg. UTCI of 0.96 ˚C. These differences in UTCI can be better observed on *Figure 64.*

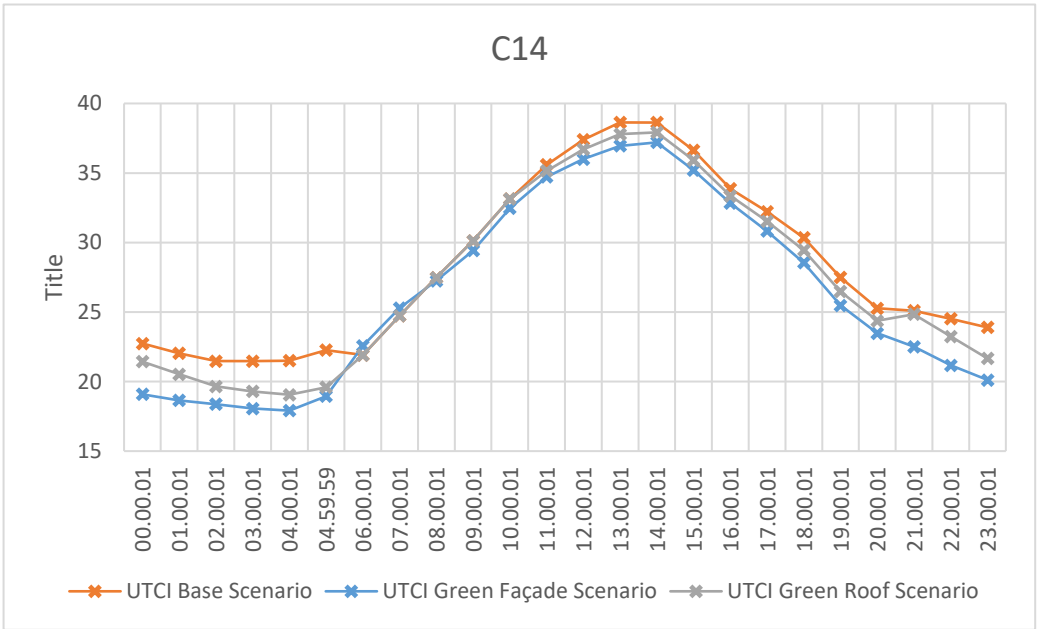

Figure 64. Graphical illustration of optimization UTCI performance of "C14"

5.2.15 Courtyard 15

Table 20. UTCI performance differences between optimization scenarios on "C15"

Name	Image	Difference (˚C)
C15 s2 optimized	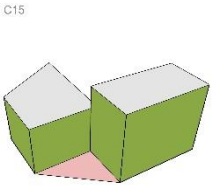	Avg. UTCI diff. = 2.06 ˚C Max. UTCI diff. = 1.23 ˚C
C15 s3 optimized	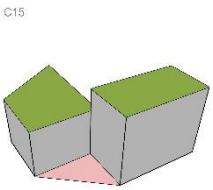	Avg. UTCI diff. = 0.59 ˚C Max. UTCI diff. = 0.01 ˚C

Table 20 and *Figure 65* illustrate the comparison of both optimization scenarios within courtyard "C15". As it is shown above the difference in UTCI from the base model during the hottest hour of the day on the green façade "s2 optimized" is 1.23˚C, while the difference of average UTCI from the base/current state model is 2.06 ˚C. The other optimization scenario displays a difference in UTCI during the hottest hour of the day of 0.01 ˚C and a difference on avg. UTCI of 0.59 ˚C. These differences in UTCI can be better observed on *Figure 65.*

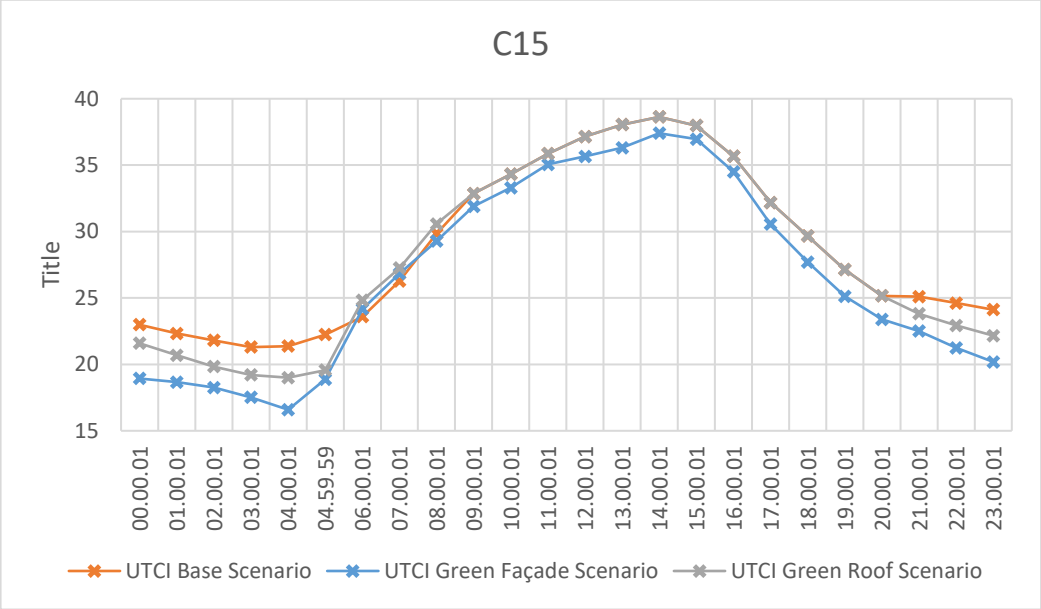

Figure 65. Graphical illustration of optimization UTCI performance of "C15"

5.2.16 Courtyard 16

Table 21. UTCI performance differences between optimization scenarios on "C16"

Name	Image	Difference (˚C)
C16 s2 optimized	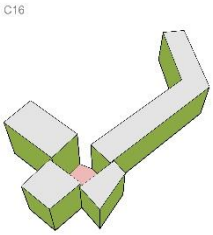	Avg. UTCI diff. = 1.97 ˚C Max. UTCI diff. = 2.43 ˚C

C16 s3 optimized	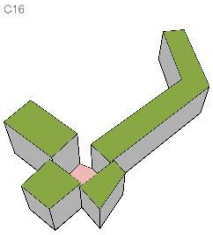	Avg. UTCI diff. = 0.58 ˚C Max. UTCI diff. = 0.82 ˚C

Table 21 and *Figure 66* illustrate the comparison of both optimization scenarios within courtyard "C16". As it is shown above the difference in UTCI from the base model during the hottest hour of the day on the green façade "s2 optimized" is 2.43˚C, while the difference of average UTCI from the base/current state model is 1.97 ˚C. The other optimization scenario displays a difference in UTCI during the hottest hour of the day of 0.82 ˚C and a difference on avg. UTCI of 0.58 ˚C. These differences in UTCI can be better observed on *Figure 66.*

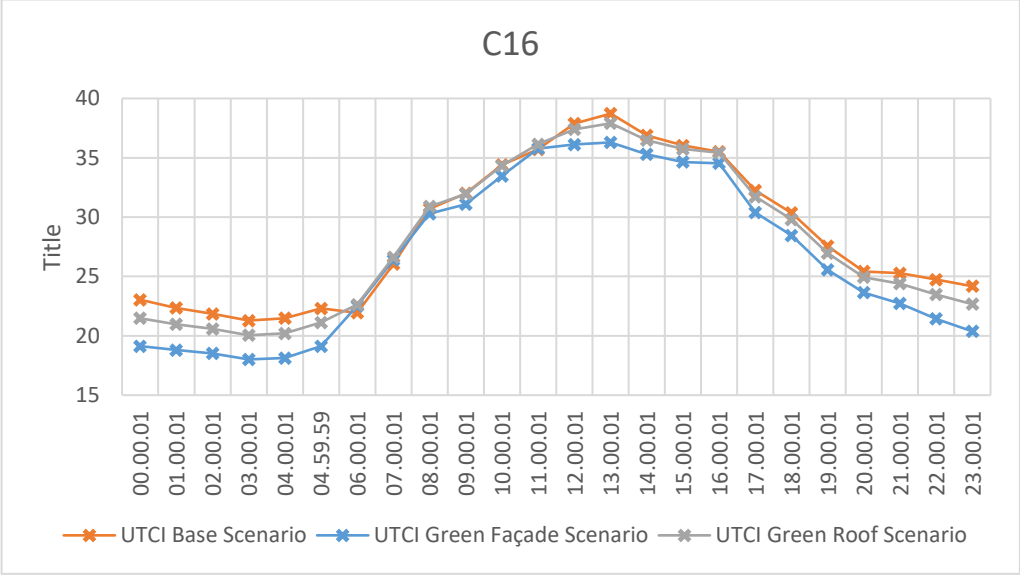

Figure 66. Graphical illustration of optimization UTCI performance of "C16"

5.2.17 Courtyard 17

Table 22 and *Figure 67* illustrate the comparison of both optimization scenarios within courtyard "C17". As it is shown above the difference in UTCI from the base model during the hottest hour of the day on the green façade "s2 optimized" is 1.42˚C, while the difference of average UTCI from the base/current state model is 1.42 ˚C. The other optimization scenario displays a difference in UTCI during the hottest hour of the day of 0.41 ˚C and a difference on avg. UTCI of 0.32 ˚C. These differences in UTCI can be better observed on *Figure 67.*

Table 22. UTCI performance differences between optimization scenarios on "C17"

Name	Image	Difference (˚C)
C17 s2 optimized	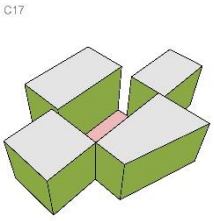	Avg. UTCI diff. = 1.99 ˚C Max. UTCI diff. = 1.42 ˚C
C17 s3 optimized	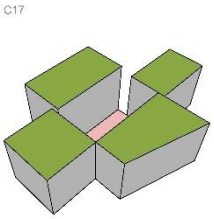	Avg. UTCI diff. = 0.32 ˚C Max. UTCI diff. = 0.41 ˚C

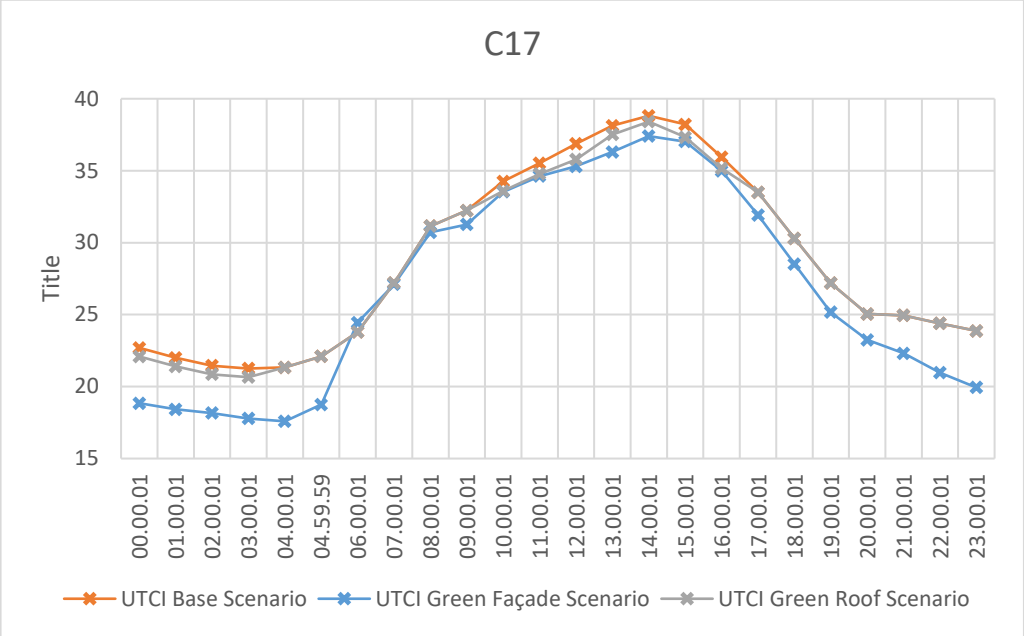

Figure 67. Graphical illustration of optimization UTCI performance of "C17"

5.2.18 Courtyard 18

Table 23 and *Figure 68* illustrate the comparison of both optimization scenarios within courtyard "C18". As it is shown above the difference in UTCI from the base model during the hottest hour of the day on the green façade "s2 optimized" is 1.42˚C, while the difference of average UTCI from the base/current state model is 1.42 ˚C. The other optimization scenario displays a difference in UTCI during the hottest hour of the day of 0.41 ˚C and a difference on avg. UTCI of 0.32 ˚C. These differences in UTCI can be better observed on *Figure 68.*

Table 23. UTCI performance differences between optimization scenarios on "C18"

Name	Image	Difference (˚C)

C18 s2 optimized	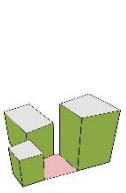	Avg. UTCI diff. = 1.63 ˚C Max. UTCI diff. = 1.95 ˚C
C18 s3 optimized	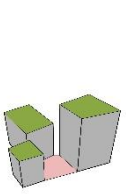	Avg. UTCI diff. = 0.1 ˚C Max. UTCI diff. = 0.2 ˚C

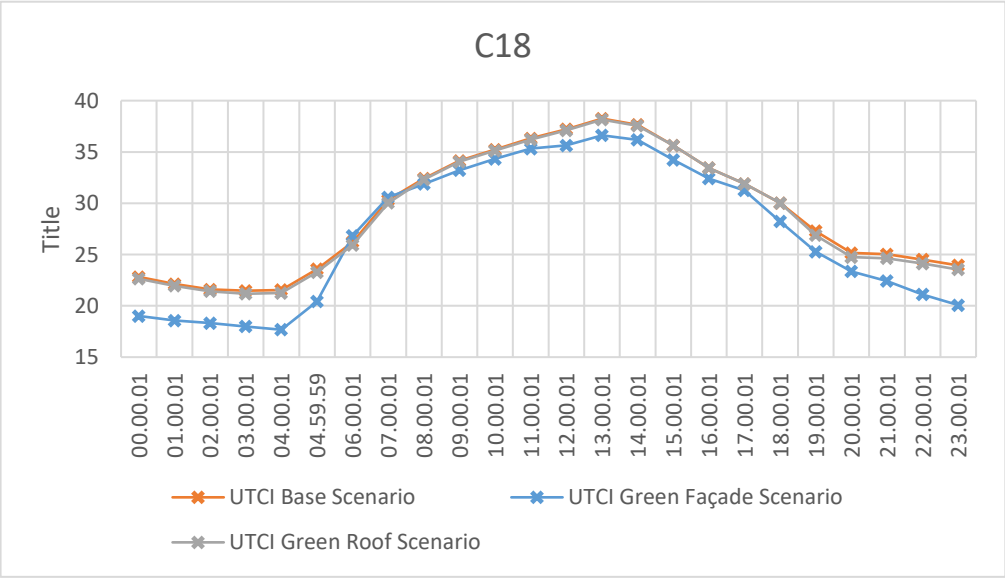

Figure 68. Graphical illustration of optimization UTCI performance of "C18"

5.2.19 Courtyard 19

Table 24 and *Figure 69* illustrate the comparison of both optimization scenarios within courtyard "C19". As it is shown above the difference in UTCI from the base model during the hottest hour of the day on the green façade "s2 optimized" is 1.27˚C, while the difference of average UTCI from the base/current state model is 2.32 ˚C. The other optimization scenario displays a difference in UTCI during the hottest hour of the day of 0.5 ˚C and a difference on avg. UTCI of 0.75 ˚C. These differences in UTCI can be better observed on *Figure 69.*

Table 24. UTCI performance differences between optimization scenarios on "C19"

Name	Image	Difference (˚C)
C19 s2 optimized	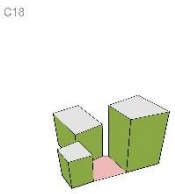	Avg. UTCI diff. = 2.32 ˚C Max. UTCI diff. = 1.27 ˚C
C19 s3 optimized	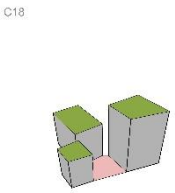	Avg. UTCI diff. = 0.75 ˚C Max. UTCI diff. = 0.5 ˚C

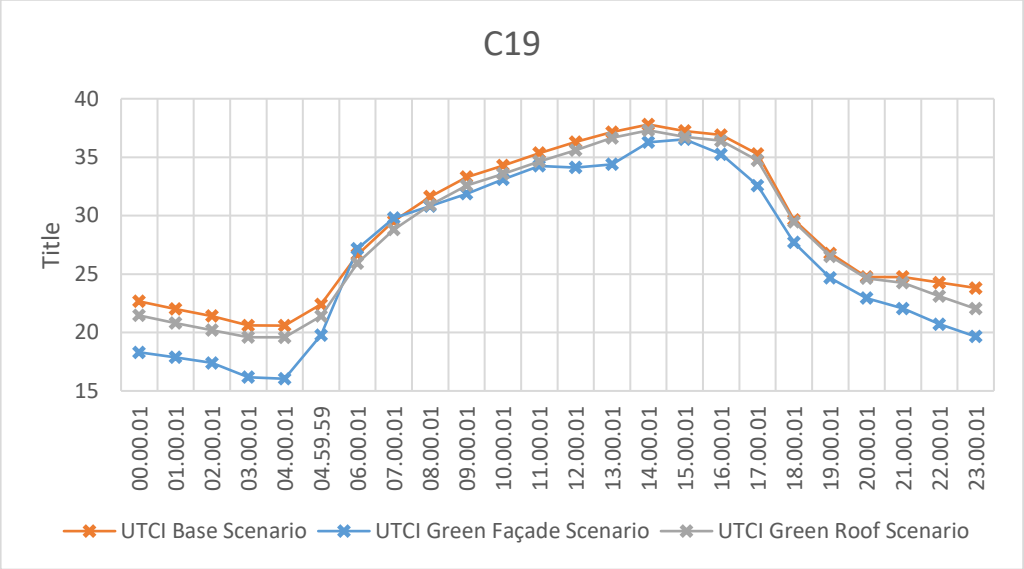

Figure 69. Graphical illustration of optimization UTCI performance of "C19"

5.2.20 Courtyard 20

Table 25 and *Figure 70* illustrate the comparison of both optimization scenarios within courtyard "C20". As it is shown above the difference in UTCI from the base model during the hottest hour of the day on the green façade "s2 optimized" is 1.37˚C, while the difference of average UTCI from the base/current state model is 2.1 ˚C. The other optimization scenario displays a difference in UTCI during the hottest hour of the day of 1.38 ˚C and a difference on avg. UTCI of 0.91 ˚C. These differences in UTCI can be better observed on *Figure 70.*

Table 25. UTCI performance differences between optimization scenarios on "C20"

Name	Image	Difference (˚C)

C20 s2 optimized	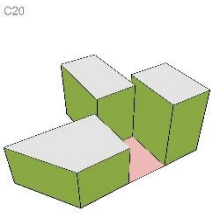	Avg. UTCI diff. = 2.1 ˚C Max. UTCI diff. = 1.37 ˚C
C20 s3 optimized	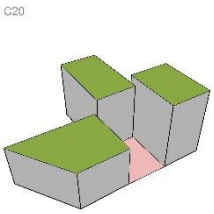	Avg. UTCI diff. = 0.91 ˚C Max. UTCI diff. = 1.38 ˚C

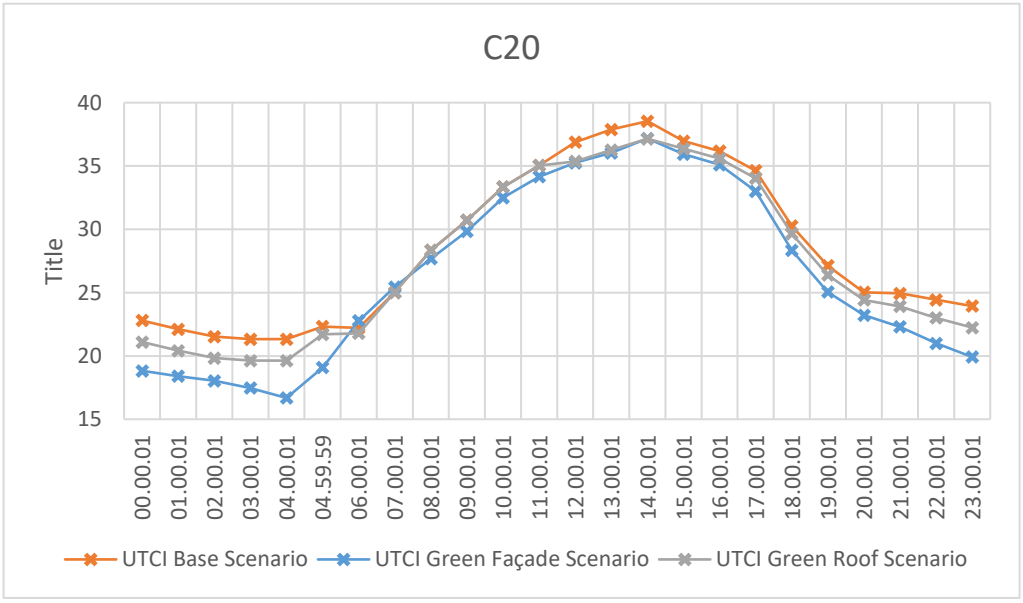

Figure 70. Graphical illustration of optimization UTCI performance of "C20"

5.2.21 Courtyard 21

Table 26 and *Figure 71* illustrate the comparison of both optimization scenarios within courtyard "C21". As it is shown above the difference in UTCI from the base model during the hottest hour of the day on the green façade "s2 optimized" is 2.21˚C, while the difference of average UTCI from the base/current state model is 2 ˚C. The other optimization scenario displays a difference in UTCI during the hottest hour of the day of 0.01 ˚C and a difference on avg. UTCI of 0.14 ˚C. These differences in UTCI can be better observed on *Figure 71*.

Table 26. UTCI performance differences between optimization scenarios on "C21"

Name	Image	Difference (˚C)
C21 s2 optimized	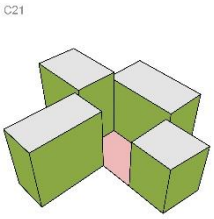	Avg. UTCI diff. = 2 ˚C Max. UTCI diff. = 2.21 ˚C
C21 s3 optimized	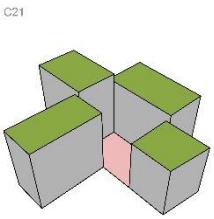	Avg. UTCI diff. = 0.14 ˚C Max. UTCI diff. = 0.01 ˚C

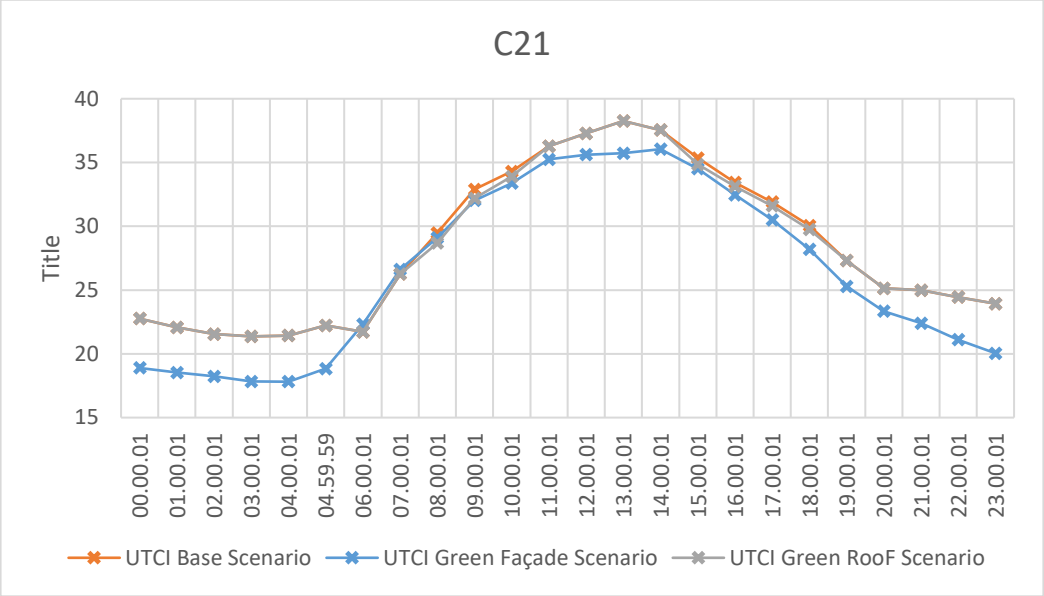

Figure 71. Graphical illustration of optimization UTCI performance of "C21"

5.2.22 Courtyard 22

Table 27 and *Figure 72* illustrate the comparison of both optimization scenarios within courtyard "C22". As it is shown above the difference in UTCI from the base model during the hottest hour of the day on the green façade "s2 optimized" is 1.95˚C, while the difference of average UTCI from the base/current state model is 1.37 ˚C. The other optimization scenario displays a difference in UTCI during the hottest hour of the day of 0.5 ˚C and a difference on avg. UTCI of 0.13 ˚C. These differences in UTCI can be better observed on *Figure 72.*

Table 27. UTCI performance differences between optimization scenarios on "C22"

Name	Image	Difference (˚C)
C22 s2 optimized	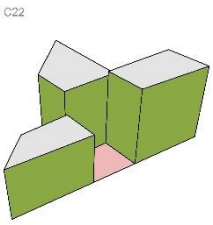	Avg. UTCI diff. = 1.37 ˚C Max. UTCI diff. = 1.95 ˚C
C22 s3 optimized	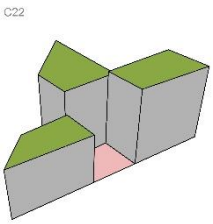	Avg. UTCI diff. = 0.13 ˚C Max. UTCI diff. = 0.5 ˚C

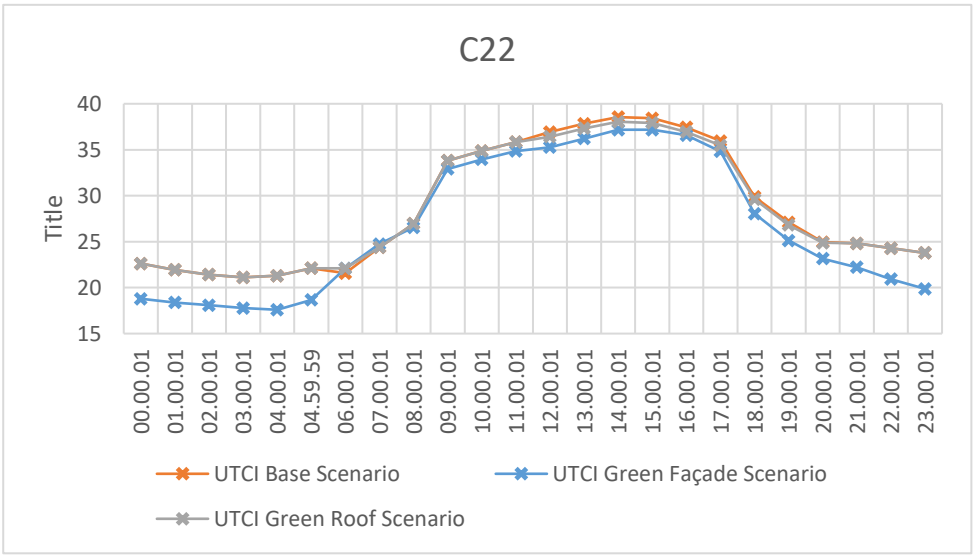

Figure 72. Graphical illustration of optimization UTCI performance of "C22"

5.2.23 Courtyard 23

Table 28 and *Figure 73* illustrate the comparison of both optimization scenarios within courtyard "C23". As it is shown above the difference in UTCI from the base model during the hottest hour of the day on the green façade "s2 optimized" is 1.32˚C, while the difference of average UTCI from the base/current state model is 1.92 ˚C. The other optimization scenario displays a difference in UTCI during the hottest hour of the day of 0.04 ˚C and a difference on avg. UTCI of 0.37 ˚C. These differences in UTCI can be better observed on *Figure 73.*

Table 28. UTCI performance differences between optimization scenarios on "C23"

Name	Image	Difference (˚C)
C23 s2 optimized	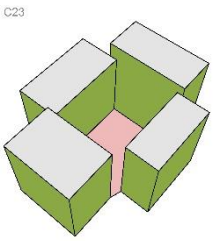	Avg. UTCI diff. = 1.92 ˚C Max. UTCI diff. = 1.32 ˚C
C23 s3 optimized	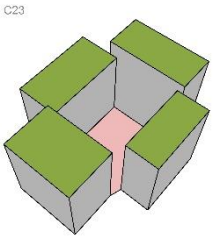	Avg. UTCI diff. = 0.37 ˚C Max. UTCI diff. = 0.04 ˚C

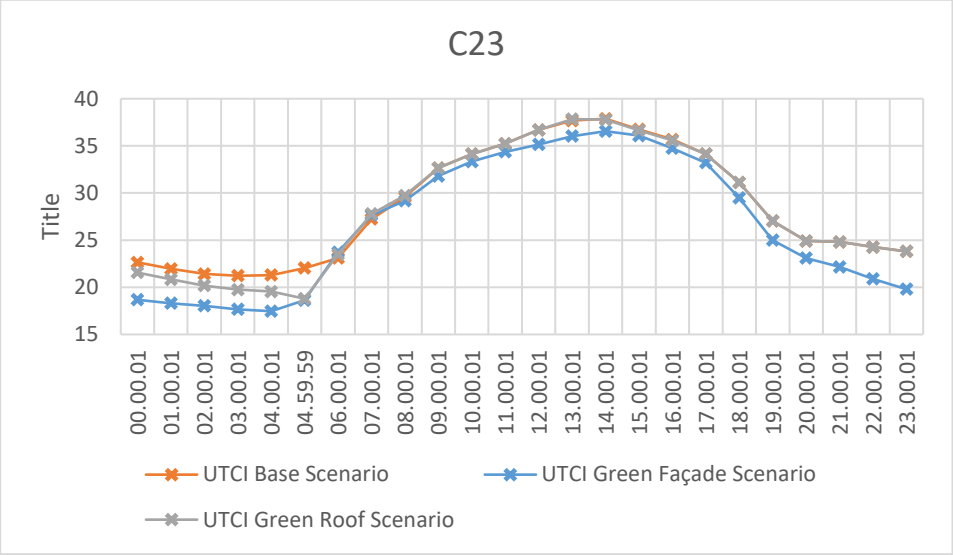

Figure 73. Graphical illustration of optimization UTCI performance of "C23"

5.2.24 Courtyard 24

Table 29 and *Figure 74* illustrate the comparison of both optimization scenarios within courtyard "C24". As it is shown above the difference in UTCI from the base model during the hottest hour of the day on the green façade "s2 optimized" is 1.46˚C, while the difference of average UTCI from the base/current state model is 2.14 ˚C. The other optimization scenario displays a difference in UTCI during the hottest hour of the day of 0.07 ˚C and a difference on avg. UTCI of 0.29 ˚C. These differences in UTCI can be better observed on *Figure 74.*

Table 29. UTCI performance differences between optimization scenarios on "C24"

Name	Image	Difference (˚C)
C24 s2 optimized	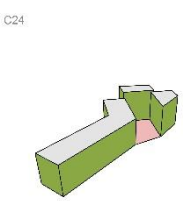	Avg. UTCI diff. = 2.14 ˚C Max. UTCI diff. = 1.46 ˚C

C24

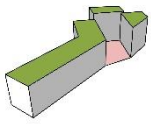

C24 s3 optimized

Avg. UTCI diff. = 0.29 ˚C

Max. UTCI diff. = 0.07 ˚C

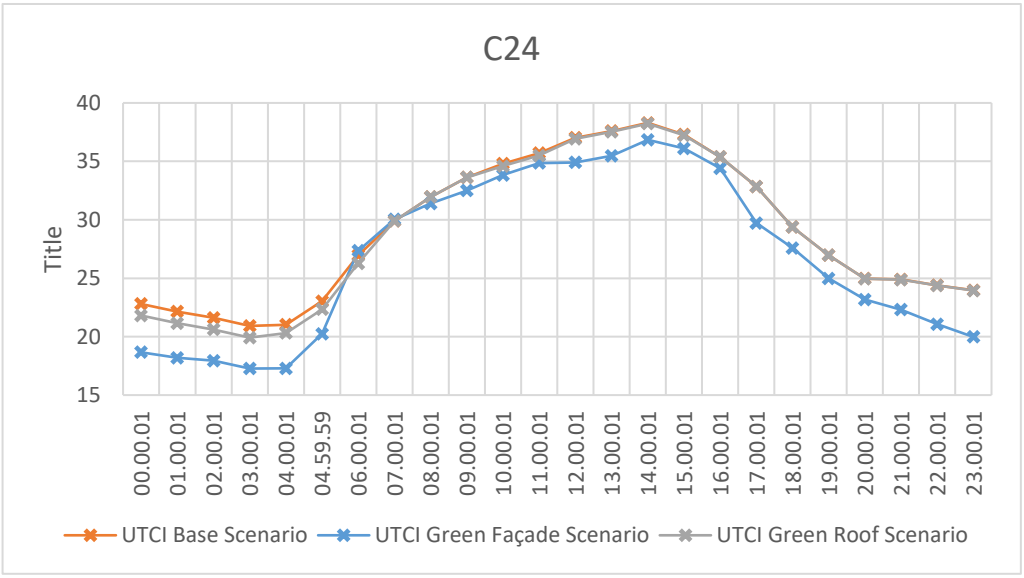

Figure 74. Graphical illustration of optimization UTCI performance of "C24"

5.2.25 Courtyard 25

Table 30 and *Figure 75* illustrate the comparison of both optimization scenarios within courtyard "C25". As it is shown above the difference in UTCI from the base model during the hottest hour of the day on the green façade "s2 optimized" is 1.23˚C, while the difference of average UTCI from the base/current state model is 2.18 ˚C. The other optimization scenario displays a difference in UTCI during the hottest hour of the day of 0.25 ˚C and a difference on avg. UTCI of 0.25 ˚C. These differences in UTCI can be better observed on *Figure 75*.

Table 30. UTCI performance differences between optimization scenarios on "C25"

Name	Image	Difference (˚C)
C25 s2 optimized	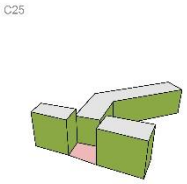	Avg. UTCI diff. = 2.18 ˚C Max. UTCI diff. = 1.23 ˚C
C25 s3 optimized	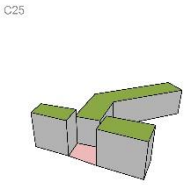	Avg. UTCI diff. = 0.04 ˚C Max. UTCI diff. = 0.25 ˚C

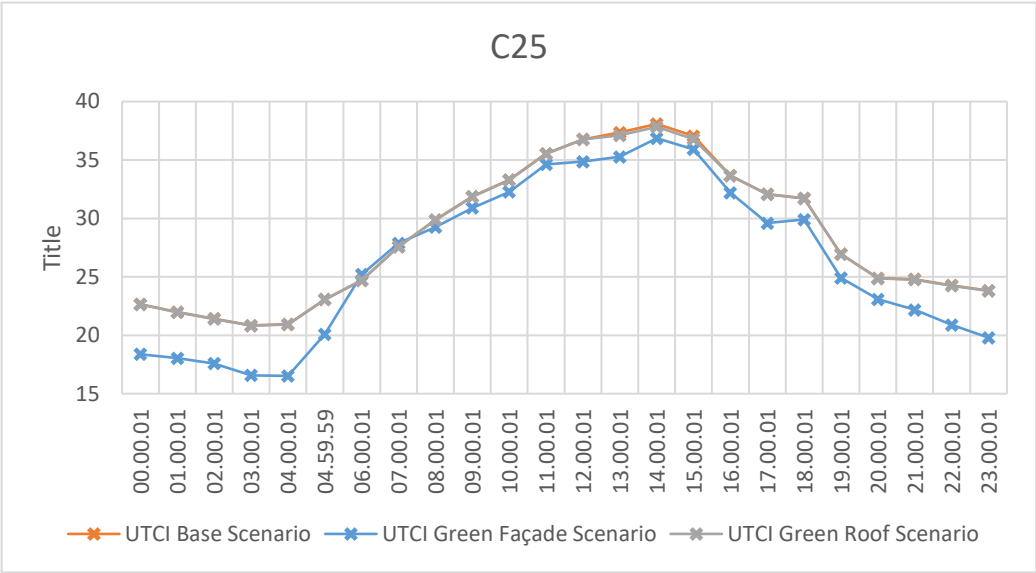

Figure 75. Graphical illustration of optimization UTCI performance of "C25"

5.2.26 Courtyard 26

Table 31 and *Figure 76* illustrate the comparison of both optimization scenarios within courtyard "C26". As it is shown above the difference in UTCI from the base model during the hottest hour of the day on the green façade is 1.31˚C, while the difference of average UTCI from the base/current state model is 2.17 ˚C. The other optimization scenario displays a difference in UTCI during the hottest hour of the day of 0.5 ˚C and a difference on avg. UTCI of 0.14 ˚C. These differences in UTCI can be better observed on *Figure 76.*

Table 31. UTCI performance differences between optimization scenarios on "C26"

Name	Image	Difference (˚C)
C26 s2 optimized	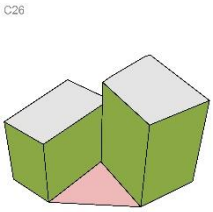	Avg. UTCI diff. = 2.17 ˚C Max. UTCI diff. = 1.31 ˚C
C26 s3 optimized	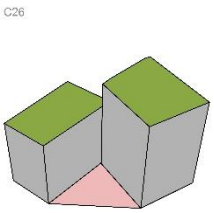	Avg. UTCI diff. = 0.14 ˚C Max. UTCI diff. = 0.5 ˚C

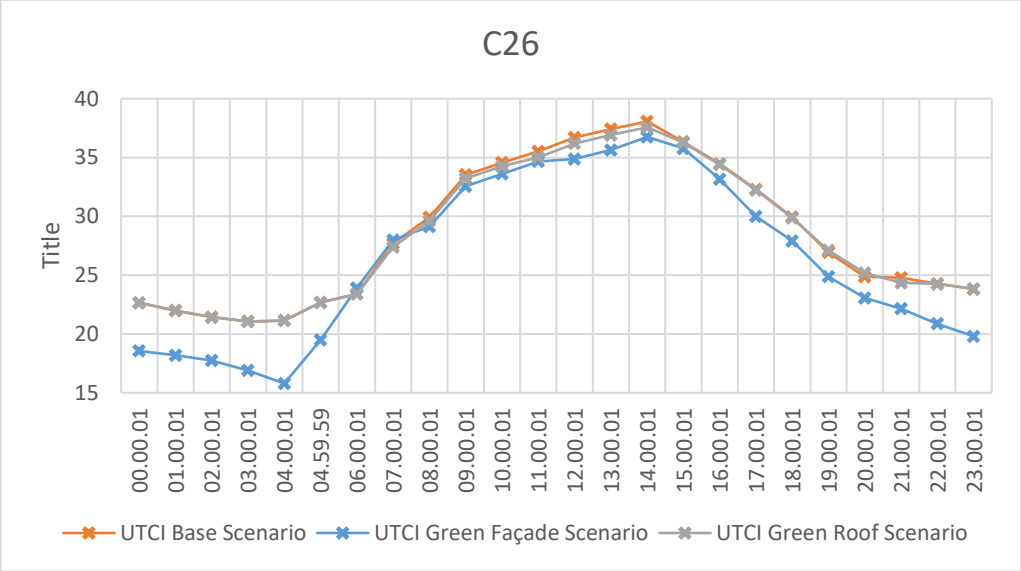

Figure 76. Graphical illustration of optimization UTCI performance of "C26"

5.2.27 Courtyard 27

Table 32 and *Figure 77* illustrate the comparison of both optimization scenarios within courtyard "C27". As it is shown above the difference in UTCI from the base model during the hottest hour of the day on the green façade is 1.12˚C, while the difference of average UTCI from the base/current state model is 2.26 ˚C. In the alternative optimization scenario, there is a difference in UTCI of 0.09 degrees Celsius during the warmest hour of the day, and there is a difference in UTCI of 0.24 degrees Celsius on average. These differences in UTCI can be better observed on *Figure 77.*

Table 32. UTCI performance differences between optimization scenarios on "C27"

Name	Image	Difference (˚C)
C27 s2 optimized	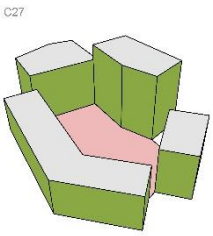	Avg. UTCI diff. = 2.26 ˚C Max. UTCI diff. = 1.12 ˚C
C27 s3 optimized	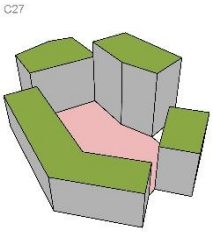	Avg. UTCI diff. = 0.24 ˚C Max. UTCI diff. = 0.09 ˚C

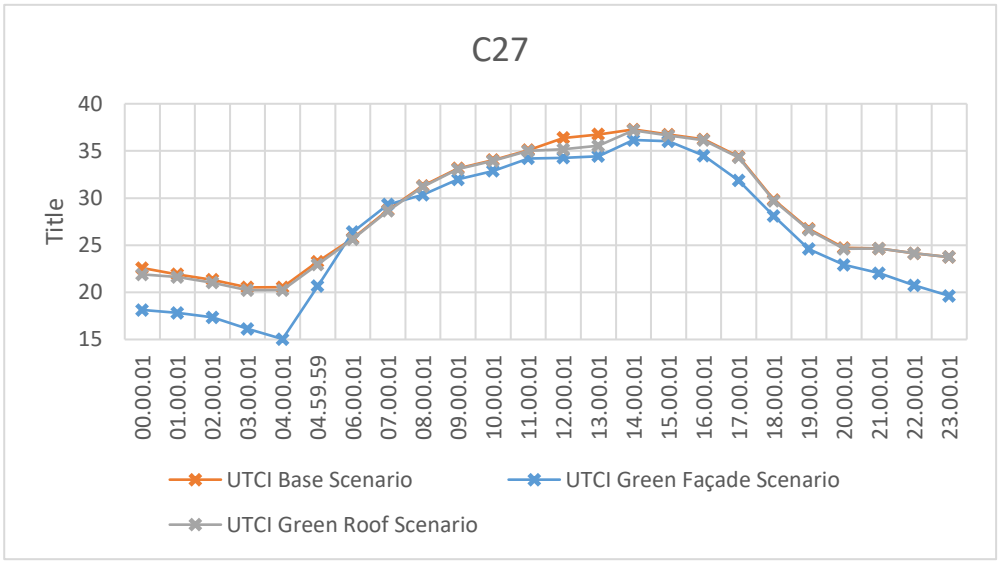

Figure 77. Graphical illustration of optimization UTCI performance of "C27"

5.2.28 Courtyard 28

Table 33 and *Figure 78* illustrate the comparison of both optimization scenarios within courtyard "C28". As it is shown above the difference in UTCI from the base model during the hottest hour of the day on the green façade "s2 optimized" is 1.26˚C, while the difference of average UTCI from the base/current state model is 2.32 ˚C. The other optimization scenario displays a difference in UTCI during the hottest hour of the day of 1.2 ˚C and a difference on avg. UTCI of 0.47 ˚C. These differences in UTCI can be better observed on *Figure 78.*

Table 33. UTCI performance differences between optimization scenarios on "C28"

Name	Image	Difference (˚C)
C28 s2 optimized	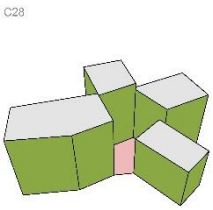	Avg. UTCI diff. = 2.32 ˚C Max. UTCI diff. = 1.26 ˚C
C28 s3 optimized	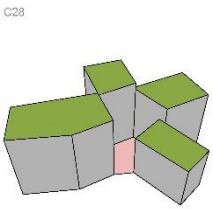	Avg. UTCI diff. = 0.47 ˚C Max. UTCI diff. = 1.2 ˚C

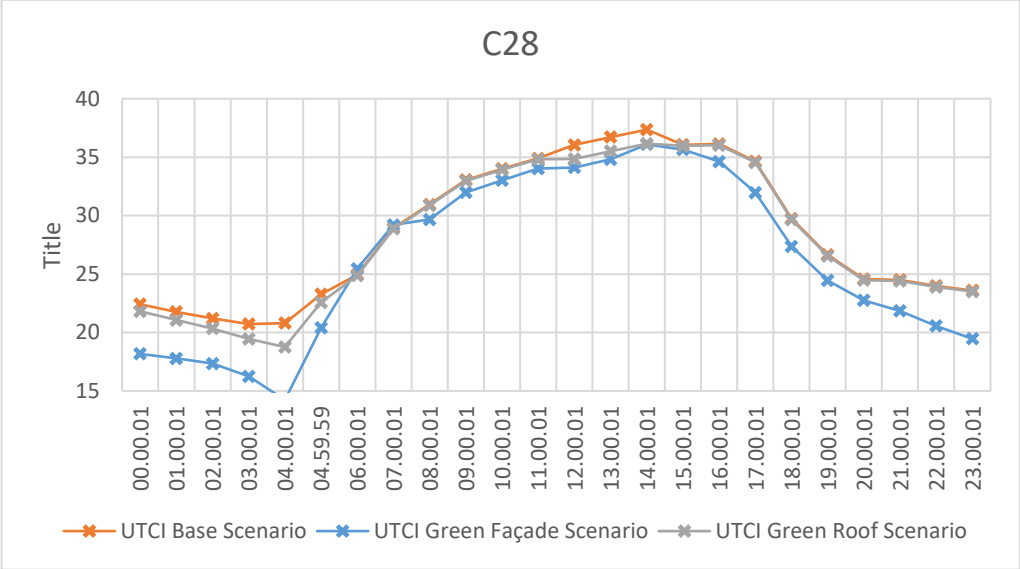

Figure 78. Graphical illustration of optimization UTCI performance of "C28"

5.2.29 Courtyard 29

Table 34 and *Figure 79* illustrate the comparison of both optimization scenarios within courtyard "C29". As it is shown above the difference in UTCI from the base model during the hottest hour of the day on the green façade "s2 optimized" is 1.4˚C, while the difference of average UTCI from the base/current state model is 2.01 ˚C. The other optimization scenario displays a difference in UTCI during the hottest hour of the day of 1.2 ˚C and a difference on avg. UTCI of 0.42 ˚C. These differences in UTCI can be better observed on *Figure 79.*

Table 34. UTCI performance differences between optimization scenarios on "C29"

Name	Image	Difference (˚C)
C29 s2 optimized	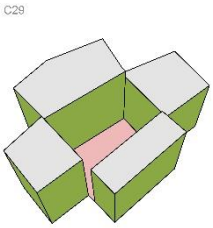	Avg. UTCI diff. = 2.01 ˚C Max. UTCI diff. = 1.4 ˚C
C29 s3 optimized	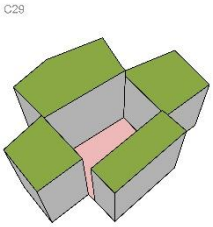	Avg. UTCI diff. = 0.42 ˚C Max. UTCI diff. = 1.2 ˚C

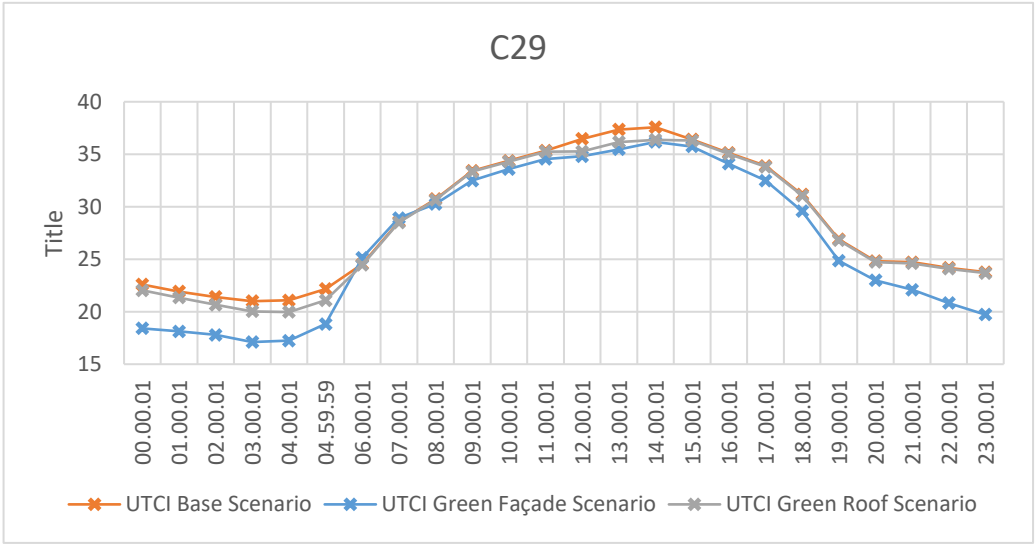

Figure 79. Graphical illustration of optimization UTCI performance of "C29"

5.2.30 Courtyard 30

Table 35 and *Figure 80* illustrate the comparison of both optimization scenarios within courtyard "C30". As it is shown above the difference in UTCI from the base model during the hottest hour of the day on the green façade "s2 optimized" is 1.09˚C, while the difference of average UTCI from the base/current state model is 2.01 ˚C. The other optimization scenario displays a difference in UTCI during the hottest hour of the day of 0.14 ˚C and a difference on avg. UTCI of 0.5 ˚C. These differences in UTCI can be better observed on *Figure 80.*

Table 35. UTCI performance differences between optimization scenarios on "C30"

Name	Image	Difference (˚C)
C30 s2 optimized	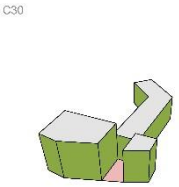	Avg. UTCI diff. = 2.01 ˚C Max. UTCI diff. = 1.09 ˚C
C30 s3 optimized	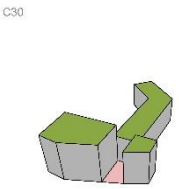	Avg. UTCI diff. = 0.5 ˚C Max. UTCI diff. = 0.14 ˚C

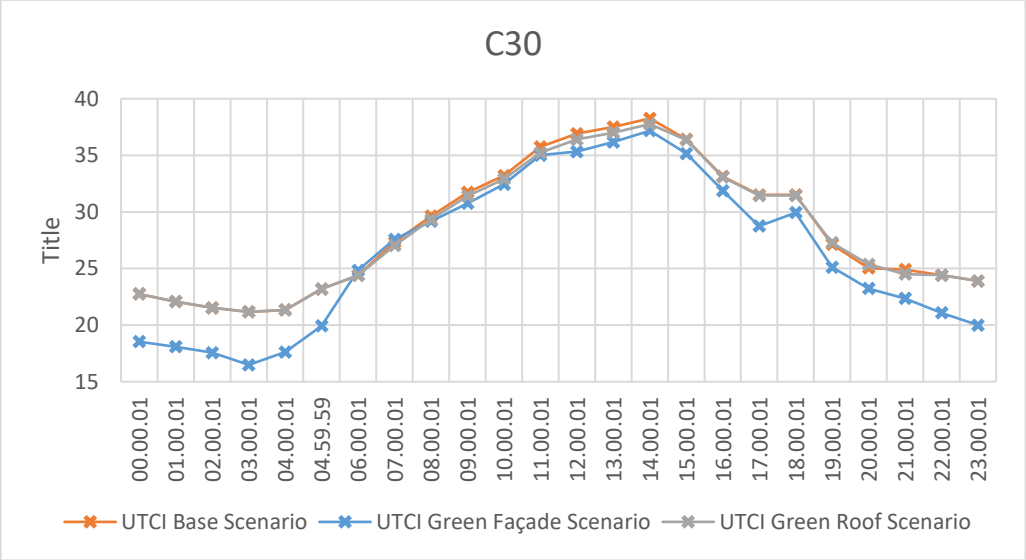

Figure 80. Graphical illustration of optimization UTCI performance of "C30"

5.2.29 Courtyard 29

Table 36 and *Figure 81* illustrate the comparison of both optimization scenarios within courtyard "C29". As it is shown above the difference in UTCI from the base model during the hottest hour of the day on the green façade "s2 optimized" is 1.4˚C, while the difference of average UTCI from the base/current state model is 2.01 ˚C. The other optimization scenario displays a difference in UTCI during the hottest hour of the day of 1.2 ˚C and a difference on avg. UTCI of 0.42 ˚C. These differences in UTCI can be better observed on *Figure 81*.

Table 36. UTCI performance differences between optimization scenarios on "C29"

Name	Image	Difference (˚C)
C29 s2 optimized	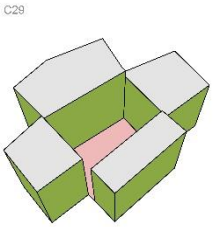	Avg. UTCI diff. = 2.01 ˚C Max. UTCI diff. = 1.4 ˚C
C29 s3 optimized	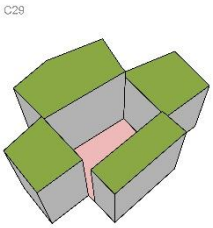	Avg. UTCI diff. = 0.42 ˚C Max. UTCI diff. = 1.2 ˚C

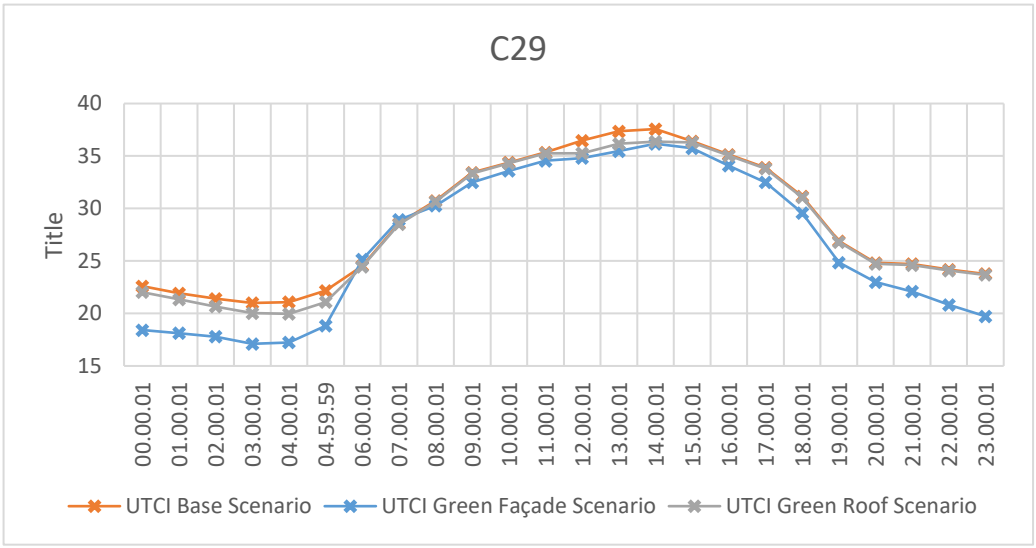

Figure 81. Graphical illustration of optimization UTCI performance of "C29"

5.2.31 Courtyard 31

Table 37 and *Figure 82* illustrate the comparison of both optimization scenarios within courtyard "C31". As it is shown above the difference in UTCI from the base model during the hottest hour of the day on the green façade "s2 optimized" is 0.86˚C, while the difference of average UTCI from the base/current state model is 2.28 ˚C. The other optimization scenario displays a difference in UTCI during the hottest hour of the day of 0.11 ˚C and a difference on avg. UTCI of 0.07 ˚C. These differences in UTCI can be better observed on *Figure 82.*

Table 37. UTCI performance differences between optimization scenarios on "C31"

Name	Image	Difference (˚C)
C31 s2 optimized	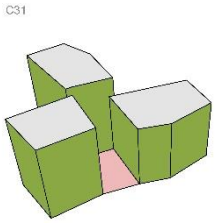	Avg. UTCI diff. = 2.28 ˚C Max. UTCI diff. = 0.86 ˚C
C31 s3 optimized	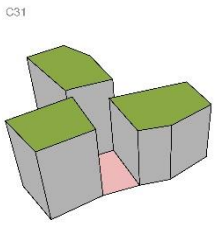	Avg. UTCI diff. = 0.07 ˚C Max. UTCI diff. = 0.11 ˚C

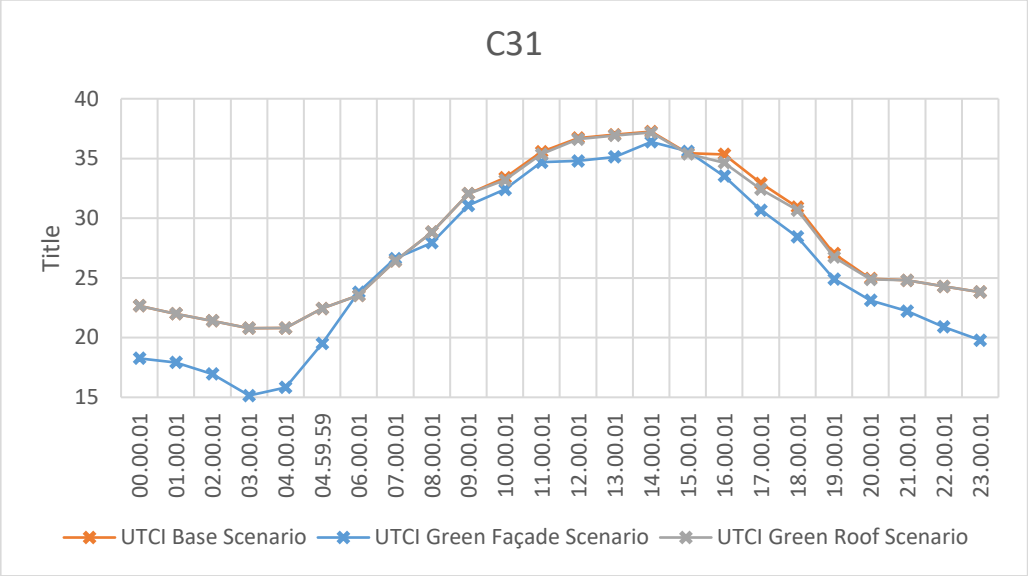

Figure 82. Graphical illustration of optimization UTCI performance of "C31"

5.2.32 Courtyard 32

Table 38 and *Figure 83* illustrate the comparison of both optimization scenarios within courtyard "C32". As it is shown above the difference in UTCI from the base model during the hottest hour of the day on the green façade "s2 optimized" is 1.46˚C, while the difference of average UTCI from the base/current state model is 1.98 ˚C. The other optimization scenario displays a difference in UTCI during the hottest hour of the day of 0.09 ˚C and a difference on avg. UTCI of 0.07 ˚C. These differences in UTCI can be better observed on *Figure 83.*

Table 38. UTCI performance differences between optimization scenarios on "C32"

Name	Image	Difference (˚C)
C32 s2 optimized	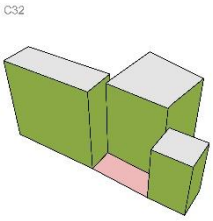	Avg. UTCI diff. = 1.98 ˚C Max. UTCI diff. = 1.46 ˚C
C32 s3 optimized	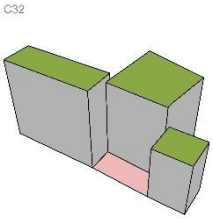	Avg. UTCI diff. = 0.07 ˚C Max. UTCI diff. = 0.09 ˚C

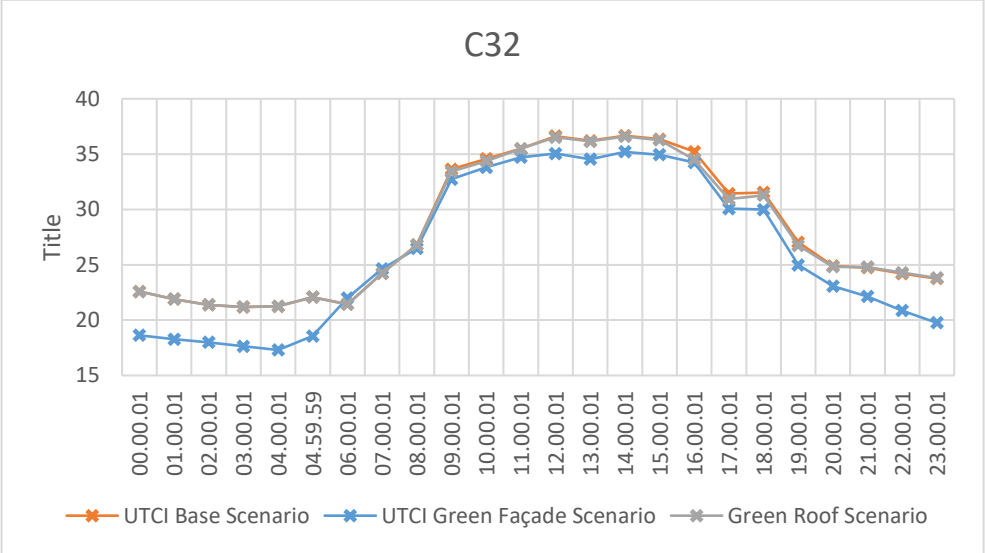

Figure 83. Graphical illustration of optimization UTCI performance of "C32"

5.2.33 Courtyard 33

Table 39 and *Figure 84* illustrate the comparison of both optimization scenarios within courtyard "C32". As it is shown above the difference in UTCI from the base model during the hottest hour of the day on the green façade "s2 optimized" is 0.58˚C, while the difference of average UTCI from the base/current state model is 2.77 ˚C. The other optimization scenario displays a difference in UTCI during the hottest hour of the day of 0.1 ˚C and a difference on avg. UTCI of 0.11 ˚C. These differences in UTCI can be better observed on *Figure 84.*

Table 39. UTCI performance differences between optimization scenarios on "C33"

Name	Image	Difference (˚C)
C33 s2 optimized	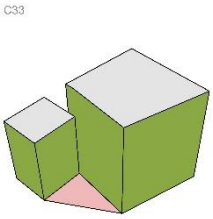	Avg. UTCI diff. = 2.77 ˚C Max. UTCI diff. = 0.58 ˚C
C33 s3 optimized	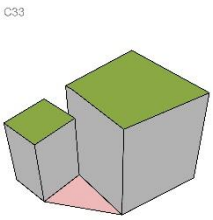	Avg. UTCI diff. = 0.11 ˚C Max. UTCI diff. = 0.1 ˚C

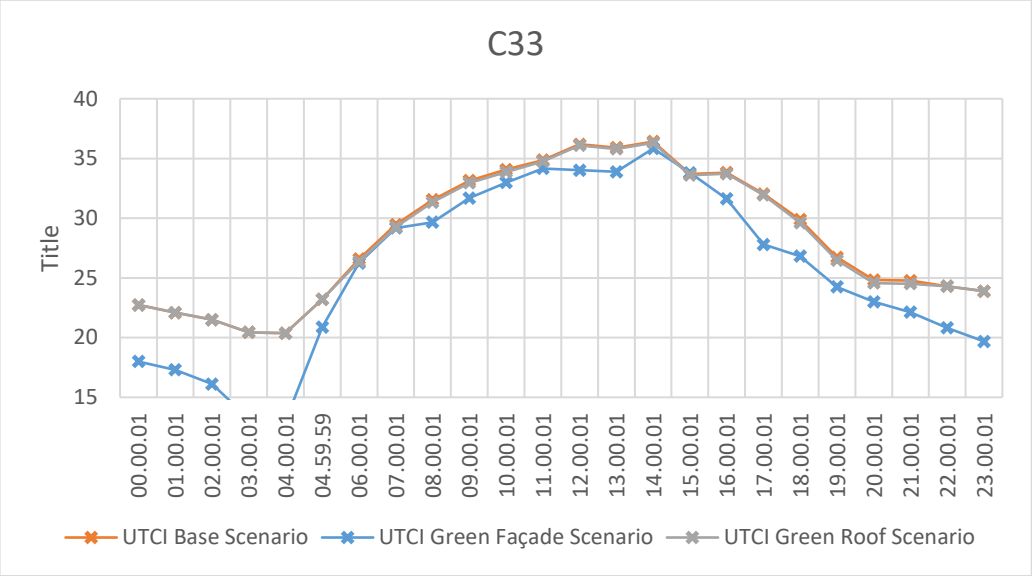

Figure 84. Graphical illustration of optimization UTCI performance of "C33"

4.3 Macroscale

In macro scale the comparison between each optimization scenario is conducted parallel to one-another, to determine how they perform. This way a better understanding towards the best performing scenario can be formed. This process consists of visualizing the maximum UTCI performances as well as the average UTCI performance of each optimization scenario. To better understand the benefits of each optimization scenario towards outdoor thermal stress, one last step was added where the proximity to the border-line of the maximum value of non-thermal stress (see *Figure 85*).

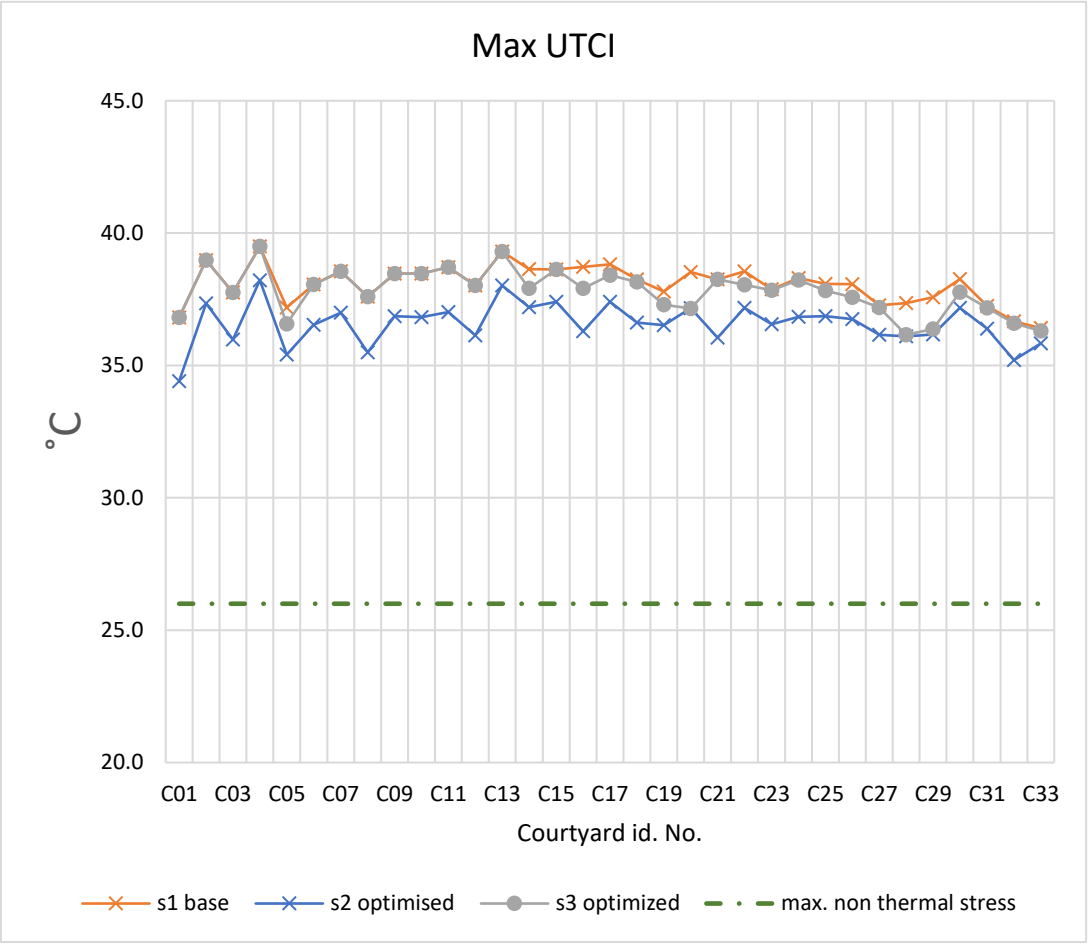

Figure 85. Graphical illustration of max. UTCI performance of all scenarios

As illustrated on *Figure 85* the optimization that provides the highest amount of UTCI reduction from the present state UTCI values of the site is the green façade optimization method (s2 optimized). The other optimization variant provides hardly any benefit in UTCI. Taking this all into account, in the figure above it is evident that the difference between the best performing optimization scenario and the maximal UTCI value associated with no thermal stress is high, a difference of 10.58 ˚C to be precise.

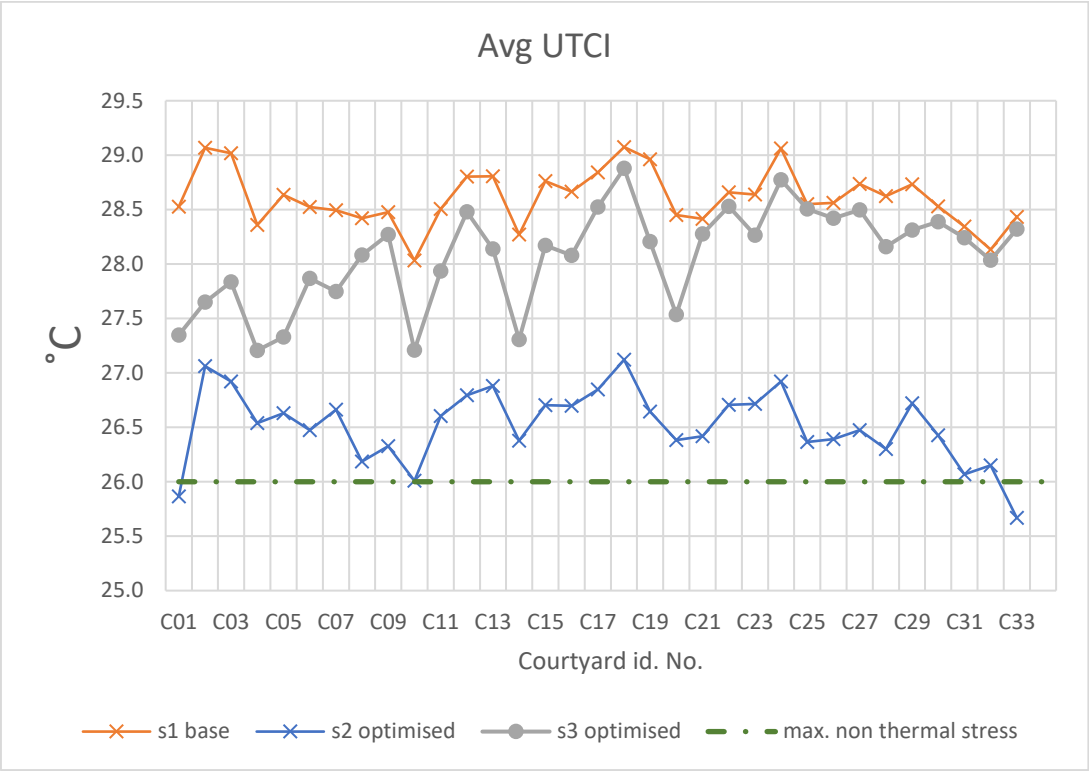

Figure 86. Graphical illustration of avg. UTCI performance of all scenarios

Figure 86 provides a different perspective on the performance of each optimization scenario and the relations they poses regarding the current state scenario and the maximal UTCI value associated with thermal stress. Throughout this representation it is visible that the green façade optimization scenario provides the best benefits in UTCI. *Figure 86* depicts that the average UTCI values of all hours of the simulated day is closer to the maximal non-thermal stress values for the "s2 optimized"/green façade optimization scenario.

Table 40. UTCI performance differences between both optimization

Optimization Scenarios	S2 optimization	S3 optimization
Images		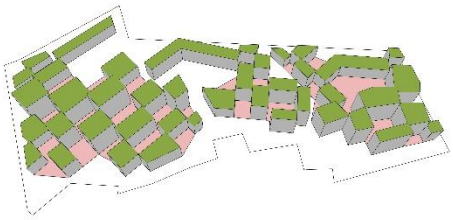
Avg. UTCI benefit (˚C)	1.5	0.28
Avg. max UTCI benefit (˚C)	2.09	0.53
UTCI benefit from base (%)	7.3%	1.9%

Table 40 illustrates the comparison of optimization scenarios in macroscale. The average UTCI benefit from optimization scenario with green façade is 1.5 ˚C lower than the current state avg. UTCI, whereas the average UTCI benefit from "s3 optimization" that consists of green roofs being 0.28 ˚C lower than the UTCI of "s1 base" scenario.

The differences in maximum UTCI value of both scenarios with regard to the current state one are 2.09 ˚C and 0.53 ˚C respectively. This further reinforces the deduction that the green façade optimization performs best out of the two.

During this 24h interval the benefit in UTCI of the green façade optimization scenario stands at 7.3%, a value 5.4% higher than that of the green roof optimization scenario.

From the observations made throughout this evaluation, the green façade optimization seems to have a more positive impact on UTCI.

CHAPTER 6

CONCLUSIONS

6.1 Conclusions

This paper evaluated the impact of large scale building fabric on outdoor thermal comfort in three different scenarios where the morphological indicators remained constant and two common ways of optimization through the use of vertical and horizontal greenery. This paper presents a comprehensive analysis of simulations and comparisons to determine the most effective optimization strategy for Tirana's climate conditions. The data underwent analysis at both micro and macroscale levels, incorporating four distinct variables, namely air temperature, mean radiant temperature, wind speed, and relative humidity. These variables are incorporated into a single indicator, the UTCI.

In microscale it is concluded that the best performing optimization out of the two is the green façade optimization for Tirana in terms of UTCI.

In macroscale the green façade optimization outperforms the green roof optimization in terms of UTCI. The comparison was done using the average and maximal UTCI values as well as the proximity to the maximal 'no thermal stress' boundary. "s2 optimization" lowers the average of maximum UTCI throughout the all outdoor areas by 2.09 ˚C (7.3%) and the average UTCI for the 24h by 0.28 ˚C compared to "s3 optimization". The present study reveals that the most notable associations between Universal Thermal Climate Index (UTCI) in courtyards and built environment indicators are the ratio of façade area to site area and the average depth of the courtyard.

6.2 Recommendations for further research

In entirety, the results substantiate the influence of neighborhood morphology on outdoor thermal comfort. The process of model development and analysis adheres to pertinent scientific research and experimentation that has undergone scrutiny, while considering the impact of building height, voids, and shape. Several priority areas are suggested for further exploration in the research.

- Extending the research to indoor thermal comfort and the energy requirements of each building, to understand each optimization's impact in building scale as well as in urban scale.
- Considering different varieties of vertical and horizontal greenery to optimize the outdoor thermal comfort.
- Using different programs like Dynamo for Revit in order to involve different attributes within each optimization model utilizing the powers of genetic algorithms for further research.
- Considering daylight as a significant variable in the assessment process due to its potential to significantly influence design optimizations.

As a conclusion, this research states once more that the early design stage, if it is properly evaluated and analyzed can have significant impact in the outdoor thermal comfort.

REFERENCES

Mirza, S., Niwalkar, A., Anjum, S., Bherwani, H., Singh, A., & Kumar, R. (2022, June). Studying impact of infrastructure development on urban microclimate: Integrated multiparameter analysis using OpenFOAM. Energy Nexus, 6, 100060. https://doi.org/10.1016/j.nexus.2022.100060

Brozovsky, J., Radivojevic, J., & Simonsen, A. (2022, September). Assessing the impact of urban microclimate on building energy demand by coupling CFD and building performance simulation. Journal of Building Engineering, 55, 104681. https://doi.org/10.1016/j.jobe.2022.104681

Mughal, M. O., Kubilay, A., Fatichi, S., Meili, N., Carmeliet, J., Edwards, P., & Burlando, P. (2021, September). Detailed investigation of vegetation effects on microclimate by means of computational fluid dynamics (CFD) in a tropical urban environment. Urban Climate, 39, 100939. https://doi.org/10.1016/j.uclim.2021.100939

Abdollahzadeh, N., & Biloria, N. (2022, June). Urban microclimate and energy consumption: A multi-objective parametric urban design approach for dense subtropical cities. Frontiers of Architectural Research, 11(3), 453–465. https://doi.org/10.1016/j.foar.2022.02.001

Kamal, A., Abidi, S. M. H., Mahfouz, A., Kadam, S., Rahman, A., Hassan, I. G., & Wang, L. L. (2021, December). Impact of urban morphology on urban microclimate and building energy loads. Energy and Buildings, 253, 111499. https://doi.org/10.1016/j.enbuild.2021.111499

Banerjee, S., Ching N. Y, G., Yik, S. K., Dzyuban, Y., Crank, P. J., Pek Xin Yi, R., & Chow, W. T. (2022, November). Analysing impacts of urban morphological variables and density on outdoor microclimate for tropical cities: A review and a framework proposal for future research directions. Building and Environment, 225, 109646. https://doi.org/10.1016/j.buildenv.2022.109646

Salvati, A., Kolokotroni, M., Kotopouleas, A., Watkins, R., Giridharan, R., & Nikolopoulou, M. (2022, January). Impact of reflective materials on urban canyon albedo, outdoor and indoor microclimates. Building and Environment, 207, 108459. https://doi.org/10.1016/j.buildenv.2021.108459

Schaefer, M., Ebrahimi Salari, H., Köckler, H., & Thinh, N. X. (2021, November). Assessing local heat stress and air quality with the use of remote sensing and pedestrian perception in urban microclimate simulations. Science of the Total Environment, 794, 148709. https://doi.org/10.1016/j.scitotenv.2021.148709

Ragheb, A. A., El-Darwish, I. I., & Ahmed, S. (2016, June). Microclimate and human comfort considerations in planning a historic urban quarter. International Journal of Sustainable Built Environment, 5(1), 156–167. https://doi.org/10.1016/j.ijsbe.2016.03.003

Katal, A., Mortezazadeh, M., Wang, L. L., & Yu, H. (2022, July). Urban building energy and microclimate modeling – From 3D city generation to dynamic simulations. Energy, 251, 123817. https://doi.org/10.1016/j.energy.2022.123817

Hang, J., & Chen, G. (2022, December). Experimental study of urban microclimate on scaled street canyons with various aspect ratios. Urban Climate, 46, 101299. https://doi.org/10.1016/j.uclim.2022.101299

Fisk, W. J. (2018, May 18). How home ventilation rates affect health: A literature review. Indoor Air, 28(4), 473–487. https://doi.org/10.1111/ina.12469

Abdollahzadeh, N., & Biloria, N. (2022, June). Urban microclimate and energy consumption: A multi-objective parametric urban design approach for dense subtropical cities. Frontiers of Architectural Research, 11(3), 453–465. https://doi.org/10.1016/j.foar.2022.02.001

Jia, W., Cheng, P., Ma, L., Wang, S., Qian, H., & Li, Y. (2022, December). Individual heterogeneity and airborne infection: Effect of non-uniform air distribution. Building and Environment, 226, 109674. https://doi.org/10.1016/j.buildenv.2022.109674

Conceição, E., Gomes, J., Lúcio, M., & Awbi, H. (2022). Application of Cold Radiant Surfaces in the Buildings Development in Summer Conditions. E3S Web of Conferences, 362, 05002. https://doi.org/10.1051/e3sconf/202236205002

Zoure, A. N., & Genovese, P. V. (2023, December). Implementing natural ventilation and daylighting strategies for thermal comfort and energy efficiency in office buildings in Burkina Faso. Energy Reports, 9, 3319–3342. https://doi.org/10.1016/j.egyr.2023.02.017

Wang, X., Li, H., & Sodoudi, S. (2022, June). The effectiveness of cool and green roofs in mitigating urban heat island and improving human thermal comfort. Building and Environment, 217, 109082. https://doi.org/10.1016/j.buildenv.2022.109082

Diz-Mellado, E., López-Cabeza, V. P., Roa-Fernández, J., Rivera-Gómez, C., & Galán-Marín, C. (2023, February). Energy-saving and thermal comfort potential of vernacular urban block porosity shading. Sustainable Cities and Society, 89, 104325. https://doi.org/10.1016/j.scs.2022.104325

Tabadkani, A., Aghasizadeh, S., Banihashemi, S., & Hajirasouli, A. (2022, October). Courtyard design impact on indoor thermal comfort and utility costs for residential households: Comparative analysis and deep-learning predictive model. Frontiers of Architectural Research, 11(5), 963–980. https://doi.org/10.1016/j.foar.2022.02.006

Nosek, T., Kluková, Z., Jakubcová, M., & Jaňour, Z. (2022, January). The effect of courtyard buildings on the ventilation of street canyons: A wind-tunnel study.

Journal of Wind Engineering and Industrial Aerodynamics, 220, 104885. https://doi.org/10.1016/j.jweia.2021.104885

Zhu, J., Feng, J., Lu, J., Chen, Y., Li, W., Lian, P., & Zhao, X. (2023, May). A review of the influence of courtyard geometry and orientation on microclimate. Building and Environment, 236, 110269. https://doi.org/10.1016/j.buildenv.2023.110269

Lizana, J., López-Cabeza, V. P., Renaldi, R., Diz-Mellado, E., Rivera-Gómez, C., & Galán-Marín, C. (2022, March). Integrating courtyard microclimate in building performance to mitigate extreme urban heat impacts. Sustainable Cities and Society, 78, 103590. https://doi.org/10.1016/j.scs.2021.103590

Leng, J., Wang, Q., & Liu, K. (2020, November). Sustainable design of courtyard environment: From the perspectives of airborne diseases control and human health. Sustainable Cities and Society, 62, 102405. https://doi.org/10.1016/j.scs.2020.102405

Diz-Mellado, E., Ruiz-Pardo, L., Rivera-Gómez, C., Sanchez de la Flor, F. J., & Galán-Marín, C. (2023, June). Unravelling the impact of courtyard geometry on cooling energy consumption in buildings. Building and Environment, 237, 110349. https://doi.org/10.1016/j.buildenv.2023.110349

Lopez-Cabeza, V. P., Alzate-Gaviria, S., Diz-Mellado, E., Rivera-Gomez, C., & Galan-Marin, C. (2022, June). Albedo influence on the microclimate and thermal comfort of courtyards under Mediterranean hot summer climate conditions. Sustainable Cities and Society, 81, 103872. https://doi.org/10.1016/j.scs.2022.103872

Enríquez, E., Fuertes, V., Cabrera, M., Seores, J., Muñoz, D., & Fernández, J. (2017, June). New strategy to mitigate urban heat island effect: Energy saving by combining high albedo and low thermal diffusivity in glass ceramic materials. Solar Energy, 149, 114–124. https://doi.org/10.1016/j.solener.2017.04.011

Taha, H., Douglas, S., & Haney, J. (1997, January). Mesoscale meteorological and air quality impacts of increased urban albedo and vegetation. Energy and Buildings, 25(2), 169–177. https://doi.org/10.1016/s0378-7788(96)01006-7

Palomo Amores, T. R., Sánchez Ramos, J., Guerrero Delgado, M., Castro Medina, D., Cerezo-Narvaéz, A., & Álvarez Domínguez, S. (2023, April). Effect of green infrastructures supported by adaptative solar shading systems on livability in open spaces. Urban Forestry & Urban Greening, 82, 127886. https://doi.org/10.1016/j.ufug.2023.127886

Vox, G., Blanco, I., Convertino, F., & Schettini, E. (2022, November). Heat transfer reduction in building envelope with green façade system: A year-round balance in Mediterranean climate conditions. Energy and Buildings, 274, 112439. https://doi.org/10.1016/j.enbuild.2022.112439

Mazzeo, D., Matera, N., Peri, G., & Scaccianoce, G. (2022). Forecasting Green Roofs' Potential in Improving Building Thermal Performance and Mitigating Urban Heat Island in the Mediterranean Area: An Artificial Intelligence-Based Approach. SSRN Electronic Journal. https://doi.org/10.2139/ssrn.4155132

Mazzeo, D., Matera, N., Peri, G., & Scaccianoce, G. (2022). Forecasting Green Roofs' Potential in Improving Building Thermal Performance and Mitigating Urban Heat Island in the Mediterranean Area: An Artificial Intelligence-Based Approach. SSRN Electronic Journal. https://doi.org/10.2139/ssrn.4155132

Ysebaert, T., Koch, K., Samson, R., & Denys, S. (2021, April). Green walls for mitigating urban particulate matter pollution—A review. Urban Forestry & Urban Greening, 59, 127014. https://doi.org/10.1016/j.ufug.2021.127014

Seyam, S. (2019, November). The impact of greenery systems on building energy: Systematic review. Journal of Building Engineering, 26, 100887. https://doi.org/10.1016/j.jobe.2019.100887

Zare, S., Hasheminejad, N., Shirvan, H. E., Hemmatjo, R., Sarebanzadeh, K., & Ahmadi, S. (2018, March). Comparing Universal Thermal Climate Index (UTCI) with selected thermal indices/environmental parameters during 12 months of the year. Weather and Climate Extremes, 19, 49–57. https://doi.org/10.1016/j.wace.2018.01.004

Jendritzky, G., de Dear, R., & Havenith, G. (2011, December 21). UTCI—Why another thermal index? International Journal of Biometeorology, 56(3), 421–428. https://doi.org/10.1007/s00484-011-0513-7

Gómez, F., Valcuende, M., Matzarakis, A., & Cárcel, J. (2018, July 12). Design of natural elements in open spaces of cities with a Mediterranean climate, conditions for comfort and urban ecology. Environmental Science and Pollution Research, 25(26), 26643–26652. https://doi.org/10.1007/s11356-018-2736-1

APPENDIX

Figure 87 to *Figure 90* illustrate the 2D maps of the base/current state scenario, regarding the potential air temperature, mean radiant temperature, wind speed and relative humidity at 14:00.

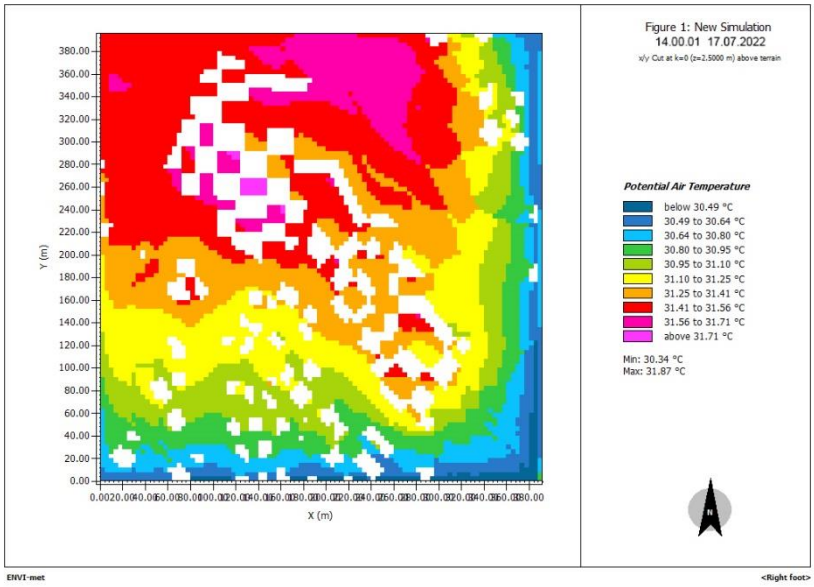

Figure 87. Potential air temperature map for s1 base at 14:00

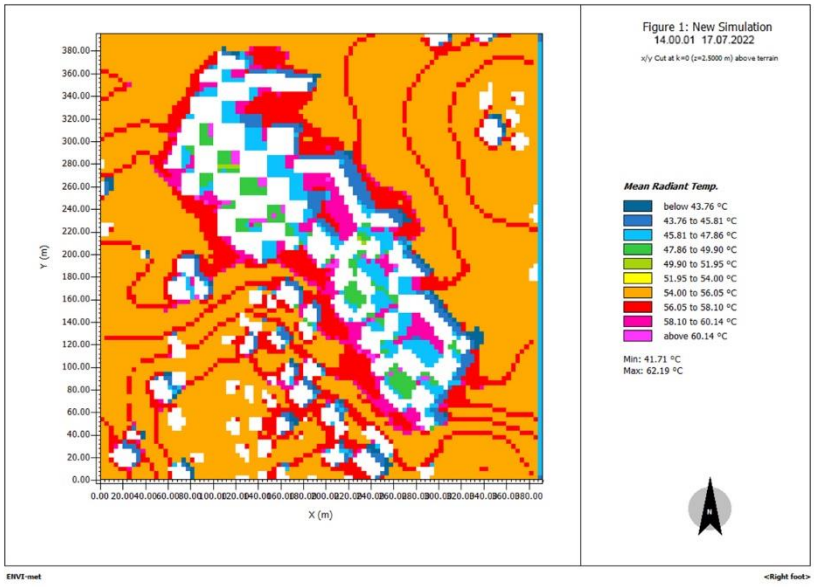

Figure 88. Mean radiant temperature map for s1 base at 14:00

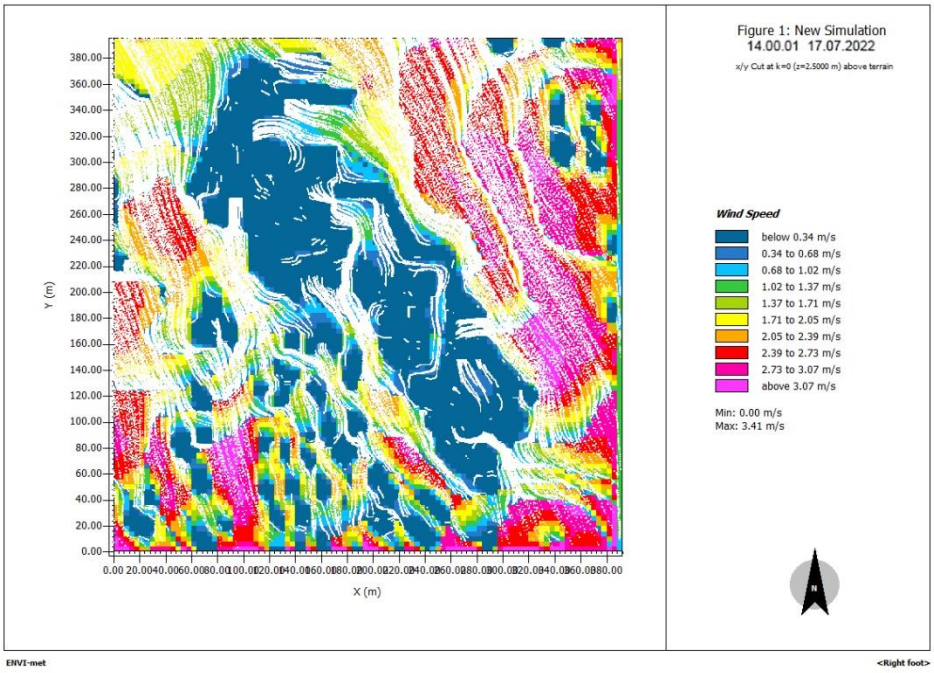

Figure 89. Wind speed map for s1 base at 14:00

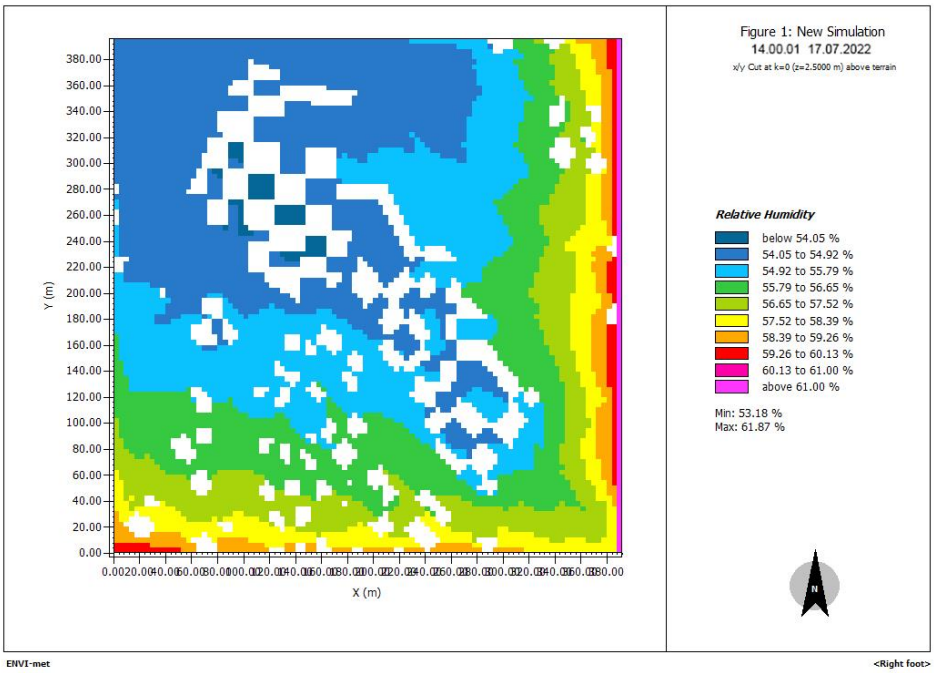

Figure 90. Relative humidity map for s1 base at 14:00

Figure 91 to *Figure 93* illustrate the 2D maps of the green roof scenario, regarding the potential air temperature, wind speed and relative humidity at 14:00.

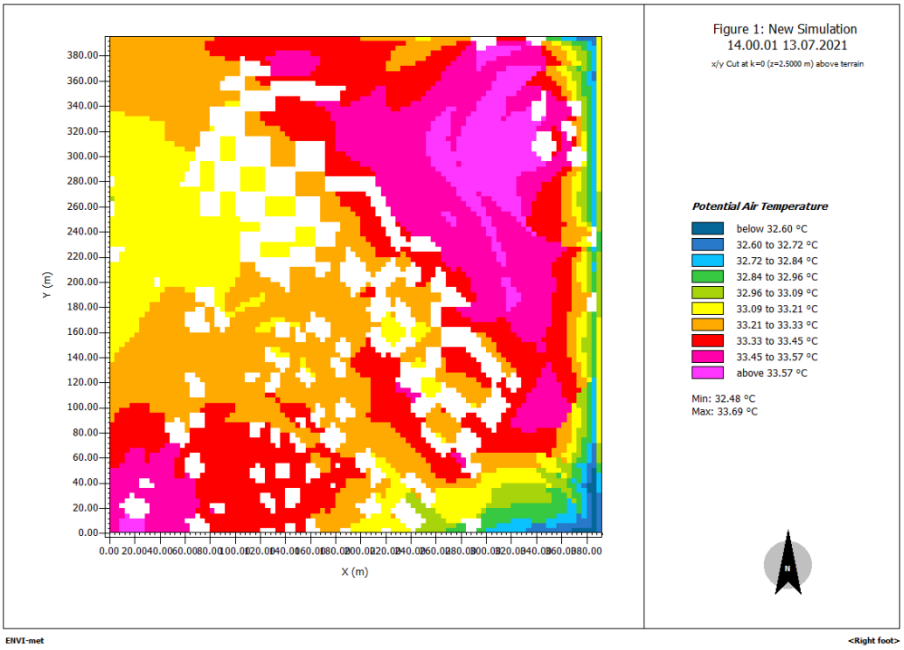

Figure 91. Potential air temperature map for s3 green roof at 14:00

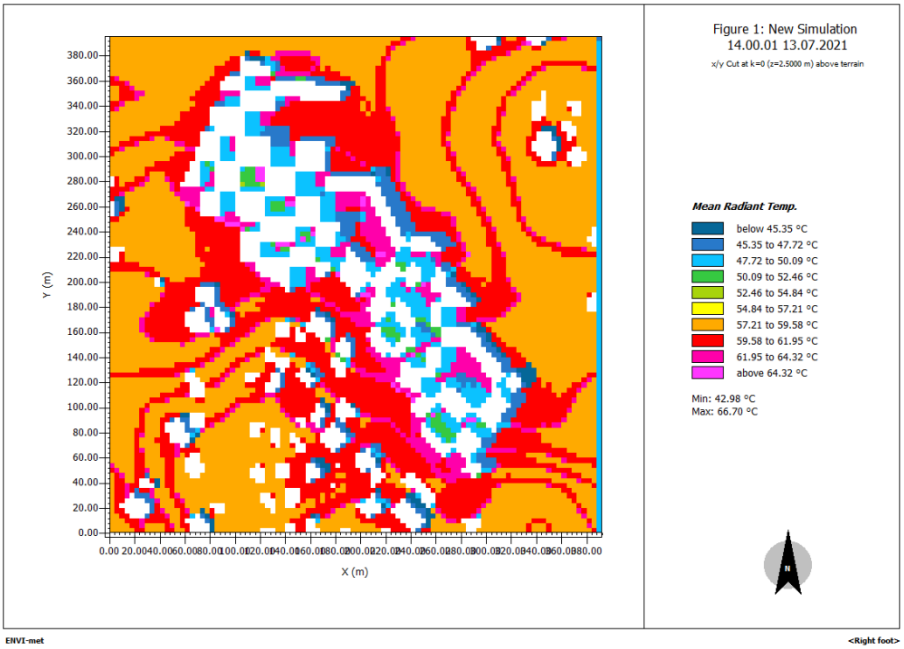

Figure 92. Mean radiant temperature map for s3 green roof at 14:00

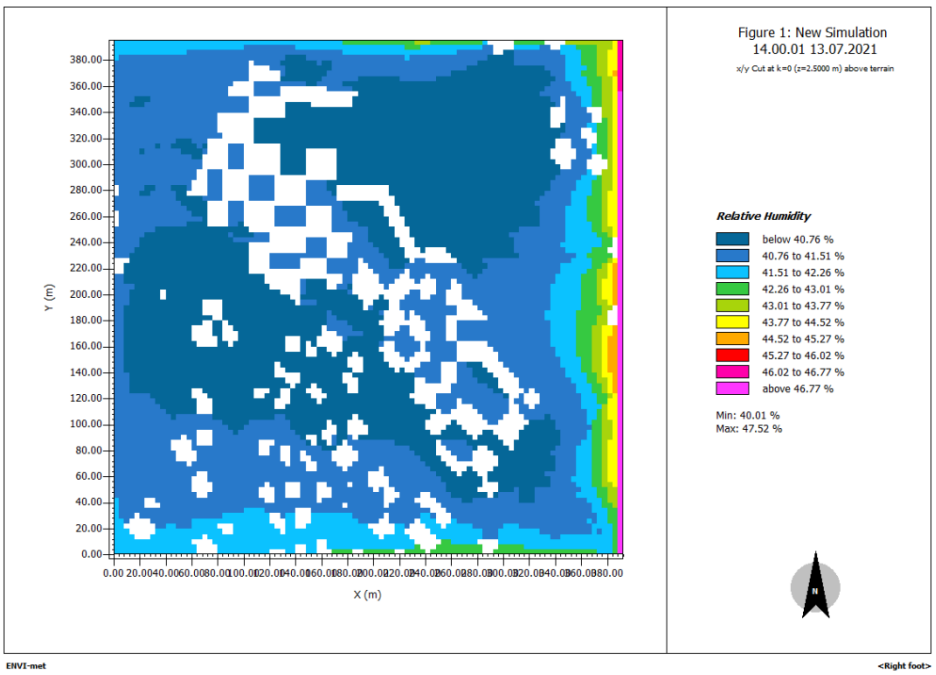

Figure 93. Mean radiant temperature map for s3 green roof at 14:00

Figure 94 to *Figure 96* illustrate the 2D maps of the green facade scenario, regarding the potential air temperature, wind speed and relative humidity at 14:00.

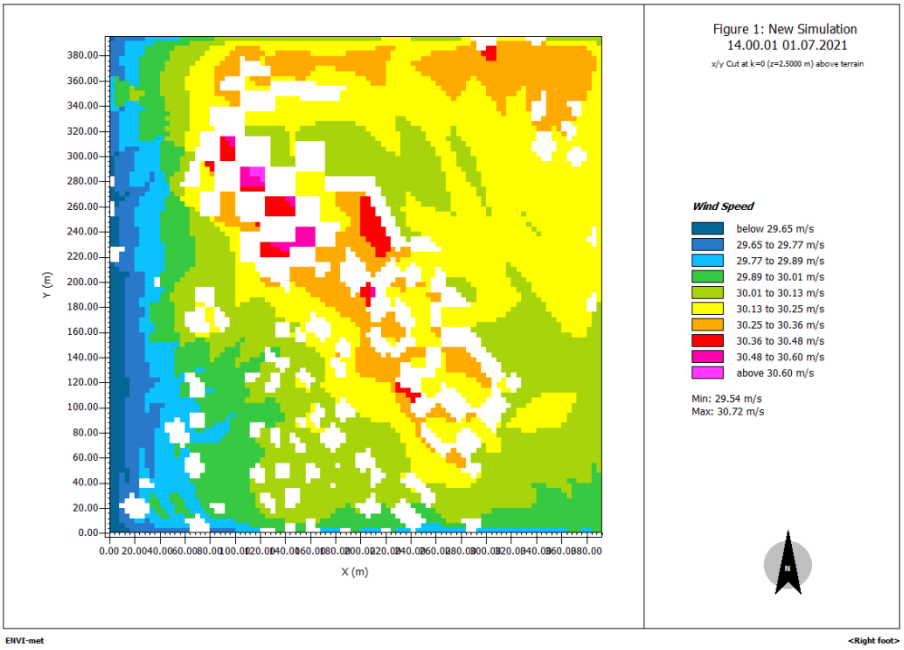

Figure 94. Potential air temperature map for s2 green facade at 14:00

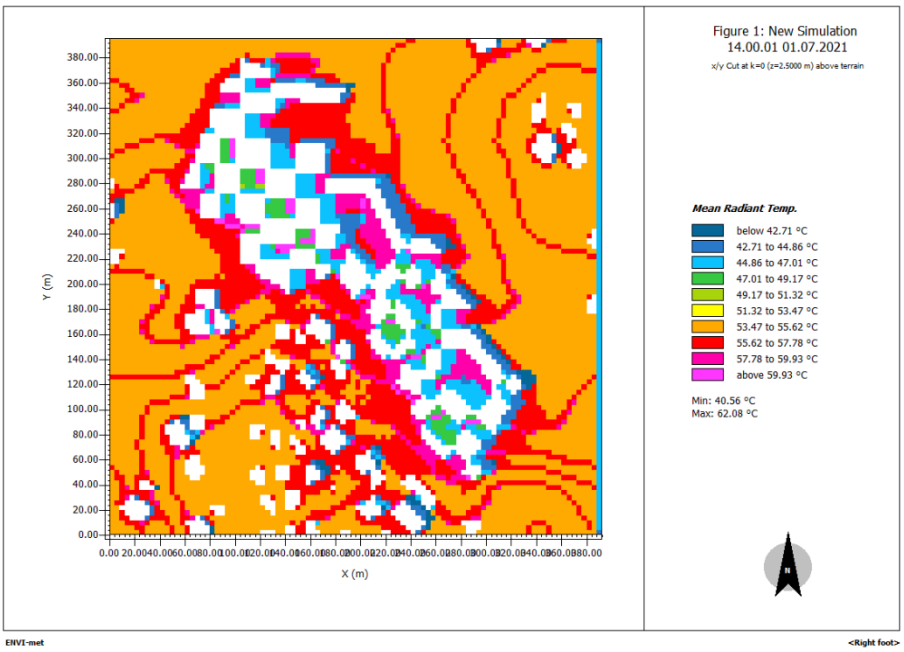

Figure 95. Mean radiant temperature map for s2 green façade at 14:00

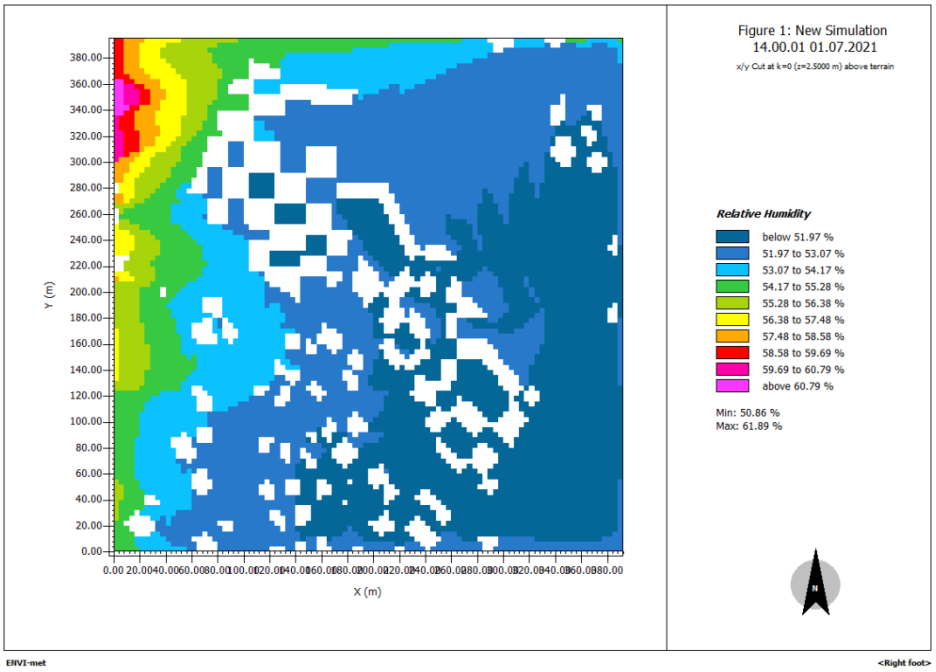

Figure 96. Relative humidity map for s2 green facade at 14:00

Figure 97 to *Figure 99* illustrate the 2D maps for the three scenarios UTCI at 14:00.

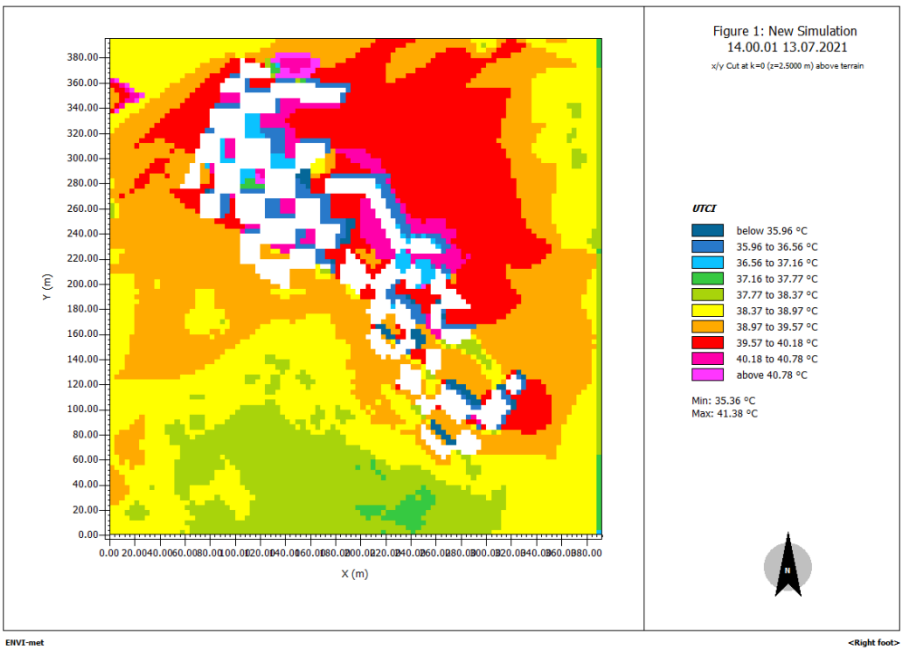

Figure 97. UTCI base model at 14:00

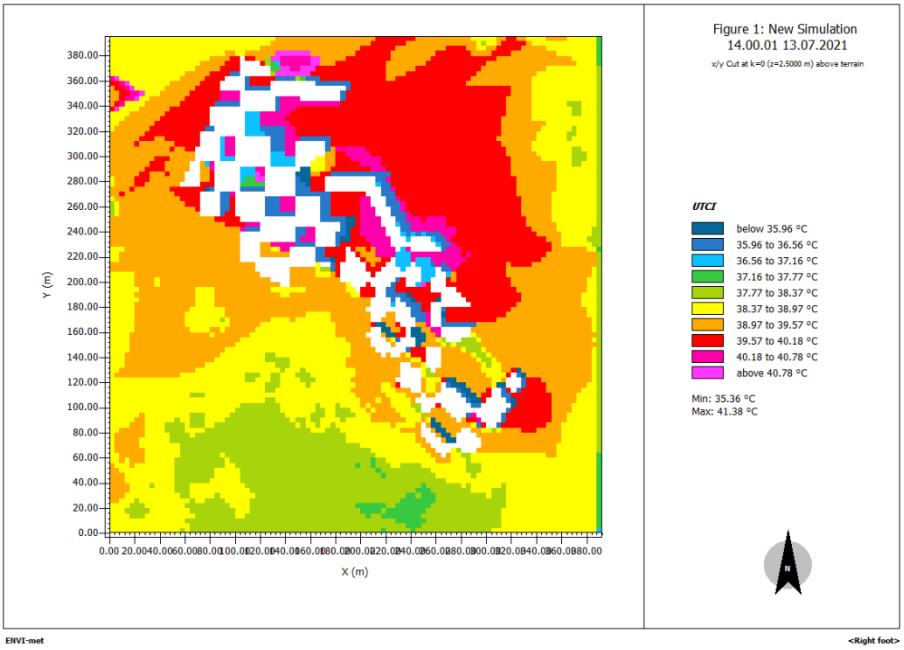

Figure 98. UTCI green roof model at 14:00

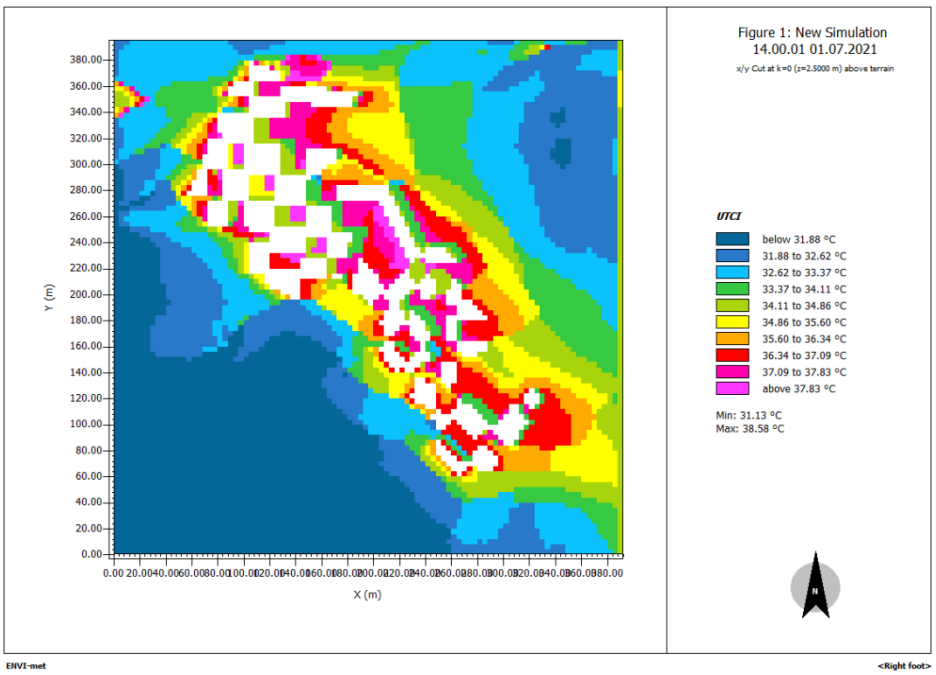

Figure 99. UTCI green façade model at 14:00

Figure 100 to *Figure 101* illustrate the process of acquiring precise data regarding the morphology of courtyards via 3D photogrammetry.

Figure 100. Courtyard 3D mesh illustration

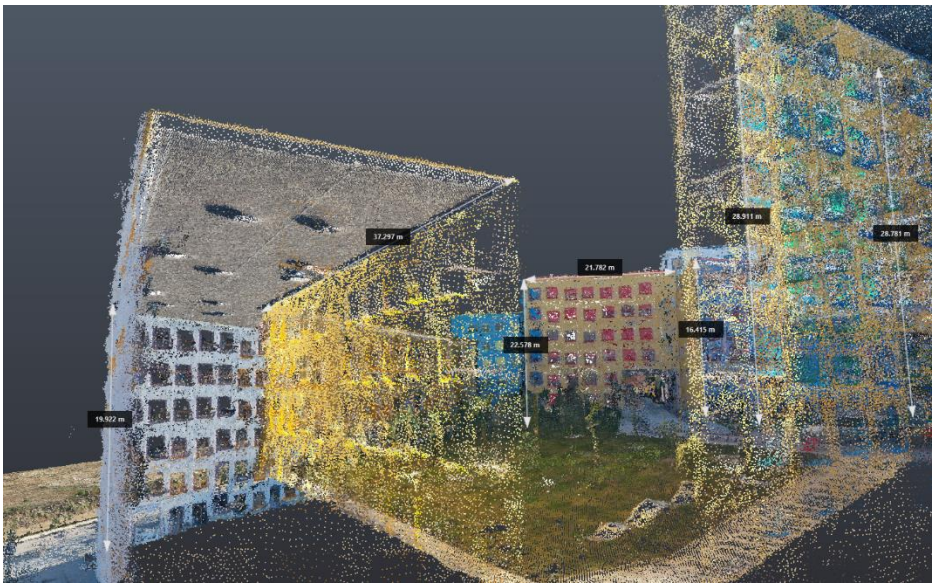

Figure 101. Courtyard 3D mesh illustration

Figure 102 illustrates the process of 3d CFD (computer fluid dynamics) wind examination.

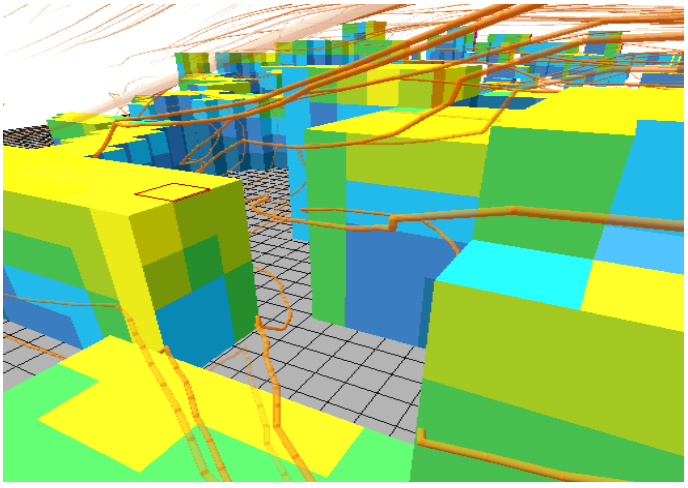

Figure 102. Courtyard 3D wind movement illustration

Figure 1033. Courtyard view

Figure 1044. Courtyard view

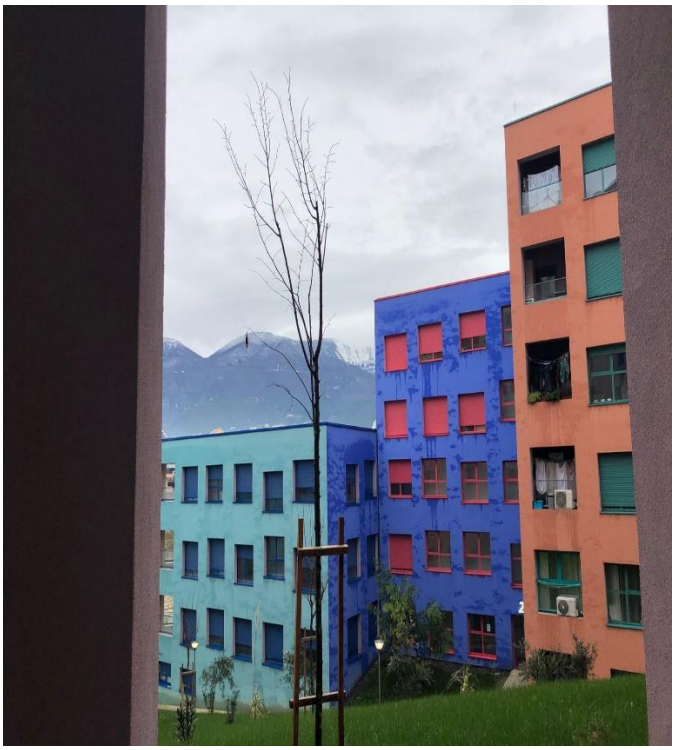

Figure 1054. Courtyard view